SEPTEMBER 2019 Ph.D. in Mechanical Engineering ÖZKAN ÖZBEK

REPUBLIC OF TURKEY

GAZİANTEP UNIVERSITY

GRADUATE SCHOOL OF NATURAL & APPLIED SCIENCES

DETERMINATION OF MECHANICAL BEHAVIORS OF FILAMENT WOUND HYBRID COMPOSITE PIPES

Ph.D. THESIS

IN

MECHANICAL ENGINEERING

BY

ÖZKAN ÖZBEK

SEPTEMBER 2019

DETERMINATION OF MECHANICAL BEHAVIORS OF FILAMENT WOUND HYBRID COMPOSITE PIPES

Ph.D. Thesis

in

Mechanical Engineering

Gaziantep University

Supervisor

Assoc. Prof. Dr. Ömer Yavuz BOZKURT

by

Özkan ÖZBEK

September 2019

REPUBLIC OF TURKEY
GAZİANTEP UNIVERSITY
GRADUATE SCHOOL OF NATURAL & APPLIED SCIENCES
MECHANICAL ENGINEERING

Name of the Thesis : Determination of Mechanical Behaviors of Filament Wound Hybrid Composite Pipes

Name of the Student : Özkan ÖZBEK

Exam Date : 20.09.2019

Approval of the Graduate School of Natural and Applied Sciences

Prof. Dr. A. Necmeddin YAZICI
Director

I certify that this thesis satisfies all the requirements as a thesis for the degree of Doctor of Philosophy.

Prof. Dr. Melda ÇARPINLIOĞLU
Head of Department

This is to certify that we have read this thesis and that in our consensus opinion it is fully adequate, in scope and quality, as a thesis for the degree of Doctor of Philosophy.

Assoc. Prof. Dr. Ömer Yavuz BOZKURT
Supervisor

Examining Committee Members:	Signature
Assoc. Prof. Dr. Recep EKİCİ	....
Assoc. Prof. Dr. Ahmet ERKLİĞ	....
Assoc. Prof. Dr. Ömer Yavuz BOZKURT	....
Asst. Prof. Dr. Mehmet Veysel ÇAKIR	....
Asst. Prof. Dr. Mehmet Tolga GÖĞÜŞ	....

I hereby declare that all information in this document has been obtained and presented in accordance with academic rules and ethical conduct. I also declare that, as required by these rules and conduct, I have fully cited and referenced all material and results that are not original to this work.

Özkan ÖZBEK

ABSTRACT

DETERMINATION OF MECHANICAL BEHAVIORS OF FILAMENT WOUND HYBRID COMPOSITE PIPES

ÖZBEK, Özkan
Ph.D. in Mechanical Engineering
Supervisor: Assoc. Prof. Dr. Ömer Yavuz BOZKURT
September 2019
111 pages

This study investigates the effects of intraply fiber hybridization on mechanical properties of composite pipes fabricated by filament winding technique. For this purpose, a 2-axis automated filament winding machine has been designed and fabricated to prepare composite pipe samples. The samples were manufactured at 6 layers at three different fiber orientations (±(40°), ±(55°) and ±(70°)) in order to investigate the effect of hybridization more effectively, by following performance at different winding angles. Split-disk test as in ASTM D2290 was used to establish apparent tensile strength of the samples. Axial compression behaviors and stiffness characteristics of the samples were determined according to ASTM D695 and ASTM D2412, respectively. In addition, the samples were separately compressed in axial and lateral directions and the crushing behaviors were determined in these directions. Finally, ignition loss tests were carried out in accordance with ASTM D2584 to determine the fiber contents of the samples. Failure modes were examined for each test separately to understand the fracture mechanisms. Tensile test results showed that apparent tensile properties of non-hybrid composite pipes are better than those of hybrid composite pipes. The quasi-static compression performance of hybrid samples was found to be marginally different in axial and radial directions such as; inclusion of carbon fiber improved compression strength in the axial direction while leading decrease of pipe stiffness in the radial direction. Crushing procdure of hybrid composite pipes were seen as more stable and regular compared to non-hybrid ones. The overall performance of the hybrid composites were found to be in the range of the results of non-hybrid composite pipes.

Key Words: Filament winding, Intraply fiber hybridization, Tensile, Compression, Crushing

ÖZET

ELYAF SARMA YÖNTEMİ İLE ELDE EDİLEN HİBRİT KOMPOZİT BORULARIN MEKANİK ÖZELLİKLERİNİN BELİRLENMESİ

ÖZBEK, Özkan
Doktora Tezi, Makine Mühendisliği
Danışman: Doç. Dr. Ömer Yavuz BOZKURT
Eylül 2019
111 sayfa

Bu çalışma, tabaka içi fiber hibridizasyonunun filament sarım tekniği ile üretilen kompozit boruların mekanik özellikleri üzerindeki etkilerini incelemektedir. Bu amaçla, kompozit boru numuneleri hazırlamak için 2 eksenli otomatik filament sargı makinesi tasarlanmış ve üretilmiştir. Örnekler, farklı sargı açılarındaki performansı izleyerek hibridizasyonun etkisini daha etkin bir şekilde araştırmak için üç farklı elyaf yöneliminde (±(40°), ±(55°) ve ±(70°)) 6 katman halinde üretilmiştir. ASTM D2290'daki gibi ayrık-disk testi, numunelerin görünür gerilme mukavemetini belirlemek için kullanılmıştır. Eksenel sıkıştırma davranışları ve numunelerin sertlik özellikleri sırasıyla ASTM D695 ve ASTM D2412'ye göre belirlenmiştir. Ek olarak, örnekler eksenel ve yanal yönlerde ayrı ayrı sıkıştırılmış ve bu yönlerde ezme davranışları belirlenmiştir. Son olarak, numunelerin elyaf içeriğini belirlemek için ASTM D2584 uyarınca yakma testleri yapılmıştır. Kırılma mekanizmalarını anlamak için her test için başarısızlık modları ayrı ayrı incelenmiştir. Çekme testi sonuçları, hibrit olmayan kompozit boruların görünen çekme özelliklerinin, hibrit kompozit borularınkinden daha iyi olduğunu göstermiştir. Hibrit numunelerin yarı-statik sıkıştırma performansının, eksenel ve radyal yönlerde marjinal olarak farklı olduğu bulundu; karbon fiberin eklenmesi, eksenel yönde sıkıştırma kuvvetini arttırırken radyal yönde boru sertliğinin azalmasına öncülük etmiştir. Hibrit kompozit boruların ezilme prosesi, hibrit olmayanlara göre daha stabil ve düzenli olarak görülmüştür. Hibrit kompozitlerin genel performansının, hibrit olmayan kompozit boruların sonuçları aralığında olduğu bulunmuştur.

Anahtar Kelimeler: Elyaf sarma, Tabaka içi fiber hibritleştirmesi, Çekme, Basma, Ezme

''Dedicated to my parents, my beloved wife and my lovely daughter''

ACKNOWLEDGEMENTS

I would like to express my special appreciation and thanks to my advisor Associate Professor Dr. Ömer Yavuz BOZKURT, you have been a tremendous mentor for me. I would like to thank you for encouraging my research and for allowing me to grow as a research scientist. Your advice on both research as well as on my career have been invaluable.

I would like to express the all staff of Gaziantep University Mechanical Engineering Department for their endless helpful characteristics and guidance.

I also thank my fellow labmates especially N. Furkan DOĞAN, Hakan ÇANDAR and Yüksel ERASLAN in for the stimulating discussions, for the sleepless nights we were working together before deadlines, and for all the fun we have had in the last four years.

Last but not the least, I would like to thank my family, my beloved wife (H. Neval ÖZBEK) and my lovely daughter (Nil ÖZBEK) for supporting me spiritually throughout writing this thesis and my life in general.

This work is supported by Gaziantep University Scientific Research Center (BAP), through project under grant number MF.DT.16.13.

TABLE OF CONTENTS

LIST OF TABLES

Page

LIST OF FIGURES

Page

LIST OF SYMBOLS

α	Fiber orientation angle
R	Mandrel radius
N_m	Mandrel rotational speed
V_c	Carriage linear speed
wt%	Fiber mass fraction
W_1	Mass of the sample before ignition loss experiments
W_2	Mass of the sample after ignition loss experiments
σ_a	Apparent hoop tensile strength
P	Maximum load on tensile tests
A	Cross-sectional area
E_m	Apparent tensile modulus
Δy	Maximum displacement
w	Width of the sample
t	Thickness of the sample
r_{mean}	Mean radius
σ_c	Compression strength
F	Load per unit length
d	Inside diameter
E	Total energy absorption
S_i	Initial stroke on crushing
S_f	Final stroke on crushing
P_m	Mean crushing load
P_i	Initial peak load
η_f	Crushing load efficiency
m_{crush}	Mass of the crushing sample

LIST OF ABBREVIATIONS

CAD	Computer Aided Design
FW	Filament Wound
ASTM	American Society for Testing and Materials
SEM	Scanning Electron Microscope
FEA	Finite Element Analysis
FRP	Fiber Reinforced Pipe
BFRP	Basalt Fiber/Epoxy Reinforced Pipe
GFRP	Glass Fiber/Epoxy Reinforced Pipe
CFRP	Carbon Fiber/Epoxy Reinforced Pipe
BGFRP	Basalt-Glass Fiber/Epoxy Reinforced Pipe
GCFRP	Glass-Carbon Fiber/Epoxy Reinforced Pipe
CBFRP	Carbon-Basalt Fiber/Epoxy Reinforced Pipe
PS	Pipe Stiffness
SF	Stiffness Factor
PPD	Percentage Pipe Deflection

CHAPTER I

INTRODUCTION

1.1. General Introduction

In today's world, scientists and engineers are widely focusing on research studies related with the performance improvements of engineering products in various fields in order to meet efficiently the rising consumption demands parallel to increase in human population. In this context, development of new materials having better properties with low weight stands out as one of the most important research activities of last few decades. As a result of these research activities, significant progresses in material science put forward the use of composite materials instead of traditional metallic-based engineering materials in numerous applications such as defense industry, aviation industry, automotive industry, marine industry, power transmission lines, electrical power transmission lines, electronics, construction, agriculture, household appliances and sports equipment. Compared with traditional metallic materials, polymeric composite materials with several unique properties, including higher specific strength and stiffness, longer service life, and better damping are regarded as one of the popular composite types.

There are different manufacturing methods for the production of polymeric composite materials such as hand layup, pultrusion, filament winding, resin transfer molding, injection molding, in accordance with the target properties of relevant product. The filament winding based on wrapping of a fiber reinforcement around a rotary mandrel with a desired settlement by controlling the axis velocities of the machine is considered as the most promising technique with respect to the minimum material waste, automated structure, flexibility and feasibility in design stage. It is the most preferred method for rounded products (tube, internal pressure tank, profile, etc.) with a positive curved surface (convex). Nowadays, high pressure vessels, sewer pipe systems, high pressure piping systems, water tanks, large underground tanks, oxygen and fire extinguisher tubes for firemen, helicopter rotor, golf clubs, wind turbine blades, transmission shafts, bus shafts, aircraft body parts, ship body parts, radom, space shuttles are some of the popular applications of filament winding. With the appropriate choose of several fabrication parameters such as fiber orientation angle, fiber type, mandrel diameter, mandrel type and resin type, the method enables great tailorability on final properties of the product.

In the literature, different application procedures such as resin bath-based impregnation, wet- and dry-type winding and prepreg winding are presented for the filament winding method [1-4]. Resin bath-based impregnation are commonly used in thermosetting industrial applications. Prepreg winding is preferred in high sensitivity applications because of its high cost. Unlike prepreg winding, wet filament winding has low cost, rapid fabrication and allowance to change resin content. Because of that; it has the widest commercial applications. In the wet filament winding method, two different applications are seen to resin impregnation. These are fiber immersion that the fiber is completely immersed into resin and drum type that impregnated fiber passes on a drum. Also, resin viscosity and curing temperature are important factors that affect the application selection except that fiber material types.

Reasons behind the popularity of filament winding technique can be summarized as [5, 6]:

- Fiber settlement with the desired fiber orientation angle at the same or different layers,
- Use of continuous fiber reinforcement in the whole structure,
- Fabrication of the products with high fiber volume fraction,
- Low cost production (due to low fiber and resin waste rate),
- Faster production (winding speed>50 m/min) compared to other composite material production techniques.

Despite having these features, it has also some drawbacks as follows [5, 6]:

- Inability to produce geometries in reverse curvature forms,
- Impossibility to modify the shape of fiber winding in a layer,
- Specific mandrel requirements depending on product geometry,
- Poor surface quality of fabricated materials,
- Chemical solvent requirements for purification of equipment from resin after production,

- Limitation on resin type selection due to curing and overheat during the production.

Recently, hybrid fiber reinforced composite pipes fabricated by filament winding method are preferred with the employment of two or more fiber reinforcements simultaneously in the scientific studies. This hybridization can provide fabrication of a product with attractive mechanical and physical properties by reducing the adverse effects or increasing the positive effects, of each component. For example, in a glass/carbon hybrid fiber reinforced composite material; glass fiber enables more protection against the impact and lower the cost, while carbon fiber provides higher tensile properties, better abrasion and good fatigue behavior.

1.2. Research Objectives and Tasks

The main goals of this thesis are the investigation of effect of the intraply fiber hybridization on the mechanical behaviors of filament wound composite pipes under tensile, compression and crushing loadings.

The research tasks can be shown as follows:

I. An overview of filament wound composite pipes in the literature.
II. Detailed review of fiber hybridizations (interply and intraply) in filament winding technique.
III. Determination of raw materials to be used in studies.
IV. Designing a 2-axis filament winding machine on CAD programs.
V. Construction of a 2-axis filament winding machine.
VI. Revising the mathematical aspect of filament winding technique to create motion codes (G-codes).
VII. Fabrication of non-hybrid fiber reinforced composite pipes.
VIII. Implementation the intraply fiber hybridization process.
IX. Performing of apparent hoop tensile experiments by split-disk method.
X. Conduction of quasi-static compression tests in axial and radial direction.
XI. Evaluation of axial and lateral crushing experiments.
XII. Assessment of results obtained from above tests, respectively.
XIII. Discussions on effect of intraply fiber hybridization on the considered mechanical responses of pipes.

1.3. Layout of Thesis

A brief literature survey about non-hybrid fiber reinforced composite pipes and a special review of hybrid fiber reinforced composite pipes are presented in Chapter 2. The materials used in studies and methods including fabrication technique and experimental tests are given in Chapter 3. The fiber mass fractions, apparent hoop tensile and quasi-static compression results are summarized in Chapter 4. The crushing responses in axial and lateral direction of samples are presented in Chapter 5. The conclusions are revealed in Chapter 6. Finally, future works are present in Chapter 7.

CHAPTER II

LITERATURE SURVEY

2.1 Introduction

The use of fiber reinforced composite pipes in industrial applications have been rapidly accelerating due to their superior performance such as strength-to-weight ratio, stiffness-to-weight ratio, longer service life and higher corrosion resistance, than classical metal-based engineering materials [7, 8]. Several methods as hand layup, prepreg winding, filament winding etc. [2, 4, 6] are present to obtain composite pipes in the literature. Among them, filament winding technique based on wrapping of a fiber reinforcement around a rotary mandrel with a desired settlement by controlling the axis velocities of the machine is considered as the most promising technique with respect to the minimum material waste, automated structure, flexibility and feasibility in design stage.

In the present study, the effort is devoted to examine the effect of intraply fiber hybridization on the mechanical behaviors of filament wound composite pipes in the view of apparent tensile, quasi-static compression and crushing experiments. In this context, a basic literature survey about non-hybrid fiber reinforced composite pipes and special review of hybrid fiber reinforced composite pipes are carried out, respectively.

2.2 Literature Survey on Non-Hybrid Fiber Reinforced Composite Pipes

Up to today, a large number of published studies regarding the mechanical characteristics of filament wound (FW) composite pipes subjected to fatigue loading [9-10], internal and external pressure [11-12], compression and crushing loading [13-16], and impact loading [16-19], are found in the literature. Some of them are given in this section.

Mertiny et al. [20] performed the experimental stress analysis to determine hoop and axial stresses at different winding process having multi-angles. Also, they examined the failure modes of the samples and gave the images of failures. They expressed that the multi-angle is valuable method for tubular structures if variable loading conditions need to be considered.

Sayman [21] developed a general stress analysis under the hygrothermal loading for thick and thin composite cylinders having the fiber orientation of $(0°/90°)_2$, $(30°/-30°)_2$, $(45°/-45°)_2$ and $(60°/-60°)_2$. He conducted a numerical analysis on ANSYS 7.0 software and compared with the analytical solutions.

Kim et al. [22] aimed to establish a design rule for filament winding process. They used to semi-geodesic path algorithm for calculating possible winding patterns taking into account the windability. Also, finite element analysis using ABAQUS were performed to predict the behaviors of the technique.

Kaynak et al. [23] conducted the split-disk tests to determine hoop tensile properties of the samples having different fiber reinforcement, resin type, winding angles. The samples were manufactured by wet filament winding technique. They explained that use of carbon fibers have provided 60% higher performance according to glass fibers. Resin differences had no significant effect.

Avcı et al. [10] investigated the corrosion fatigue behaviour of filament wound composite pipes. The samples having the E-glass/epoxy composites with a $\pm(75°)_6$ winding angles were subjected to fatigue loading at 0.42 Hz frequency and a stress ratio of R=0.05.

Meijer and Ellyin [24] conducted the multiaxial stress tests on glass fiber reinforced tubes manufacturing by filament winding. The first failure modes were observed and the stress and strain failure envelopes were recorded.

Akkuş et al. [25] designed a tension system for the fibers before resin impregnation of the reinforcements. They used nine pulleys (two different diameter dimensions) to supply tension in filament winding action. They found the primary test of the system showed that the fiber tension may be kept constant within the 10% of aimed tension value.

Moreno et al. [11] examined the influence of winding pattern on the mechanical response of filament wound glass/epoxy composite cylinders under external pressure.

They evaluated the analytical and experimental studies. Diameter to thickness ratio was chosen as variable.

Tarakçıoğlu et al. [26] investigated the fatigue failure behavior of glass fiber reinforced filament wound composite pipes having ±(75°)$_4$ fiber orientation angle under pure internal pressure. The samples were exposed to different load levels from 30% to 70%. S-N curves of samples and observation of leakage were carried out. Three main parts as whitening, leakage initiation and final failure were observed as damage behaviors. They found that when the applied load is high the pipe suddenly bursts without any leakage.

Moon et al. [27] examined the buckling and failure behaviors of carbon fiber reinforced composite pipes for underwater vehicle applications. Hydrostatic pressure analysis were performed through finite element analysis and experiments. Samples producing with helical and hoop winding techniques had the winding angles of ±(30°/90°), ±(45°/90°) and ±(60°/90°). Analysis and test results showed that the cylinders do not recover the initial buckling pressure after buckling and that this leads directly to the collapse.

Arıkan [28] performed a failure analysis of E-glass fiber reinforced composite pipes fabricated by filament winding technique. The samples had six antisymmetric layers with ±(55°)$_6$ winding angles. The burst strengths of the samples having seven different crack angles were determined by open-ended internal pressure. It can be said that as the angle of the crack in pipes increases, the burst pressure increases and effect of the crack angle decreases. Highest burst strength was obtained from 90° surface crack angle.

Khalifa et al. [29] examined the mechanical characterization of glass/vinylester composite pipes having ±(55°) winding angle under axial monotonic loading. Their experiments determined the damage mode using acoustic emission and tensile test. They observed the damage steps, and shared the SEM microscopic photographs.

Sarı et al. [30] investigated the residual failure pressures and fatigue life of composite pipes subjected to lateral impact. Specimens having glass fiber reinforcement with ±(55°)$_6$ winding angle were exposed to three different energy levels for impact tests.

They revealed that failure pressure of non-impacted pipe has higher than the impacted one at 5.0 J energy level about 34% and 40%.

Deniz et al. [31] carried out the fatigue behaviors of E-glass reinforced and epoxy matrix filament wound composite pipes having six layers and ±(55°) winding angle. An artificial seawater having 3.5% salinity was used and the samples were examined after 3, 6 and 9 months. After the impact tests were performed at three different energy levels (5.0 J, 7.5 J and 10.0 J) fatigue experiments were carried out on the samples. According to obtained results non-impacted samples showed the greater fatigue life than impacted ones. After the 3 months immersion time, fatigue life of the samples were decreased.

Rodriguez et al. [32] evaluated the failure analysis of glass fiber reinforced composite pipes having epoxy-anhydride as matrix for oil transport. The electron microscopy images showed a concentration of the defects relatively low, but a generalized irreversible hydrolytic attack.

Rafiee [33] examined the experimental and theoretical studies based on the failure of glass/polyester composite pipes. An algorithm was developed at different input parameters of the pipes such as winding angle, number of layers and sand ratio. Sand was used as filler in the specimens.

Martins et al. [34] investigated the effect of stress ratio on the fracture morphology of filament wound composite tubes having glass fiber reinforcement and epoxy matrix. A comparative study was evaluated with two typical loading conditions as closed-end and restrained-end in the piping system.

Jia et al. [13] examined the effect of geometric factor, winding angle and pre-crack angle on quasi-static crushing behavior of filament wound carbon fiber reinforced composite cylinders. They found the compressive strength, compressive modulus and crack length exhibited the decrease trend and crushing efficiency showed the opposite trend with winding angle increasing.

Uyaner et al. [35] performed the low velocity impact tests of glass fiber reinforced tubes at two different energy levels of 5.0 J and 10.0 J. Damaged zones of the samples were observed and force-time, force-displacement curves were obtained. Also, burst strengths were investigated for the impacted and non-impacted samples and fatigue tests using PLC controlled fatigue testing instrument were applied to damaged and undamaged samples. The samples were exposed to five different stress levels. S-N curves of the samples were plotted. The burst strength and the fatigue life of the damaged glass fiber reinforced pipes were decreased as the impact energy increased. Also, the decrease in the fatigue life was greater than that of the burst strength.

Demirci et al. [36] investigated the Charpy impact behaviors of arc shaped samples. The samples produced by filament winding method had the six layer with ±(55°) winding angles. Basalt and glass fibers were used as reinforcement. They conducted the experiments at different notch-depth ratios. The delamination damage in glass reinforced composites was observed to be more dominant than basalt reinforced samples.

Perillo et al. [37] conducted the experimental and numerical tests on impact properties of glass fiber reinforced pipes. Samples having eight layers with two different fiber orientation angles were observed on drop weight impact experiments according to ASTM D2444. Abaqus Software was used to perform 3D finite element numerical analysis.

Pranesh et al. [38] performed the stress analysis of filament wound composite pipes having glass fiber reinforcement under multiaxial stress ratios. They conducted a short term test as Ultimate Elastic Wall Stress to observe change in stress-strain relationships.

Vacher et al. [39] evaluated the split disk and biaxial tests of the glass/epoxy and carbon/epoxy filament wound composite tubes. The material strength and the modulus in the fiber direction were obtained. Also, they performed failure analysis and obtained results come from experimental studies were compared with the Puck's failure theory.

Krishnan et al. [40] examined the effects of winding angle of glass fiber reinforced composite pipes under multiaxial cyclic loading. The samples having three different fiber orientation angles as $\pm(45°)_4$, $\pm(55°)_4$ and $\pm(63°)_4$ were tested using indigenous automated test.

Mahdavi et al. [41] performed the tensile test of ring samples to determine hoop strengths of filament wound glass fiber reinforced composite pipes having nine layers and ±(55°) winding angles. Also, acoustic emission technique was used to characterize the different failure mechanisms of the fabricated samples. The results were compared with the scanning electron microscope images.

Taşyürek ve Tarakçıoğlu [42] conducted the internal pressure tests of glass fiber reinforced composite pipes having six layer with ±(55°) winding angle. They added to carbon nanotubes filler with 0.5% and 1.0% within the epoxy resin having medium viscosity. The wall thickness ratio of surface cracks on each sample (w/t) was opened as 0.25 and 0.5. The results were compared with the samples including pure epoxy resin as matrix. The samples including carbon nanotubes showed the higher internal pressure than others. The observations on the samples were examined up to failure and detected to some whitenings on surface.

Misri et al. [16] carried out the effect of winding angles as ±(45°) and ±(90°) on the crushing behavior of hollow kenaf fiber and hybrid aluminum/kenaf fiber reinforced unsaturated polyester composites produced by the filament winding technique. They found the hollow composites having ±(45°) winding angle exhibited the more energy in crushing due to their longest distance in the post-crushing zone.

Hafeez and Almaskari [43] conducted an experimental study related to scaling laws in laterally indented filament wound tubes supported with V-shaped cradles. The scaling factors of the tubes having glass fiber reinforcement and epoxy matrix were determined by using Buckingham Pi theorem for geometric dimensions of the samples.

Hawa et al. [44] examined the effects of water ageing and low-velocity impact loadings on E-glass fiber/epoxy composite pipes subjected to monotonic internal pressure. The composite pipes having six antisymmetric layers and ±(55°) winding angles were manufactured by filament winding technique. To perform ageing process, samples were immersed in ±80°C water for 500h, 1000h and 1500h. For impact loadings, the energy levels having 5.0 J, 7.5 J and 10.0 J were applied and then monotonic burst tests were conducted. The results explained that samples applying ageing and impact application yielded at lower burst strength. SEM photographs of the damaged samples were also examined in study.

Almeida et al. [45] performed the external pressure tests of the carbon/epoxy filament wound composite tubes, experimentally. The tubes were manufactured by dry-filament winding using T700 towpregs to evaluate computational analysis. Numerical results have been indicated the tubes fail by buckling when the diameter to thickness ratio is 20:1.

Üstün et al. [46] conducted the hybrid nanofillers (carbon nanotubes and boron nitride nanoplates) in the epoxy matrix of the filament wound composite pipes. Carbon fiber was used as reinforcement. S-N curves of the samples were drawn and SEM views of the damaged samples were given in study. The samples having carbon nanotubes as fillers were exhibited the better fatigue behavior than other ones.

Sebaey and Mahdi [47] examined the crashworthiness behaviors of glass/epoxy composite tubes fabricated by filament winding. The samples were compressed after impacted by charpy impact tester. Various places such as side, top, down were exposed to impact energy with more than one time. They explained that top impacted samples had less sensitivity to impact damage compared to side impacted ones.

Wang et al. [48] investigated the effects of fiber orientation and wall thickness on the energy absorption characteristics of carbon fiber reinforced composite pipes subjected to axial quasi-static loading. The winding angle and thickness showed the significant influences on the crashworthiness characteristics of the progressively crushed pipes. Brittle fracturing and lamina bending as failure modes were observed.

Roslan et al. [49] carried out on the energy absorption capacity of basalt sandwich composite cylinders having foam in core. The fiber cracking, pipe's wall folding and crumping were observed as failure modes in progressive manner.

Mahdi et al. [50] examined the influence of fiber orientation angle on the energy absorption capability of E-glass/epoxy reinforced composite pipes (GFRP) having six different winding angles (0°, 15°, 30°, 45°, 60° and 75°) and eight layers. 15°/-75° and 75°/-15° were being recommended for better load carrying and energy absorption capability. A combination of four failure modes as fiber debonding, fiber fracture, matrix cracking and delamination have been observed from samples under progressive crushing.

Farley et al. [51] examined the crushing characteristics of composite tubes and classified the crushing modes depended on the crack growth. Three basic modes as transverse shear, lamina bending and local buckling were detected. Also, combination of transverse shear and lamina bending modes was named as brittle fracturing.

Lapend and Marinucci [52] conducted a study about interlaminar shear stress and split-disk tests of basalt and glass fiber reinforced composite pipes. Superposition and interweaving winding methods were used for $[(90°)_2/\pm(30°)_2/(90°)_2]$ stacking sequences of each material. Debonding capabilities and fracture shapes were identified during the test process.

A national project [53] supported by TÜBİTAK Organization were performed related to optimum pipe design by filament winding method. Barış Electric Company conducted many mechanical test such as tensile, compression, impact, compression after impact, pressure and torsion tests for four different fiber types, two different resins, three different winding angles and three different patterns.

Also, some thesis [54-59] about filament wound composite pipes having non-hybrid type fiber reinforcement can be seen in the literature. Bora Balya [60] performed the design and analysis of filament wound composite tubes under combined loading. Emrah Salim Erdiller [61] determined the mechanical properties of composite pipes by conducting tensile and split-disk tests with five different fiber materials. Karnsten Dons [62] performed the tensile and internal pressure tests and observed the leakage at different winding angles for the composite pipes.

2.3 Literature Survey on Hybrid Fiber Reinforced Composite Pipes

Although the use of non-hybrid fiber reinforcement in the literature has many researches, fiber hybridization has become a new attractive subject in filament winding, recently, because of possibility to eliminate or reduce disadvantages of materials in applications. Two fiber hybridization as interply and intraply hybridization are mainly present in literature [63]. In this section, literature examination on hybrid fiber reinforced composite pipes are given to help for understanding the literature deficiency and the novelty of this thesis.

Xu et al. [64] performed an experimental study on the crashworthiness behaviors of glass FRP, aramid FRP, carbon FRP and their interply hybridizations, with 88°, 17.6° and 88° stacking sequences from inner to outer layers. The effects of crushing speed, temperature treatment, hybrid ratio, and wall thickness were also investigated on the energy absorption capabilities of pipes. Carbon/aramid FRP pipe after temperature treatment were exhibited the highest specific energy absorption as 98 kJ/kg in quasi-static compression tests.

Basalt fiber fabric/polyester, glass fiber fabric/polyester and their interply hybridization/polyester were subjected to quasi-static compression loading by Esnaola et al. [65]. The composites with bidirectional and unidirectional fibers having semi-hexagonal shape were fabricated by infusion method. While bidirectional basalt/polyester sample had unstable collapse resulting from higher mean load issue, the maximum collapse efficiency was acquiring by bidirectional glass/polyester sample as 82%.

Ma et al. [66] examined the effects of temperature treatment on the energy absorption behaviors of carbon/aramid interply hybrid fiber reinforced composite pipes subjected to quasi-static compression test. The samples were handled at 100°C for 100 h, 200 h and 400 h, resulted with higher energy absorption compared to without treatment ones. Bending, splaying and buckling failure modes were observed from the highest to the lowest in the aspect of energy absorption, respectively.

Zuraida et al. [67] examined the pipes with four layer and $\pm(55°)_4$ fiber orientation subjected to the quasi-static indentation loading via servo-hydraulic instron machine type. Glass fiber, carbon fiber and interply hybridization of them were used for reinforcements. The obtained results were compared with the finite element analysis.

Cicala et al. [68] examined the interply hybridization effects of the glass and natural fibers on the mechanical properties such as tensile and flexural for curved pipes. They found the natural fibers had poor properties when compared to glass ones. They achieved the 20% cost reduction and 23% weight reduction to commercial pipe construction by hybridizing of the pipes.

Talib et al. [69] performed a numerical study (FEA) related to completely composite automotive drive shaft using carbon and glass fibers at different winding angle. They investigated natural frequencies and buckling torques of the samples as interply hybridized. They found the loss in natural frequency is 44.5% and buckling strength is 46.07%.

Kim et al. [70] researched the crushing behaviors of composite tubes. Carbon/epoxy, kevlar/epoxy and interply carbon-kevlar/epoxy composite tubes were utilized to obtain specific energy absorption, maximum peak load, mean crushing load. According to results, carbon/epoxy provided to the best energy absorption capability with the value of 81.7%. Also, kevlar /epoxy gave the worst specific absorption in their studies.

Ha et al. [71, 72] performed the design optimization and fabrication of a hybrid composite flywheel rotor made of carbon-glass/epoxy interply hybridization. Hoop winding via continuous filament winding technique were considered at sample production. They determined three different rim design cases and performed stress analysis of the samples.

Kumar et al. [73] used the carbon and aramid intraply fabrics to obtain hybrid composite pipe having bisphenol resin matrix. Machinability of the samples on turning operations at different parameters such as cutting speed, feed rate, cutting force, surface roughness were performed experimentally. They also conducted genetic algorithm study on samples.

Haubler et al. [74] performed an optimization study on polymer composite pipes under consideration of interply hybridization with glass and carbon fiber reinforced polymers. Different parameters that effect the filament winding such as winding angle, layer thickness, areal cost etc were investigated. Pipe performance depended on the chosen materials' transverse tensile strengths. All analysis considered as a scenario of free pressurized pipe.

Gemi et al. [75] examined the low velocity impact response of prestressed functionally graded interply hybrid pipes. Samples with the winding angle of ±(55°) were prepared at four different arrangements having glass-glass, glass-carbon, carbon-glass, carbon-carbon fibers. After the impact tests, internal pressure was applied to see burst strengths of the damaged pipes.

Wakayama et al. [76] performed a study in order to improve the burst strength after drop weight impact of FRPs. Three types of the low-modulus pitch based carbon fiber were applied to surface of carbon fiber reinforced pipes. They found that the application of low modulus carbon reinforcements were improved the burst strength of the pipe.

2.4 Conclusion on Literature Survey

So far, most of the scientific work devoted to composite pipes has focused on the non-hybrid fiber reinforced composite pipes or effect of interply fiber hybridization. To the author's knowledge, no detailed systematic work has been reported on the influence of intraply fiber hybridization of composite pipes. This thesis describes an experimental study on the effect of intraply fiber hybridization of basalt, glass and carbon fiber reinforced filament wound composite pipes. Pipes with fiber orientation angles of ±(40°), (±55°), and ±(70°) were hybridized for six layers of considered fibers and subjected to tensile, quasi-static axial and lateral compression , axial and lateral crushing loadings.

CHAPTER III

MATERIALS AND METHODS

3.1 Materials

The fiber reinforcements used in this study, as seen in Figure 3.1, are the continuous fibers of Glass roving (Dost Kimya A. Ş., Turkey) and Carbon roving (Plasto A. Ş., Turkey), Basalt roving (Tila Kompozit Ltd. Şti., Turkey). The mechanical and physical properties of the reinforcement materials are given in Table 3.1.

a) b)

c)

Figure 3.1 Fiber reinforcements; a) glass fiber roving, b) carbon fiber roving, c) basalt fiber roving

Table 3.1 Mechanical and physical properties of fiber reinforcements

Fiber Material	Linear Density (tex)	Tensile Strength (MPa)	Tensile Modulus (GPa)	Elongation at break (%)	Filament Diameter (μm)	Specific density (g/cm^3)
Basalt Fiber	2.4K	3200	90	3.1	13	2.78
Glass Fiber	2.4K	1970	79	3.5	17	2.56
Carbon Fiber	12K	3950	238	1.5	7	1.77

For the matrix structure, a lot of resin types are present in applications, but literature examination [23] showed that there are no significant differences between the usages of resin types on the mechanical behaviors of composite materials. The epoxy and hardener types, shown in Figure 3.2, allowing 6-7 hours curing time are chosen to avoid the curing issue of epoxy-hardener mixing during the fabrication process. The epoxy (EPIKOTE MGS LR160 resin) and hardener (EPIKURE Curing Agent MGS LH260S), which are supplied from Dost Kimya A.Ş., Turkey, are blended with a stoichiometric weight ratio of 100/35 to form the matrix system.

Figure 3.2 The epoxy (EPIKOTE MGS LR160 resin) and hardener (EPIKURE Curing Agent MGS LH260S)

3.2 Filament Winding

3.2.1 About Technique

Filament winding method was firstly proposed to fabricate rocket motor body in early 1940s [4]. In 1950s, a simple filament winding machine was designed to perform basic motions with only spindle rotation and horizontal carriage (two axes motion). The fibers used as reinforcement were wrapped on the rotary shaft helping of horizontal carriage motion in this machine. The method made rapid development for the fabrication of pressure vessels, rocket motor body, rocket engine nozzle and launching tubes on military field during the years of Second World War and Cold War. In 1964, Rosato D. V. and Grove C. S. [77] published a book about design, application and development of filament winding. By mid-1970s, the advancement of servo technology entered the realm of the machine design. The machines were controlled by computers with increase in the use of computer technology. Nowadays, highly developed filament winding machines are seen with additional axes of motions allowing for four, five and even six axes of controlled motion [78, 79]. Production of some advance materials such as conical shafts, T-shaped, L-shaped and asymmetric portion have been fabricated with this development. Today, there are many industrial products [80, 81] fabricated by filament winding method such as high pressure vessels, sewage pipe systems, high pressure pipe systems, water tanks, large underground tanks (for petrol, salt, acid, water etc.), oxygen and fire extinguishers for firefighters, helicopter rotary shafts, fishing rods, golf clubs, wind turbine blades, transmission shafts, bus chassis, aircraft fuselage sections, ship hull sections, rotor bodies for space shuttles.

The method consists of fiber reinforcement and resin matrix that are the main components composing the composite material, and it performs the products at different design parameters such as the desired fiber orientation angle, fiber type, mandrel diameter, mandrel type, resin type and density. The required design according to the field of application is easily conducted on with the specified parameters. Also, the method presents the advantages such as obtaining same fiber orientations on layers and regions, connectionless fiber can be used as a single piece, the absence of high cost as in an autoclave, allowing production of large amounts of product, high fiber volume. The schematic representation of the basic working principle is given in Figure 3.3.

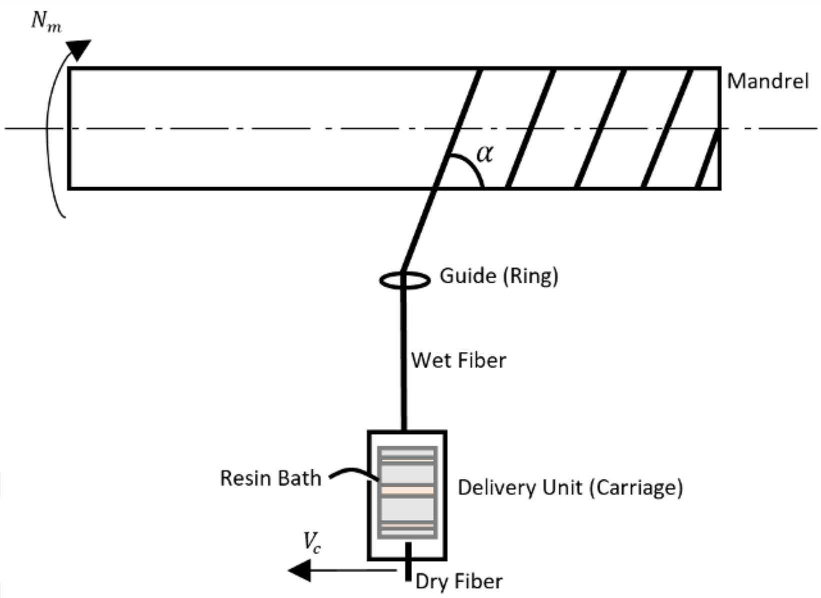

Figure 3.3 Filament winding technique

The winding angle, α which sets the layout and orientation of the fibers, is one of the most important parameter in a filament winding machine [82] since it has direct influence on response of product under mechanical loadings. It is calculated by following equation:

$$tan\alpha = \frac{2\pi R N_m}{60 V_c} \tag{3.1}$$

where R is the mandrel radius, N_m and V_c represent the mandrel rotational speed and carriage linear speed, respectively.

3.2.2 Winding Patterns

There are mainly three types of winding patterns that can be applied on filament winding method [5]. These are called as hoop, helical and polar windings that have been classified according to winding angle, α which makes with longitudinal axis as shown in Figure 3.4. If the process having the winding angle near the 90°, then it is called as hoop or circumferential winding process. Helical winding has the constant mandrel rotation when carriage unit is moving with a linear motion in forward and backward. Polar winding is generally used for fabrication of high pressure vessels since the fiber is wrapped from one end directly to another on the mandrel. The angles having close to 0° are required in this pattern. In this study, helical winding is considered for ±(40°), ±(55°) and ±(70°) fiber orientations.

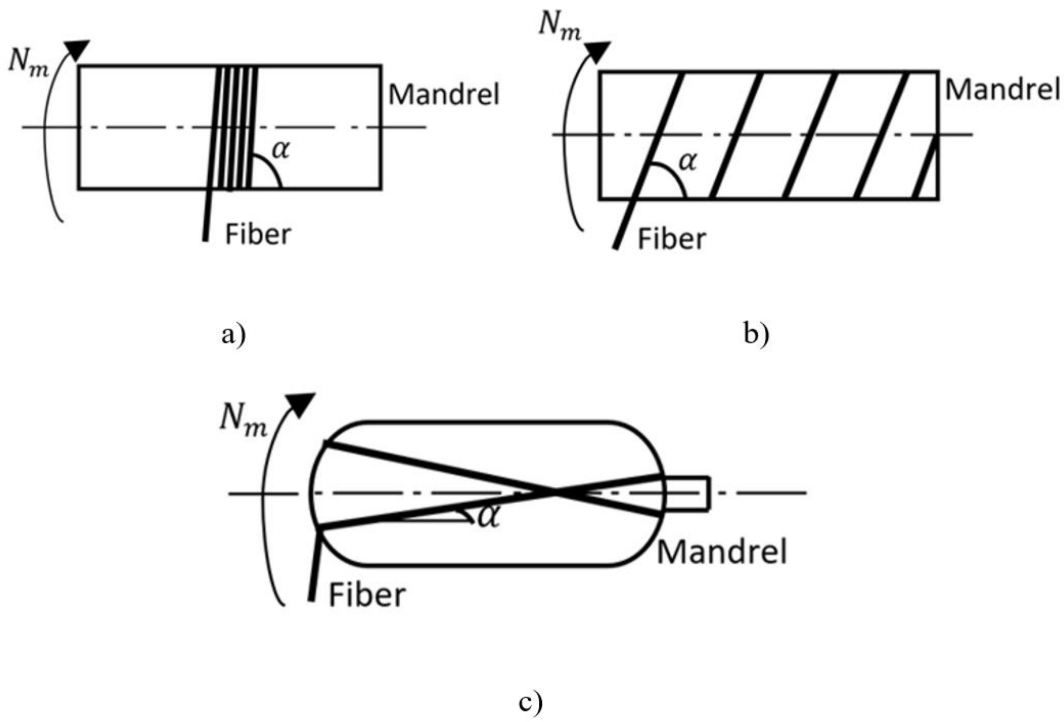

Figure 3.4 Winding patterns; a) hoop winding, b) helical winding, c) polar winding

3.2.3 Hybridization Techniques

Fiber hybridization is a promising strategy to toughen composite materials [83]. Interply and intraply techniques as two different way to hybridize of different fiber reinforcements are mainly used in literature [63]. In interply fiber hybridization, as shown in Figure 3.5a, after one layer is fully covered with 1st fiber, next layer are wrapped with another fiber reinforcement on the first one. So, different layers must have different fiber reinforcements. However, intraply fiber hybridization, as seen in Figure 3.5b, offers co-winding of at least two fiber reinforcement by considering same material for each layer of the composite pipe. There are several advantages and drawbacks to each other. For example; the interply technique requires the filament system to be re-prepared for the continuation of the process of each layer while the the process with intraply technique is completed without any intervention. However, similar filament diameter needs to be used to satisfy uniform thickness for the product in intraply technique. It is not a mandatory requirement in interply technique since different layer independency.

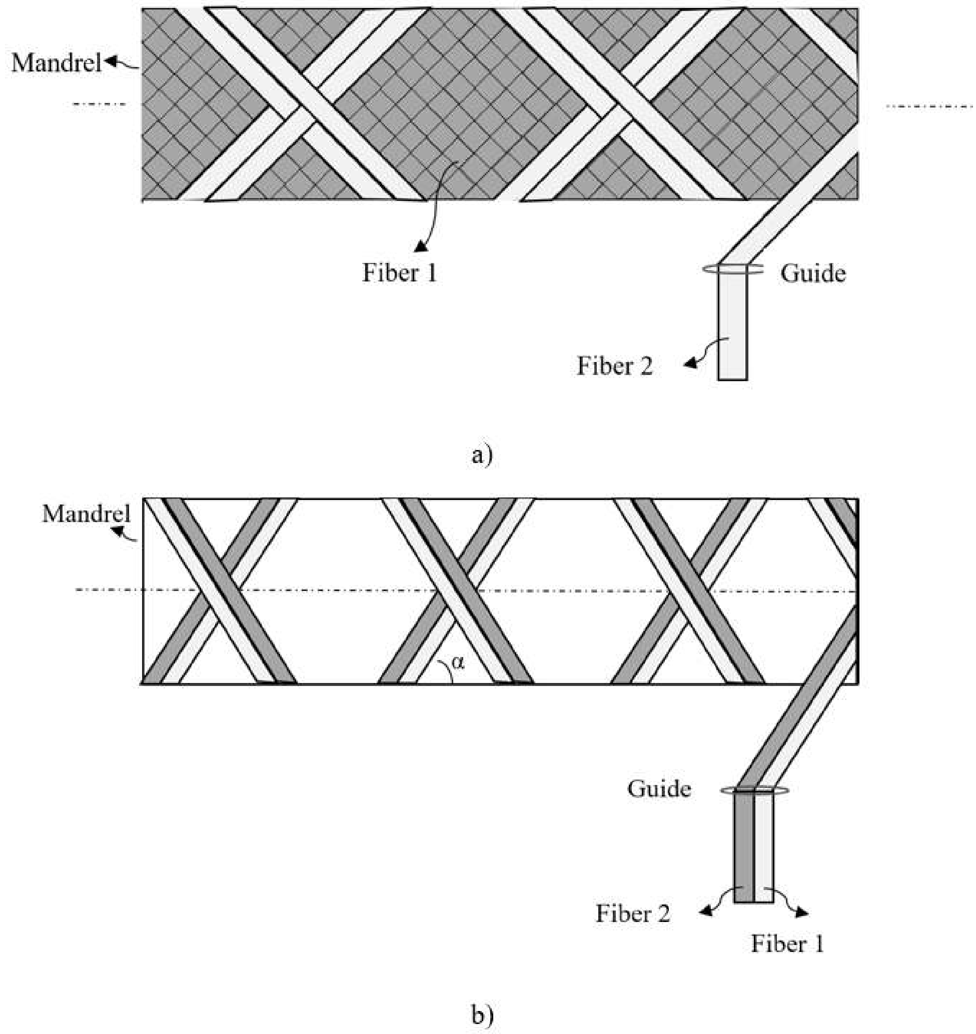

Figure 3.5 Fiber hybridization techniques; a) interply fiber hybridization, b) intraply fiber hybridization

3.3 Filament Winding Machine

A filament winding machine has been designed and installed in order to produce the required samples for the thesis. The design of machine are based on the three main parts which are mechanical section, electronic section and software section. The 2-axis movements of the fully-automated machine are linear for fiber delivery and rotational for fiber wrapping. The machine body is made of fully 6061 Aluminum material. It has 1280 x 1300 x 700 mm dimensions in height, wide, depth and its production capacity is 750 mm in length and 250 mm in diameter. Also linear axis of the machine and rotational axis can reach 8000 mm/min and 250 rpm, respectively. Details of the developed machine can be seen following sections.

The mechanical part of the machine consists of the five basic parts which are main structure, carriage (fiber delivery) unit, resin bath, control box and rotary unit, as seen in Figure 3.6.

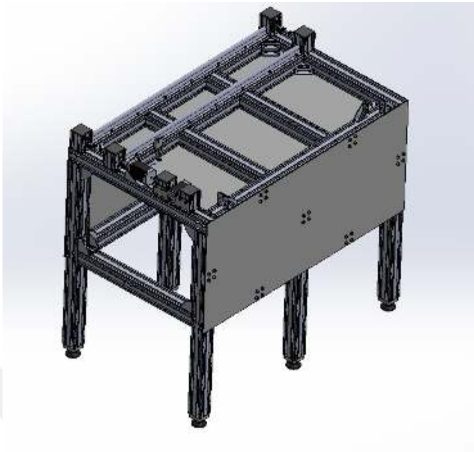

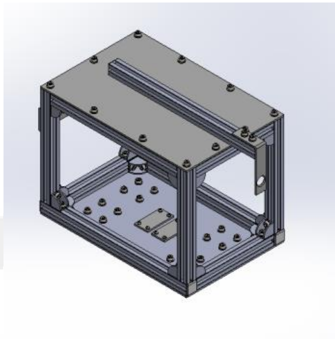

a) b)

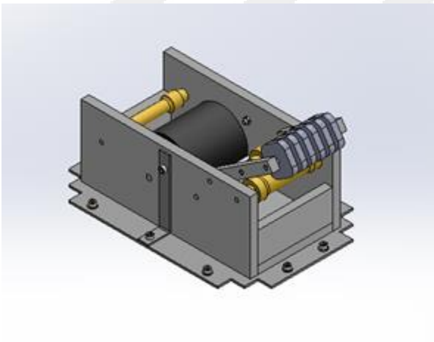

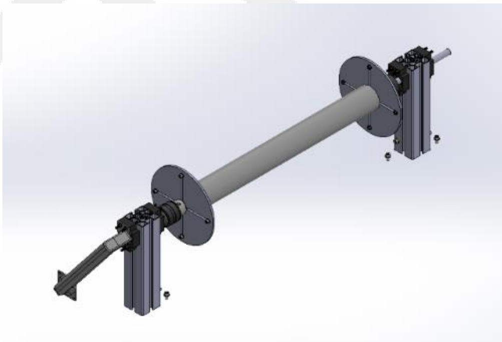

c) d)

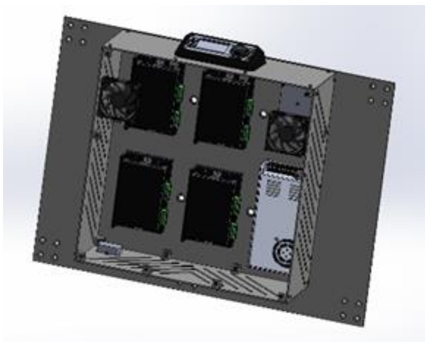

e)

Figure 3.6 Sections of filament winding machine; a) main chassis, b) carriage section, c) resin tank section, d) mandrel section, e) control box

The main structure provides the stability and continuity entire the process. It supports the all system by balancing at certain levels and prevents the possible vibrations to ensure system working without problem. The carriage unit helps to determine filament path with linear motion on the machine. Its motion is provided by stepper motor by using belt and pulley system. Fiber is directed to rotary unit by using a guide arranged on the carriage unit. This is the last fiber transition before winding. Also, carriage unit includes the resin bath and so can be protective for bath. Resin bath has a crucial importance for production of composites. It controls the tension guides by brass and delrin rollers which are placed inside the tank and wetting the fiber reinforcements entire the process. Tensional forces and excess resin back into the bath are given by these rollers. Also, the bath has three inlet and outlet ceramic rings which means the three fibers by following different paths can be used within the same winding process. Control box consists of required electronic components such as stepper motor drivers, limit switches, power supply, main board, cooling fans, control screen and stepper motors. All electronic components are positioned in this box. Rotational movements for the mandrel are conducted on the rotary unit of the machine. The unit has mandrel chucks to hold the mandrel and belt-pulley system to rotate the mandrel. The fiber is wrapped at a desired winding angle which is managed by relationship between carriage linear motion and mandrel rotation. Figure 3.6 presents important components of the machine. Figure 3.7 and Figure 3.8 present the designed version of the machine as CAD generated image and installed of the machine, respectively.

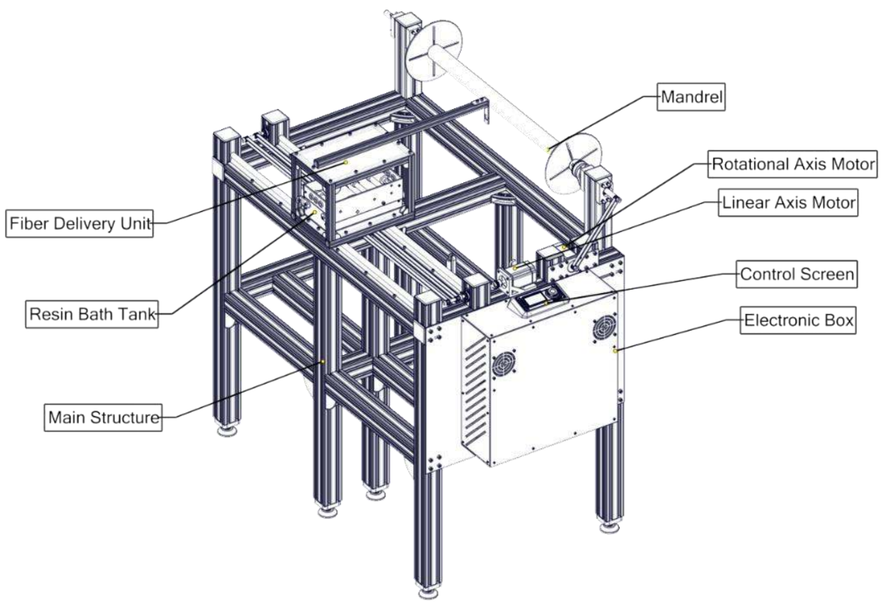

Figure 3.7 CAD generated image of filament winding machine

Figure 3.8 Final photograph of the filament winding machine

Electronic system of the machine provides high accuracy motion by using generated G-codes. It is designed as two axis. One axis is for linear motion in order to pose fiber delivery unit. Second axis is rotational axis in order to wrap fiber on round mandrel. To actuate axes two Nema 23 size stepper motors are used with stepper drivers. Winding machine controlled by low cost but highly stable main control board. Machine movements accomplished by generated G-Code and user can control machine by using embedded screen. 4 different limit switches are used in order to prevent axes damage and collisions. Two speed controlled fans are used to cool electronic components. 12V and 29.5A power supply is powering the whole system. Electronic components and their relations can be seen in Figure 3.9.

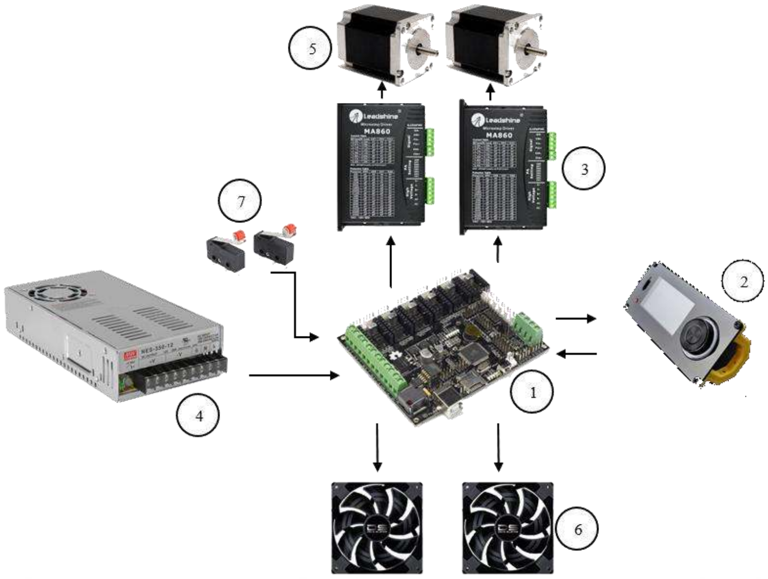

Figure 3.9 Electronic systems of filament winding machine

Electronic component list of the filament winding machine

1) Megatronics 3.1 Main Board
2) Viki LCD 2.0
3) 2 X Leadshine MA860 Stepper Motor Driver
4) MeanWell NES350-12 Power Supply
5) 2 X Leadshine Nema 23 3A Bipolar 1.8^{o} Stepper Motor
6) 2 X 12V Cooling Fan
7) 4 X Limit Switch

In order to control filament winding machine main control software is developed. Machine can be controlled by using embedded screen and also computer via USB. The system understands the motion code by using NIST RS274NGC G-code standard. The user can easily generate motion code by using winding angle, filament bandwidth, winding length, mandrel diameter and finally linear axis feed rate. After that this motion code can be easily send the machine, the software of the machine controls the axis to provide accurate winding operations.

3.4 Fabrication of FW Composite Pipes

The fabrication process of fiber reinforced composite pipes can be categorized into three distinct steps as preliminary preparations, process conducting and post processing. Firstly, release wax is applied on the mandrel and release agent film is wrapped. Afterwards, release wax is again implemented to pull out the mandrel from the pipe at the end of the winding process. The glass wool is exerted to obtain smooth surface inside the samples. Fiber(s) reinforcements are placed with helping of resin bath and rollers. By using epoxy and hardener, resin mixture is prepared with a stoichiometric ratio of 100:35. Prepared resin is deposited into the resin bath tank. After preliminary preparations is completed, the process at desired parameters is begun by loading the motion codes to machine, as seen in Figure 3.10.

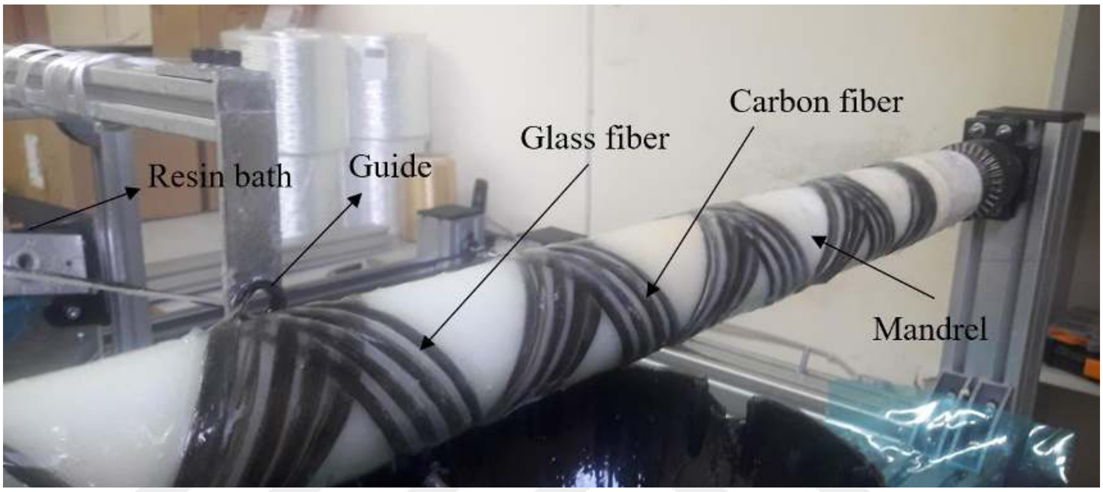

Figure 3.10 Filament winding (carbon/glass intraply fiber hybridization)

After process is completed, a heat shrinkage tape is wrapped on the mandrel and curing procedure is performed by heating the samples when it is rotating. Sanding and polishing as post processing can be conducted to obtain aesthetic appearance on the sample. The naming and thickness of the fabricated FW composite pipes are given in Table 3.2.

Table 3.2 The naming and thickness of FW composite pipes

FW Composite Pipe	Naming	Thickness (mm)
Basalt/Epoxy FRP	BFRP	4.00 ± 0.20
Glass/Epoxy FRP	GFRP	2.95 ± 0.08
Carbon/Epoxy FRP	CFRP	2.58 ± 0.08
Basalt-Glass/Epoxy FRP	BGFRP	4.00 ± 0.15
Glass-Carbon/Epoxy FRP	GCFRP	3.25 ± 0.07
Carbon-Basalt/Epoxy FRP	CBFRP	4.60 ± 0.20

3.5 Mechanical Characterization

3.5.1 Ignition Loss Test

Determination of the fiber fractions is very important since its crucial effect on the overall mechanical properties of the filament winding structure. Higher fiber fraction is resulted with the better product since the fiber reinforcement is the stronger component of a composite material.

Ignition loss experiments according to ASTM 2584 standard [84] are performed to determine fiber mass fraction for each configuration. The test procedure is based on the disappearance of the cured reinforced resin component as a result of combustion and the fact that the samples, as seen in Figure 3.11a, have a minimum surface area of 625 mm^2 regardless of shape. The samples are exposed to 650°C temperature for 1.5 hours in a high capacity furnace as shown in Figure 3.11b.

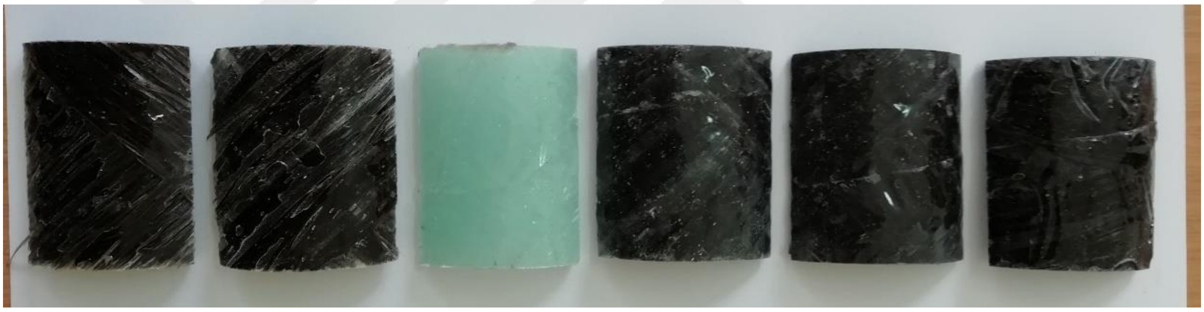

a)

b)

Figure 3.11 a) Samples, b) ignition loss test

The weight of the pipe samples before test, W_1 and after test, W_2 are precisely measured and fiber mass fraction, wt% for each pipe at different fiber orientation angles are evaluated using Equation (3.2). Four number of samples are used for each configuration.

$$\%wt = 100(W_2/W_1) \tag{3.2}$$

3.5.2 Split-Disk Method

Specification and assessment of the hoop tensile strength and modulus behaviors of the composite pipes are played a crucial role in applications, especially developing hoop stress structures caused by internal pressurized pipes, because of its direct influence on failure. Split-disk using ring shaped samples is a popular and practical method to carry out hoop tensile evaluation of the pipes [23, 85]. Apparent hoop tensile strength rather than true one are obtained from it due to bending moment imposition to samples during the loading stage of experiments.

Split-disk experiments are performed in accordance with ASTM D 2290 standard [86] which presents the procedure to determinate of hoop tensile characteristics of the FW tubular structures. The ring-shaped samples, shown in Figure 3.12a and Figure 3.12c, have reduction areas for both sides and there are semi-cylindrical metal based structures inside them to minimize bending imposition. The experiments are conducted on Shimadzu AG-X Series universal testing machine as shown in Figure 3.12b.

An apparent hoop tensile strength, $\sigma_a$is calculated from maximum load, P divided by area of the reduced-minimum section, A as given in Equation (3.3);

$$\sigma_a = P/2A \tag{3.3}$$

Hoop tensile modulus of elasticity, E_m is obtained from following equation [87];

$$E_m = \frac{0.1257 r_{mean}^3}{wt^3} \frac{P}{\Delta y} \tag{3.4}$$

where r_{mean}, w and t are the mean radius, width and thickness of the sample. Δy is defined as displacement at maximum load point. At least five number of samples for each configuration are exposed to tensile loading at 5 mm/min rate.

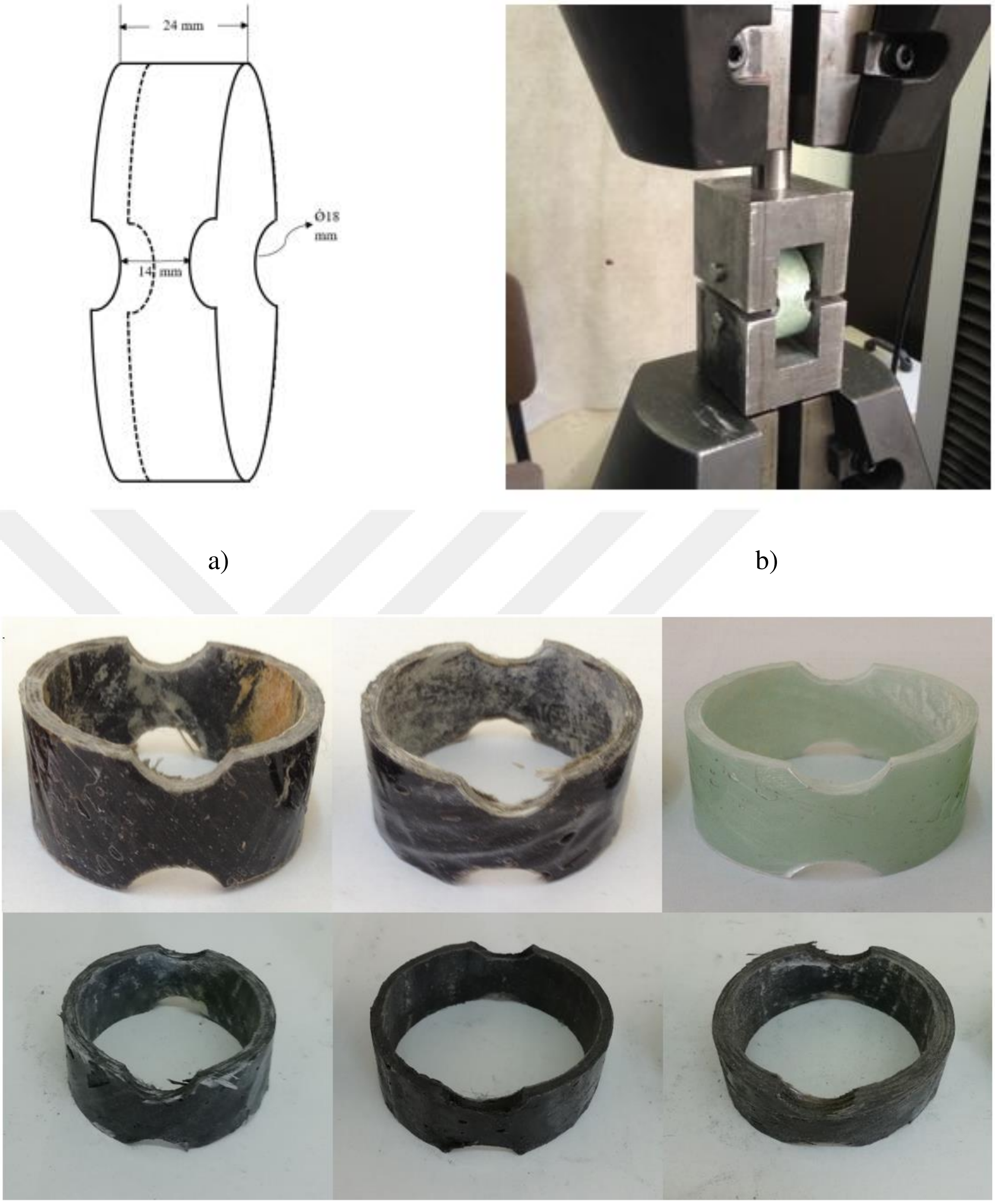

Figure 3.12 a) The geometry of ring-shaped sample, b) split-disk test, c) ring-shaped samples

3.5.3 Quasi-Static Axial and Radial Compression

The determination of the compressive strength or the response of the sample under axial compression loading is one of the key parameters for structure designs. On an atomic level, the molecules or atoms are forced apart when in tension whereas in compression they are forced together [88]. The samples for the compression test in the axial direction are prepared by sawing process in accordance with ASTM D695 standard [89] so that the length must be equal the inner diameter of the specimens. All specimens are assumed to have a length of 46.3±0.02 mm and are loaded in the axial direction at a speed of 1.3 mm/min as shown in Figure 3.13.

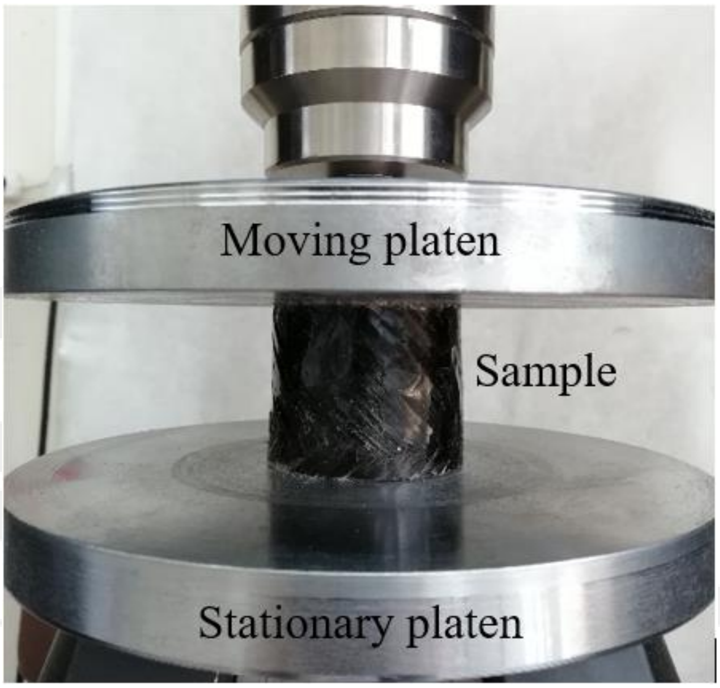

Figure 3.13 Quasi-static axial compression test

The compressive strength values of the specimens, σ_c are calculated by the following formula (Eq. (3.5)) given in the relevant standard:

$$\sigma_c = P/A \tag{3.5}$$

where, P represents the maximum load and A is the original cross-sectional area.

The example images which belong to BFRP, BGFRP, GFRP, GCFRP, CFRP and CBFRP samples are given in Figure 3.14, respectively. The contact surface of the samples are precisely flattened to provide uniform distribution of the load.

Figure 3.14 Samples for quasi-static axial compression test

Pipe stiffness, which is the ability to resist deformation under loading, is an important design parameters especially in soil-pipe interaction zones. This behavior is found from parallel-plate loading application which is the radial compression loading to samples. The samples are prepared by sawing process in accordance with ASTM D 2412 standard [90], so that the length should be at least 3 times of the diameter value. All specimens are loaded in the radial direction at a speed of 12.5 mm/min, as shown in Figure 3.15.

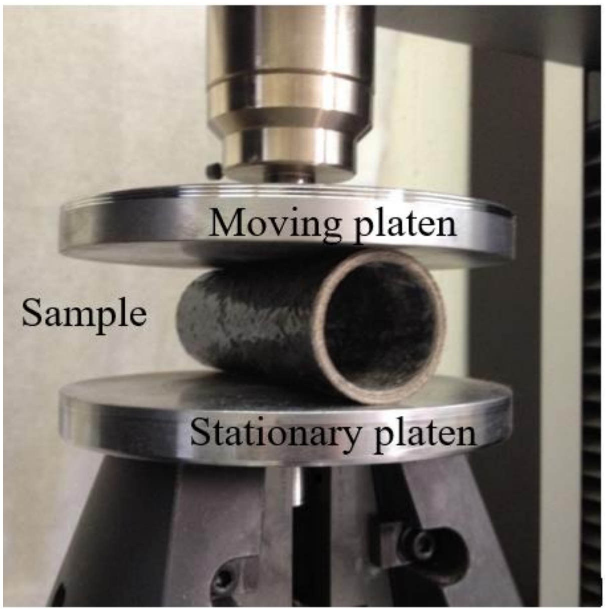

Figure 3.15 Quasi-static radial compression test

The pipe stiffness values, PS of the samples are calculated by the following formula (Equation (3.6)) given in the relevant standard:

$$PS = F/\Delta y \quad (3.6)$$

where, F and Δy are the load per unit length, N/mm, and displacement, mm, values at the first crazing or cracking point. Also, stiffness factor, SF can be calculated from the multiplication of pipe stiffness and mean radius of the pipes;

$$SF = 0.149r^3 (PS) \quad (3.7)$$

Percentage pipe deflection, PPD, which is the ratio of the reduction in pipe inside diameter, Δy to the initial inside diameter, d, is found from following equation;

$$PPD = 100(\Delta y/d) \quad (3.8)$$

All samples considered in this experiments have the $170 \pm 0.5\ mm$ in length. The example images which belong to BFRP, BGFRP, GFRP, GCFRP, CFRP and CBFRP samples are given in Figure 3.16, respectively.

Figure 3.16 Samples for quasi-static radial compression test

3.5.4 Axial and Lateral Crushing

The axial and lateral crushing experiments are performed between two flat steel platens as a continuation of quasi-static compression tests, which on a 300 kN capacity Shimadzu AG-X Series universal testing machine, to obtain crashworthiness parameters of composite pipes. All samples are compressed into 32.5 mm (about 70.2% stroke efficiency) for axial crushing and 35 mm under lateral loading. The load in crushing process versus displacement of moving platen are recorded by automatic data acquisition system. At least five replicated tests are achieved to ensure experimental reliability for both crushing. By the way, photographs are taken by a camera to monitor the crushing process history.

Crushing process, as shown in Figure 3.17, can be generally divided into three stages as pre-crushing, post-crushing and material densification [49]. In elastic region or pre-crushing, the material behaves elastically that can be returned to original length if loading is removed, and initial peak load is noted. Small inter- or intralaminar cracks as microfracture, which determinative of failure mode, are nucleated with local stress concentration on the initial peak load point. After that, post-crushing goes on with propagation of crushing in progressive or catastrophic manner. This stage is the crucial to measure crashworthiness parameters except initial peak load and to understand failure mechanisms. Lastly, when material densification is started which means load increases sharply, crushing process is done.

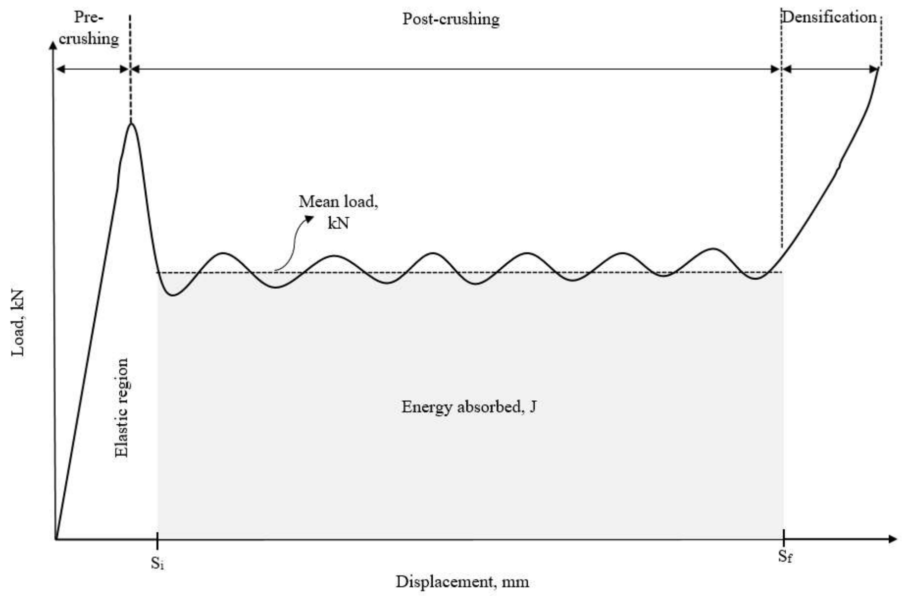

Figure 3.17 Typical load-displacement curve of crushing process

The progressive and catastrophic type failures shown in Figure 3.18 are seen for fiber reinforced composite materials in axial crushing process. A stable progressive crush is established by localized failure that initiates at one end of the specimen and progress through the sample. During catastrophic failure the initial maximum force is very high and drops rapidly, therefore the average force is low [91, 92].

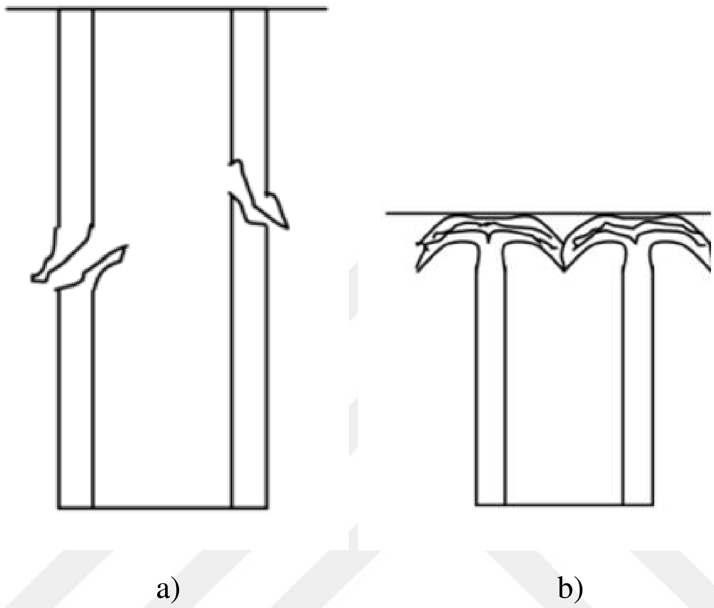

Figure 3.18 Typical collapse modes in axial crushing for composite tubes a) catastrophic failure, b) progressive failure [92]

According to Farley classification [51], four basic crushing modes as transverse shear, lamina bending, local buckling, brittle fracturing (combination of transverse shear and lamina bending) occur in brittle materials. The crushing modes caused by inter-/intralaminar crack growths and the failure of the samples are schematically demonstrated in Figure 3.19. Also, Figure 3.20 presents the summarization of the crushing process history in fiber reinforced composite pipes.

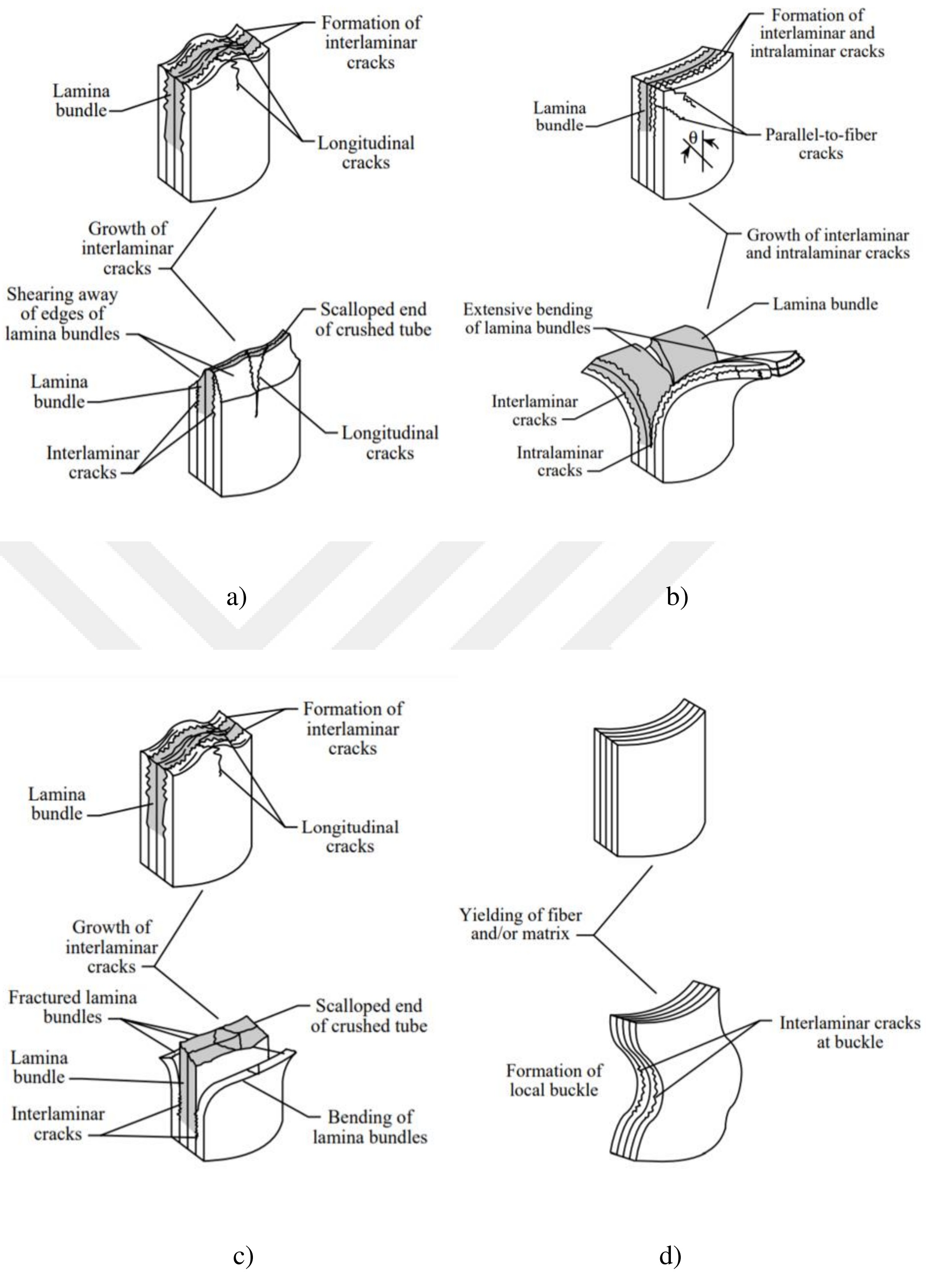

Figure 3.19 Crushing modes according to Farley's classifications a) transverse shear, b) lamina bending, c) brittle fracturing, d) local buckling [93]

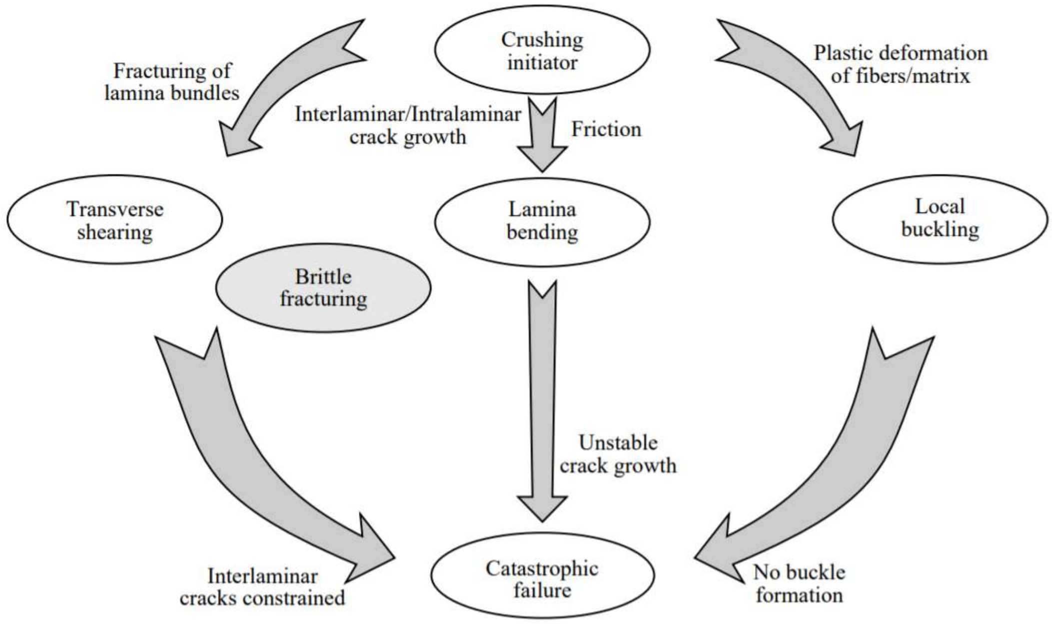

Figure 3.20 Axial crushing process for fiber reinforced composite pipes [93]

For the parallel-plate loading application in lateral direction, crushing can be categorized into two main modes as stable and unstable, which are seen in Figure 3.21, into the post-crushing zone. Cyclic regular fluctuations as up and down in load are obtained from stable crushing mode, while the unstable crushing mode presents the load drops in high deceleration after the first peak point on the load-displacement diagrams.

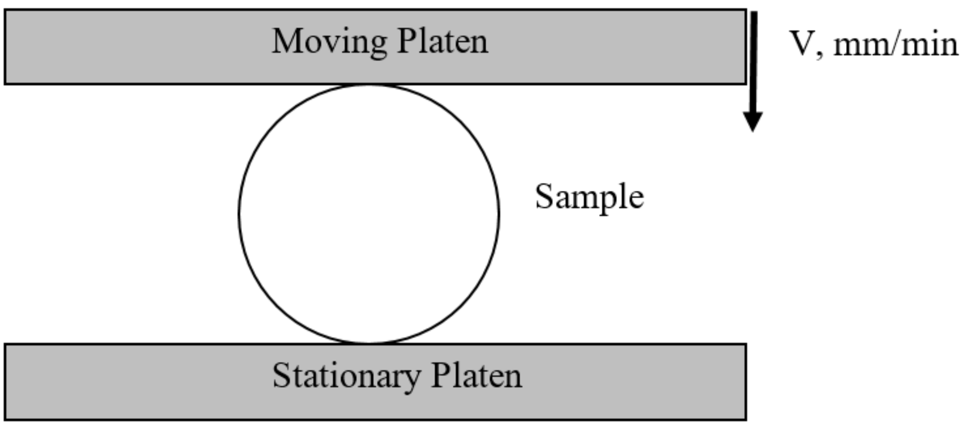

a)

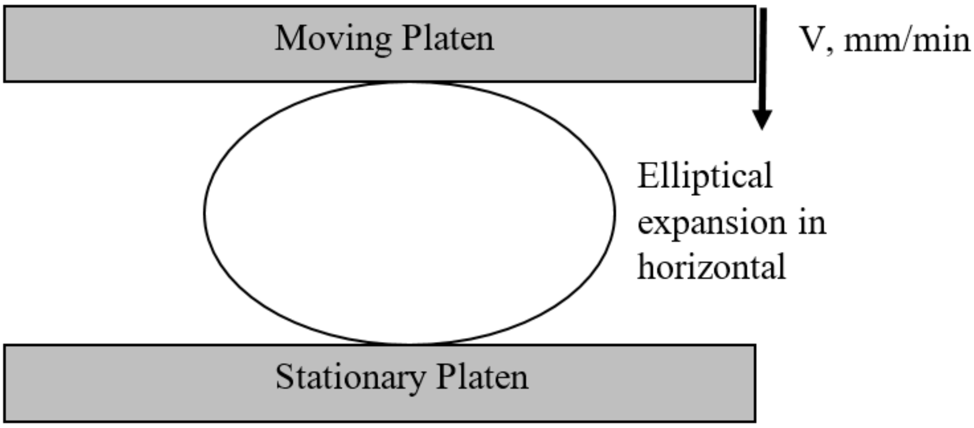

b)

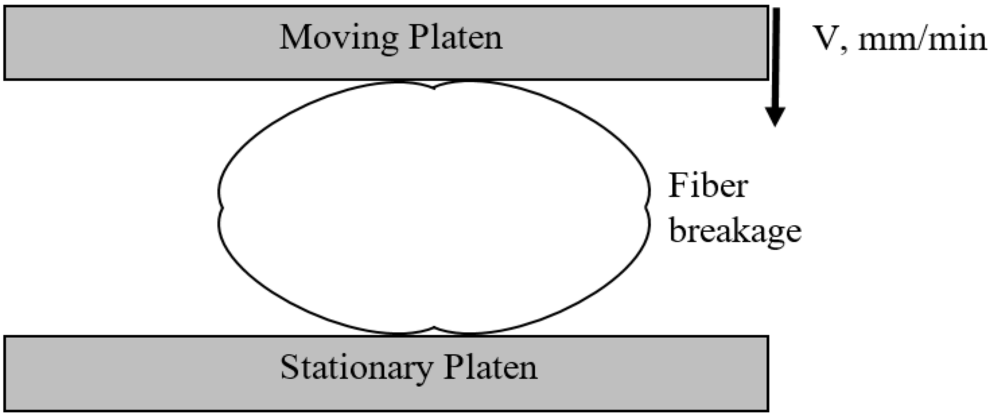

c)

Figure 3.21 Lateral crushing; a) application of the process, b) stable crushing, c) unstable crushing

The crashworthiness parameters of FRPs was calculated as follows:

Total energy absorption, E is the area under load-displacement curve between crush distances, which is shown in Figure 3.17, and calculated by integration of load, P as seen Eqn. (3.9);

$$E = \int_{S_i}^{S_f} P(s)\, ds \tag{3.9}$$

where S_i and S_f represents the initial and final stroke values in compression after the first initial peak load. Also, mean load is found from the integration of each load value depending on stroke or pipe length, P(s) in crushing propagation stage as in Eqn. (3.10);

$$P_m = \frac{\int_{S_i}^{S_f} P(s)ds}{S_f} \tag{3.10}$$

Crushing load efficiency, η_f, which is the percentage ratio of mean load and initial peak load, is the useful index to evaluate stability of the crushing process and performance of the absorber. It is obtained from Eqn. (3.11);

$$\eta_f = 100(P_m/P_i) \tag{3.11}$$

where the peak load (P_i), which is commonly maximum load, is the initial peak load in the load-displacement curve.

Specific energy absorption, E_s is the most important parameter to evaluate crushing characteristics of the material. It is the absorbed energy per unit mass of crushing sample and calculated with Eq. (3.12);

$$E_s = \frac{E}{m_{crush}} = \frac{\int_{S_i}^{S_f} P(s)ds}{m_{crush}} \tag{3.12}$$

CHAPTER IV

TENSILE AND COMPRESSION BEHAVIORS OF COMPOSITE PIPES

4.1 Introduction

In this section, the results of tensile and compression tests which are the most basic research to determine the fundamental mechanical properties of a composite pipe. The determination of the hoop strength, compression strength and pipe stiffness has been gaining great interest for engineering applications especially in the areas of the internal pressurized components, structural design and soil-pipe interaction zones, respectively. This chapter is devoted to investigate the effects of intraply fiber hybridization on filament wound composite pipes by means of tensile and compression tests. To this aim, the split-disk method for apparent hoop tensile and the quasi-static axial and radial compression by external parallel-plate have been applied to all pipe samples. Also, different fiber orientation angles have been considered to ensure more reliable interpretations regarding the influence of intraply fiber hybridization.

4.2 Fiber Mass Fraction

Ignition loss experiments in accordance with ASTM D 2584 based on the burning of fiber reinforced composite materials were conducted to determine the fiber mass fraction of FRPs. According to results, presented in Table 4.1, GFRP samples have the highest fiber mass fraction with 71.46%. The samples reinforced with carbon fiber (CFRP, GCFRP and CBFRP) gave the lower fiber and higher resin ratio than others. It can be attributed to lower specific density of carbon fiber and the higher resin volume in pipes, especially, in intraply hybrid samples due to differences in fiber diameters. Minimum fiber mass fraction was obtained from GCFRP with 53.75%. On the other hand, compared to fiber hybridization the variation of fiber orientation angle did not result with significant differences in fiber mass fraction of configurations. Some example photos which belong to samples after ignition loss experiments were given in Figure 4.1. The winding quality was looked like pretty acceptable owing to regular sequences of fiber settlement.

Table 4.1 Fiber mass fraction

Fiber Reinforcement	±(40°), wt.%	±(55°), wt.%	±(70°), wt.%	Average, wt.%
Basalt Fiber	59.95	63.40	66.01	63.12
Glass Fiber	71.27	71.37	71.75	71.46
Carbon Fiber	57.22	56.88	56.65	56.92
Basalt-Glass Fiber	63.49	63.08	69.60	65.39
Glass-Carbon Fiber	55.00	54.71	51.54	53.75
Carbon-Basalt Fiber	55.04	56.03	53.13	54.73

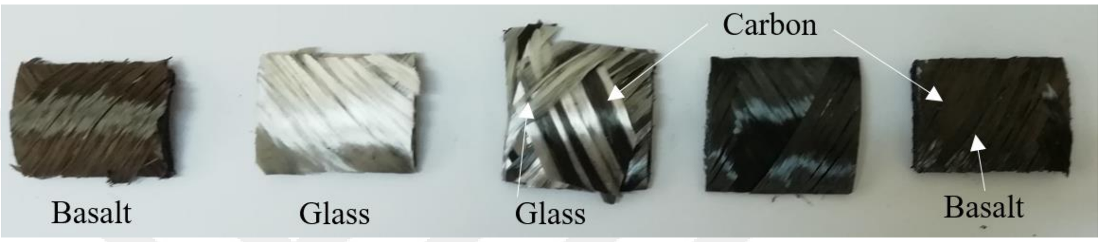

Figure 4.1 The samples after ignition loss tests

4.3 Apparent Hoop Tensile Strength

Split disk experiments were carried out to determine tensile characteristics in the hoop direction of the specimens. The apparent hoop tensile strengths of fiber reinforced composite pipes at different fiber orientation angles were given in Figure 4, respectively. The maximum apparent tensile strength was recorded in non-hybrid CFRP (580.95 MPa) at ±(70°), while the minimum one was obtained in hybrid CBFRP (47.71 MPa) at ±(40°). The negative effect as deteriorations was found in the range of 9.7% (GCFRP by GFRP with ±(70°) fiber orientation) and 66.5% (CBFRP by CFRP with $\pm(40°)_6$ fiber orientation) for all intraply hybridized of FRPs because of the poor ability to merger characteristics between the fibers reinforcements. This situation can be explained as complex tensile behavior of intraply arrangements which is progressive failure at various layers as mentioned in Pegoretti's study [94]. Also, Dehkordi et al. [95] found that tensile stress of intraply hybridization of basalt and nylon materials gave the lower values than pure ones which is explained by weak interfacial adhesion between the fibers reinforcements leading fiber pull out failure mode.

For the fiber orientation impression; all samples showed the remarkable improvements in apparent tensile strength with the increase in fiber orientation angle or, in other words, when the fiber layout direction was approached to direction of loading. The apparent hoop tensile strength values of BFRP, BGFRP, GFRP, GCFRP, CFRP and CBFRP having ±(70°) fiber orientation angle were the 5.29, 6.62, 3.31, 4.41, 4.08, 6.92 times of samples having ±(40°) fiber orientation angle, respectively.

Hoop tensile modulus for different fiber orientation angles, which was calculated by Equation 3.4 considering mean radius, load, width, thickness, elongation at break, of the sample, were given in Figure 4.3, respectively. All samples except ±(40°) fiber orientation gave the parallel trend with tensile characteristics. CFRP owing to higher specific strength possessed the maximum tensile modulus as 20.20, 52.21 and 84.84 for ±(40°), ±(55°) and ±(70°) fiber orientation angles, respectively.

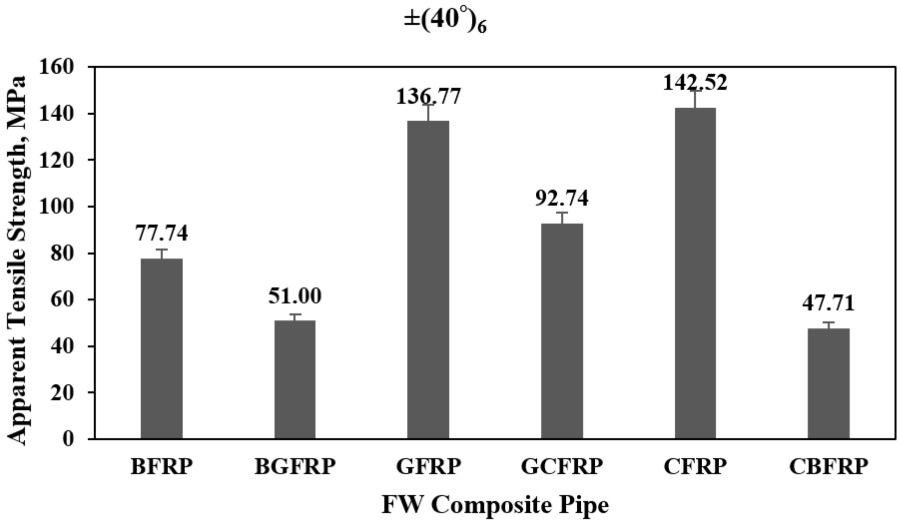

(a)

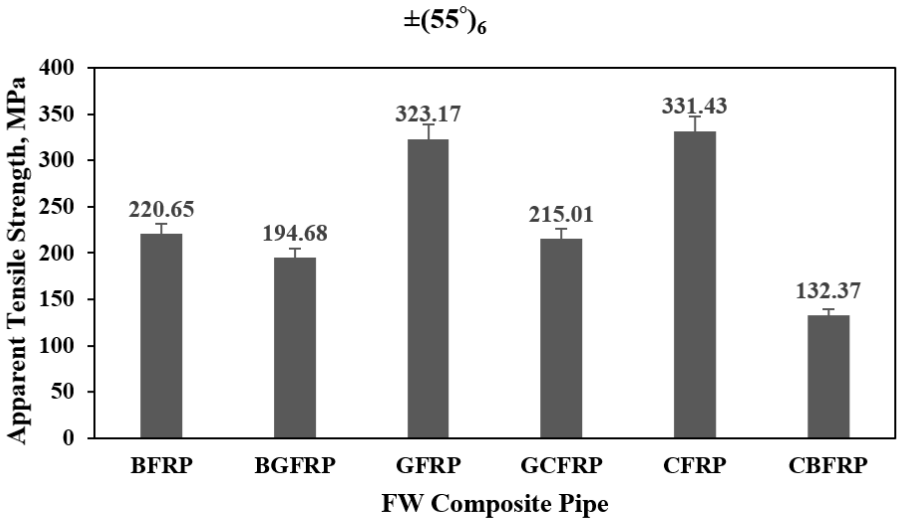

(b)

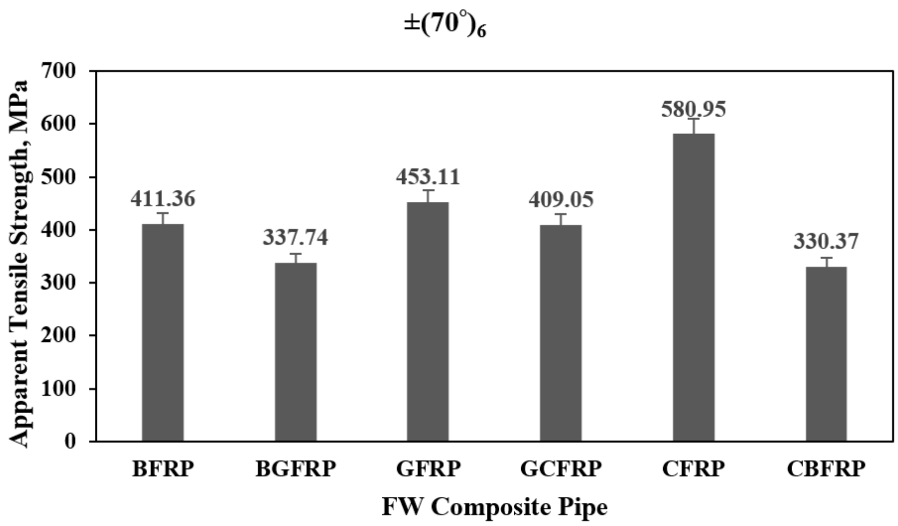

(c)

Figure 4.2 Apparent hoop tensile strength for (a) ±(40°) fiber orientation, (b) ±(55°) fiber orientation, c) ±(70°) fiber orientation

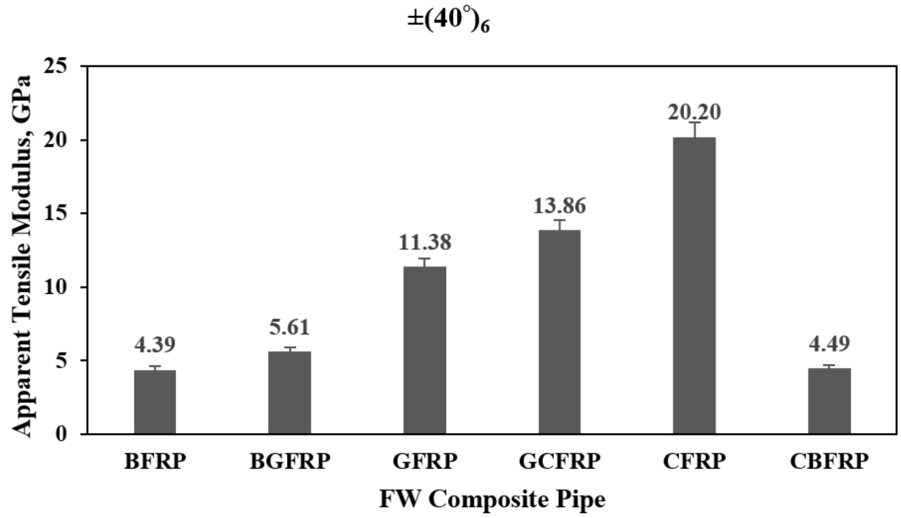

(a)

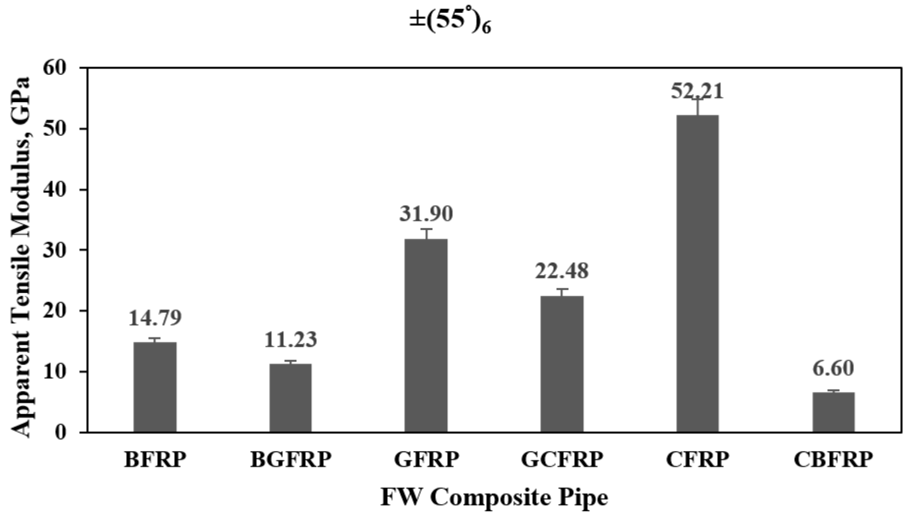

(b)

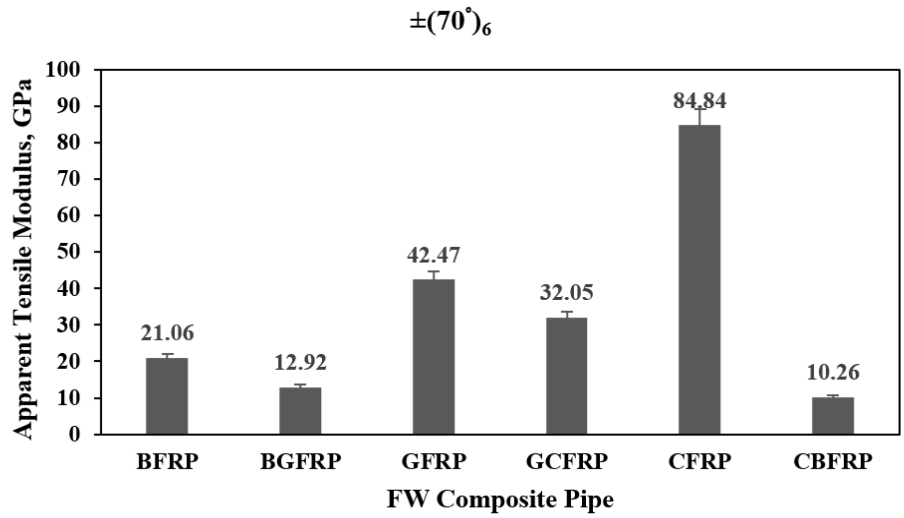

(c)

Figure 4.3 Apparent hoop tensile modulus for (a) ±(40°) fiber orientation, (b) ±(55°) fiber orientation, c) ±(70°) fiber orientation

The apparent hoop tensile strength against displacement curves were presented in Figure 4.4. With the increase in fiber orientation angle, intraply hybrid fiber reinforced pipes showed the higher displacement values at break points, while non-hybrid samples exhibited decreasing trend. Even though hybridization process had less apparent tensile strength as per non-hybrid samples, breaking elongations with increase in fiber orientation angle were enhancement unlike non-hybrid samples. Furthermore, little fluctuations at close points of maximum strength values were detected due to progressive fiber breakage.

$\pm(40^{\circ})_6$

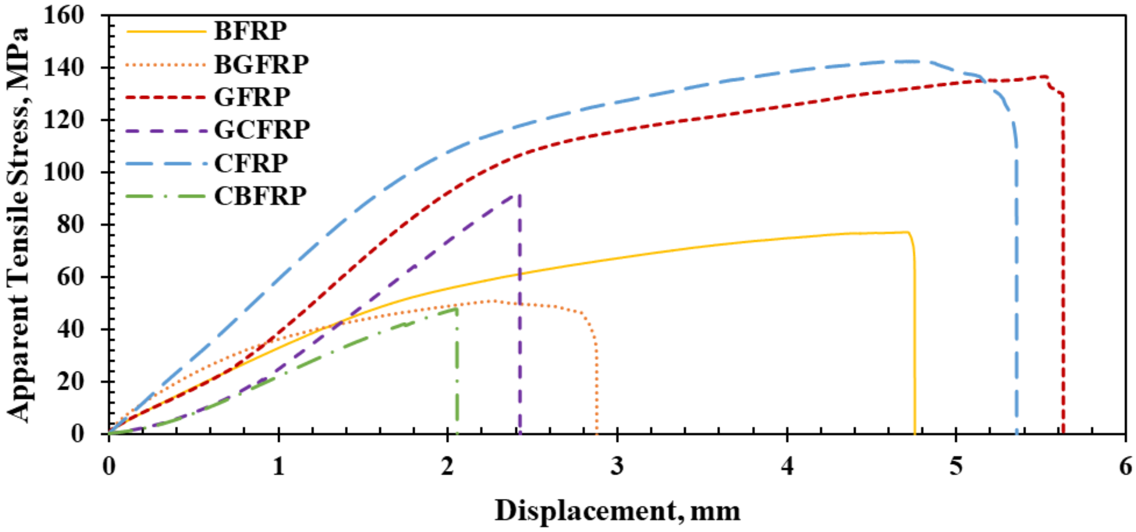

(a)

$\pm(55^{\circ})_6$

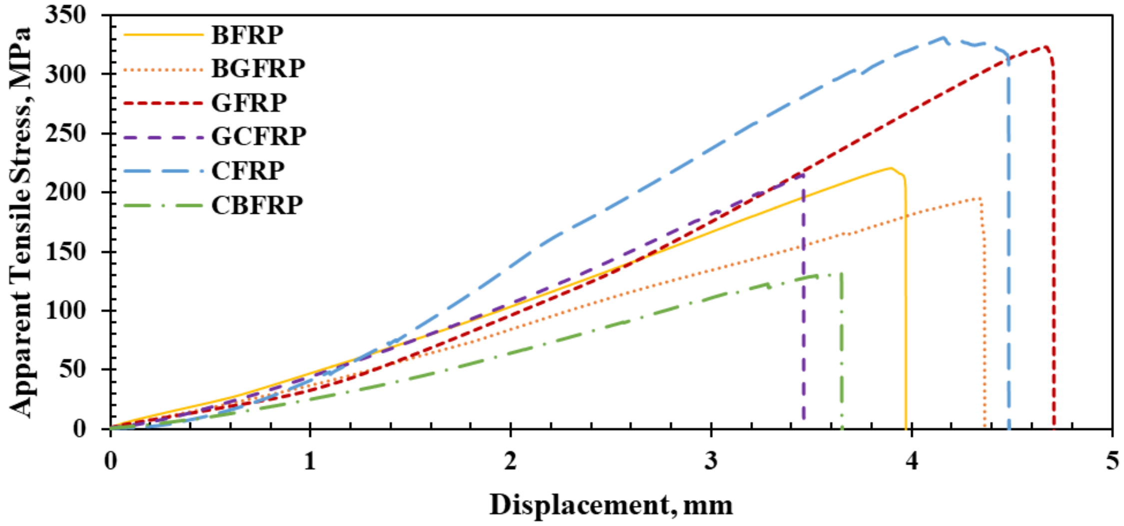

(b)

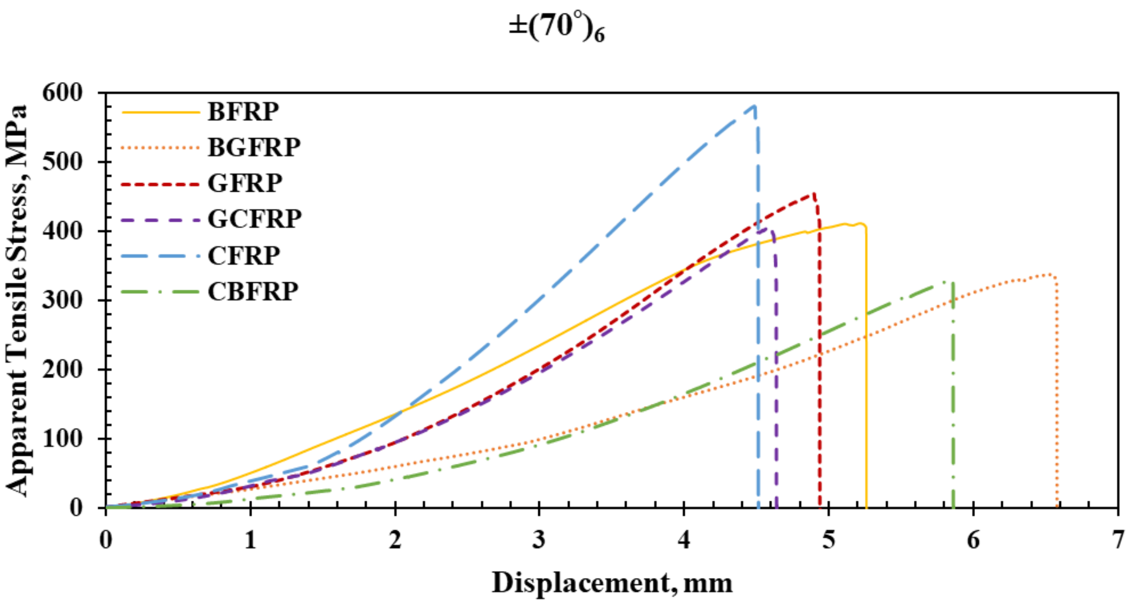

(c)

Figure 4.4 Stress-displacemet diagrams for (a) ±(40°) fiber orientation, (b) ±(55°) fiber orientation, c) ±(70°) fiber orientation

In Figure 4.5, the fracture characteristics of the FRPs can be clearly seen. Intraply hybrid FRPs showed the behavior of more fiber debonding and fiber pull out failure mode compared with non-hybrid FRP ones. This can be associated with the less tensile attribution of weaker fiber components of hybridized sample. Additionally, weak interfacial adhesion resulted with not only less tensile strength but also fiber debonding and fiber pull out in failure mode. In general, failure modes were followed as matrix fragmentation, fiber crazing, delamination, fiber breakage in winding direction for non-hybrid fiber reinforced materials and finally fiber pull out for intraply hybrid pipes, respectively.

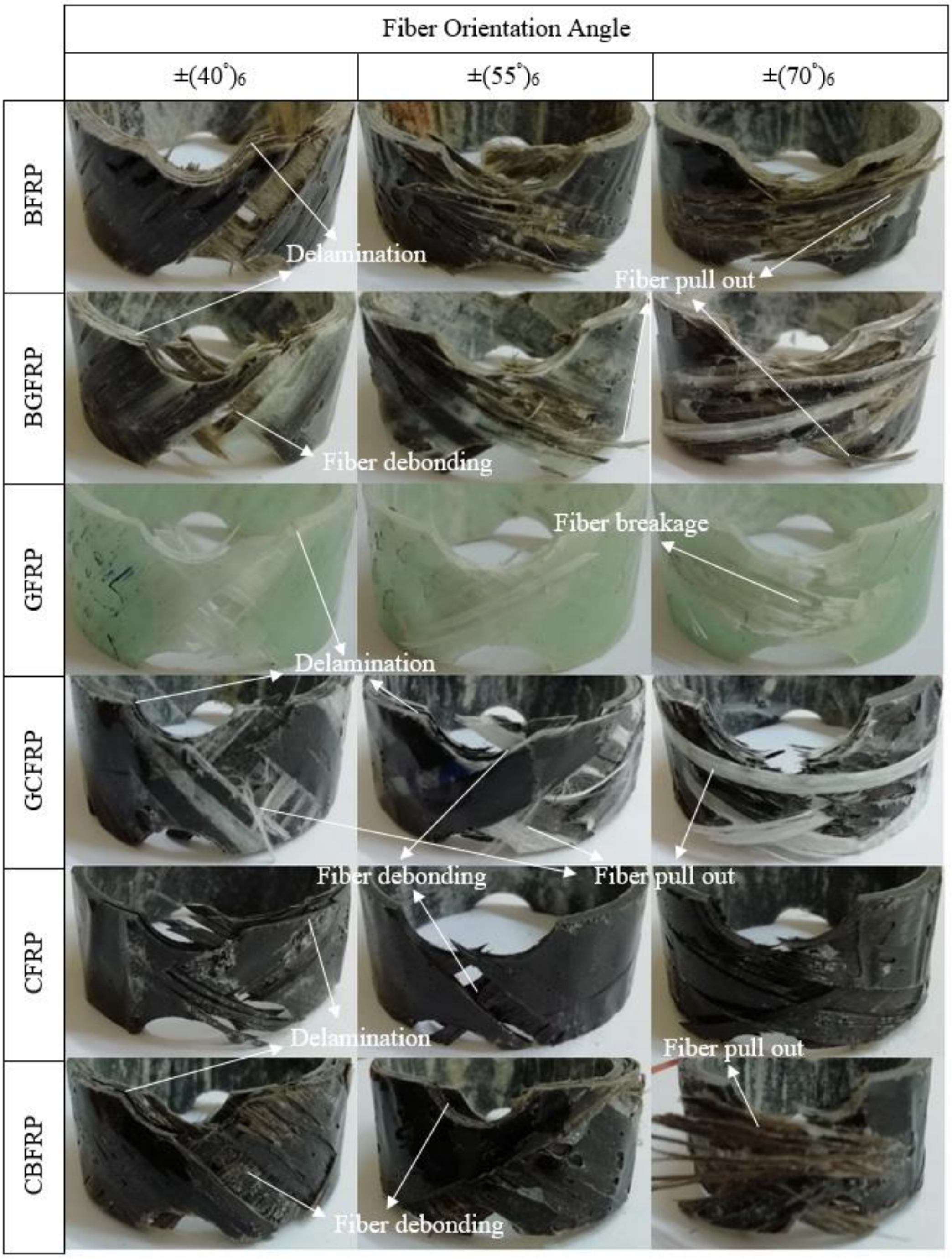

Figure 4.5 Failure shapes of the samples from split-disk experiment

4.4 Compression Strength

Quasi-static axial compression experiments were performed to determine compression strength of the FRPs. To examine the effect of intraply hybridization on compression strength of FRPs, results were given according to different fiber orientation angle as indicated in Figure 4.6. While maximum strength as 106.59 MPa was obtained from

CFRP with ±(70°), minimum strength was the 46.08 MPa from BFRP with ±(40°). Carbon fiber inclusion to GFRP and BFRP or glass fiber addition to BFRP improved the compression behaviors. From the BGFRP results, the increase in strength was 4.38%, 20.64%, and 11.78% compared to BFRP for ±(40°), ±(55°), and ±(70°) fiber orientations, respectively. Furthermore, compared to non-hybrid BFRP, 14.52%, 3.24%, and 6.47% improvements were acquired from CBFRP responses. For the GCFRP hybridized samples, carbon fiber inclusion led to 6.52%, 2.62%, and 18.70% increase in compression strength of GFRP samples of ±(40°), ±(55°), and ±(70°) fiber orientations, respectively. In all the samples, increase in fiber orientation angle resulted with decrease in compression strength of FRPs since the fiber direction was approached to loading direction as indicated Soden's study [14]. The intraply hybridization proved to have the considerable influences on the axial compression strength of the materials.

The compressive stress-strain diagrams with samples having different fiber orientation angles were presented in Figure 4.7. In general, intraply FRPs showed the strain values at maximum compressive stress point between the non-hybrid FRPs of constituent fibers. Furthermore, the slope of diagrams gave an idea about modulus of intraply FRPs looked like parallel tendency with stress characteristics.

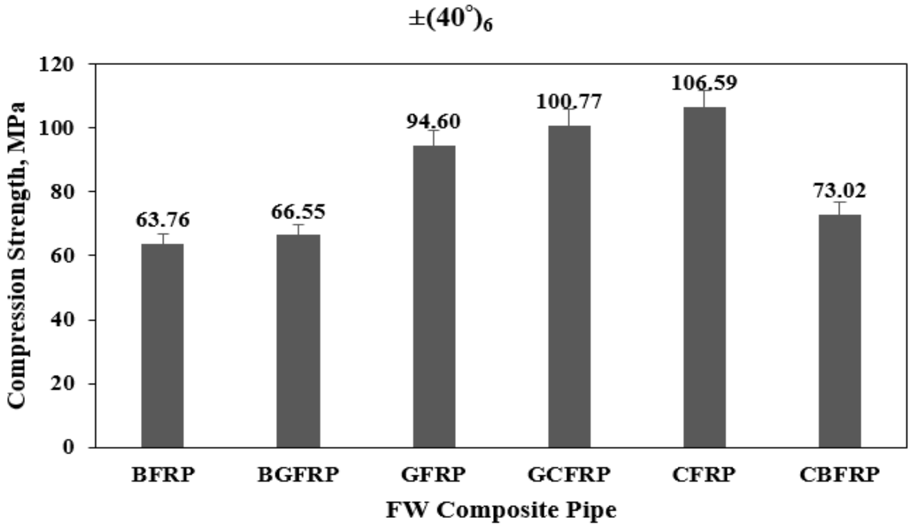

(a)

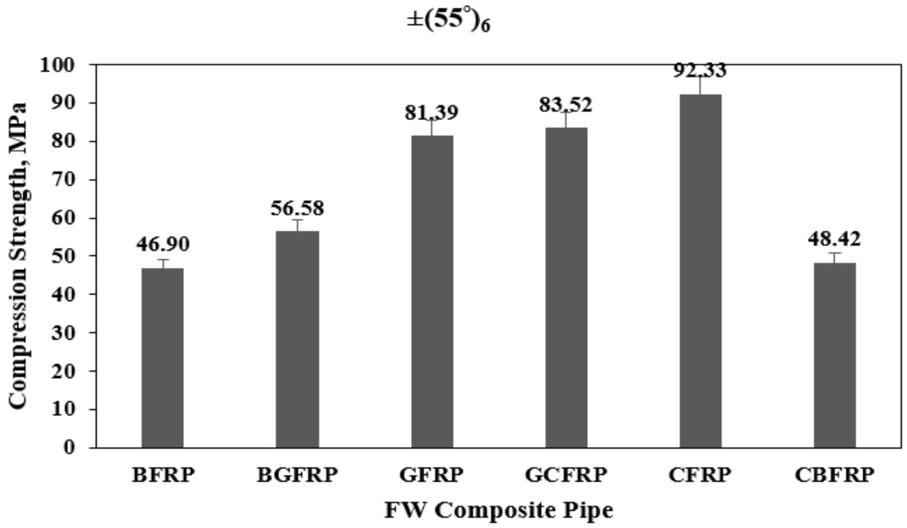

(b)

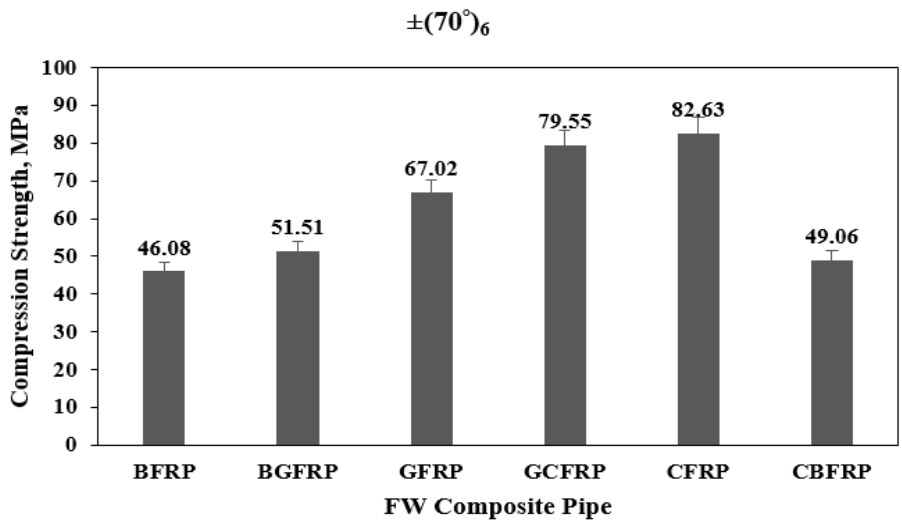

(c)

Figure 4.6 Axial compression strength for (a) ±(40°) fiber orientation, (b) ±(55°) fiber orientation, c) ±(70°) fiber orientation

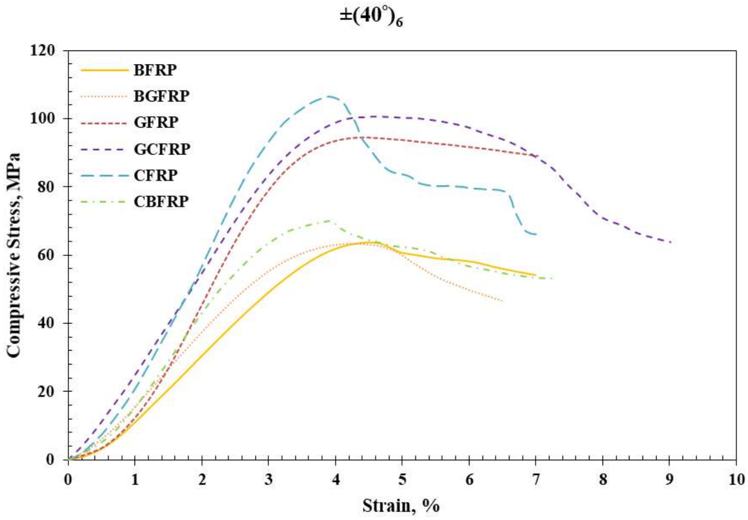

(a)

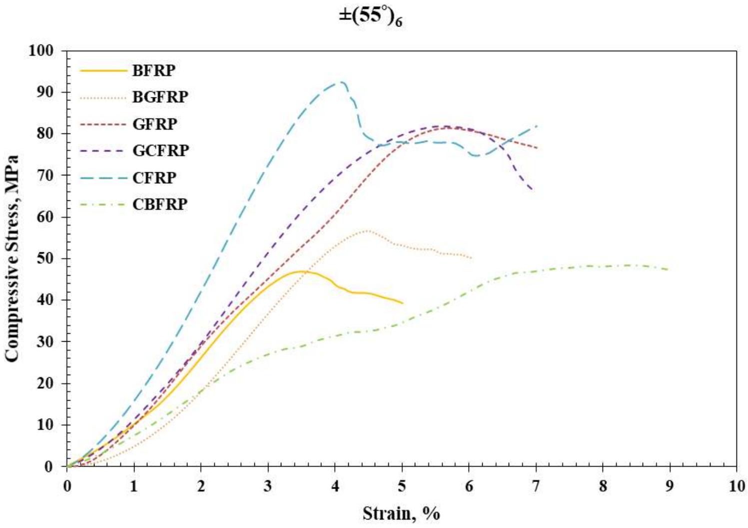

(b)

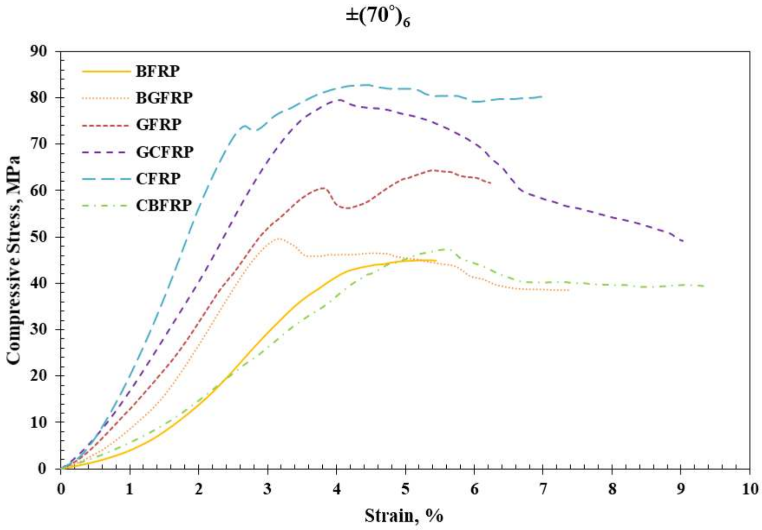

(c)

Figure 4.7 Compressive stress vs strain diagrams for (a) ±(40°) fiber orientation, (b) ±(55°) fiber orientation, c) ±(70°) fiber orientation

Images of compression damage of axial compression test samples having ±(40°), ±(55°) and ±(70°) fiber orientation angles were given in Figure 4.8. As can be observed from the images, the compression damage of non-hybrid FRPs except GFRP showed the progressive failure that begins at the top or bottom cross-section of samples. GFRP had the parallel-to-fiber cracking because of short interlaminar crack initiation. However, intraply FRP samples behaved three different failure types. BGFRP depending the fiber orientations had the parallel-to-fiber cracking and progressive failures. GCFRP and CBFRP samples regardless of fiber orientations resulted with the catastrophic and fiber pull out failure modes, respectively. Fiber orientation angles indicated no significant differences on failure modes of FRPs. Only GFRP based samples showed buckling behavior before parallel-to-fiber cracking modes especially seen in ±(40°) fiber orientations. Matrix fragmentations as first failure followed by progressive folding or parallel-to-fiber cracking were observed for all samples.

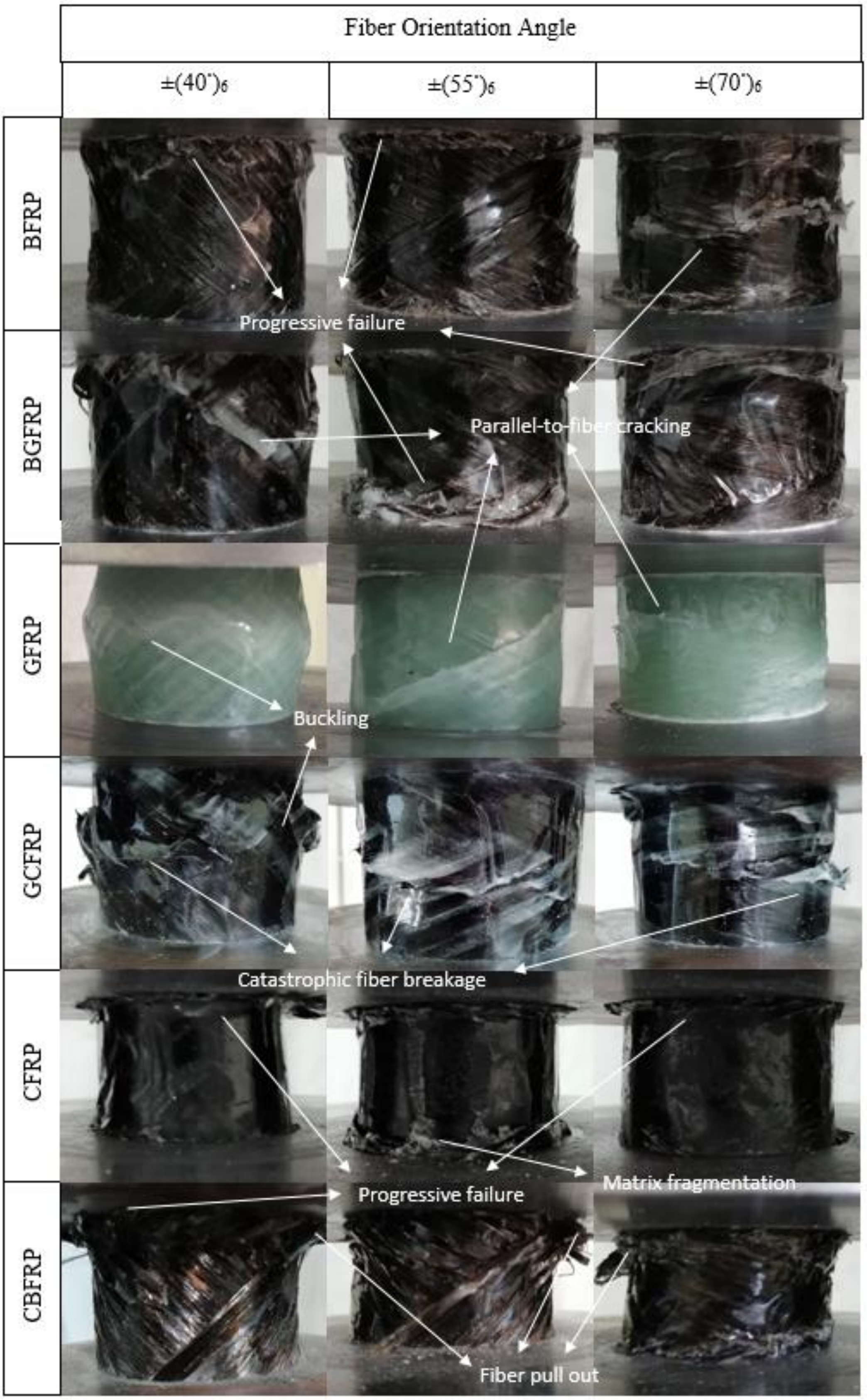

Figure 4.8 Failure shapes of samples under axial compression

4.5 Pipe Stiffness

The compression tests in radial direction by external parallel plate loading were conducted in order to determine the pipe stiffness characteristics of the samples. The pipe stiffness, as shown in Figure 4.9, were based on the force-displacement ratio of the point where the first drop in load values. According to the results, the pipe stiffness value of hybridized FRPs found between those of non-hybrid FRPs. BFRP (±(70°)) with 27.65 MPa was found as the most rigid material in terms of pipe stiffness. CFRP characteristics, which had the lowest values, were increased by addition of glass and basalt fibers. That is, GCFRP compared to CFRP responded 12.43%, 62.53% and 7.38% higher values in pipe stiffness for ±(40˚), ±(55°) and ±(70°) fiber orientation angles, respectively. Furthermore, basalt fiber inclusion (CBFRP) improved the CFRP pipe stiffness with an amount of 35.25%, 75.19% and 27.84% for ±(40˚), ±(55°) and ±(70°) fiber orientations, respectively. When the effect of the fiber orientation angle was considered, the material gained the better rigidity in terms of pipe stiffness with increase in fiber orientation angle.

Figure 4.10 presents the stiffness factor of FRP samples with different fiber orientations. Intraply hybridized FRP samples showed the parallel trend with the pipe stiffness characteristics. As the fiber orientation angle increased, higher stiffness factor values were obtained for all samples.

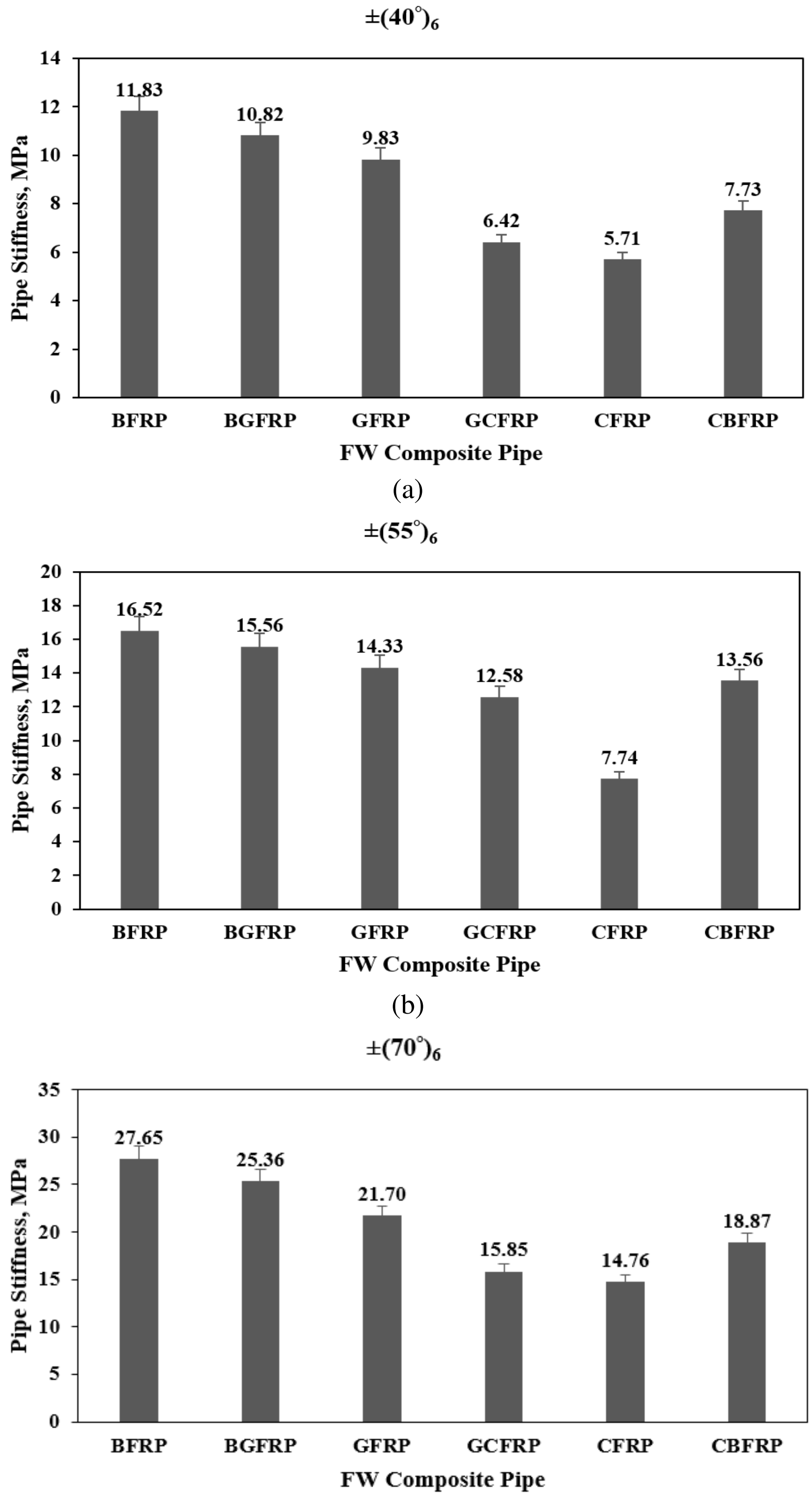

(c)

Figure 4.9 Pipe stiffness for (a) ±(40°) fiber orientation, (b) ±(55°) fiber orientation, c) ±(70°) fiber orientation

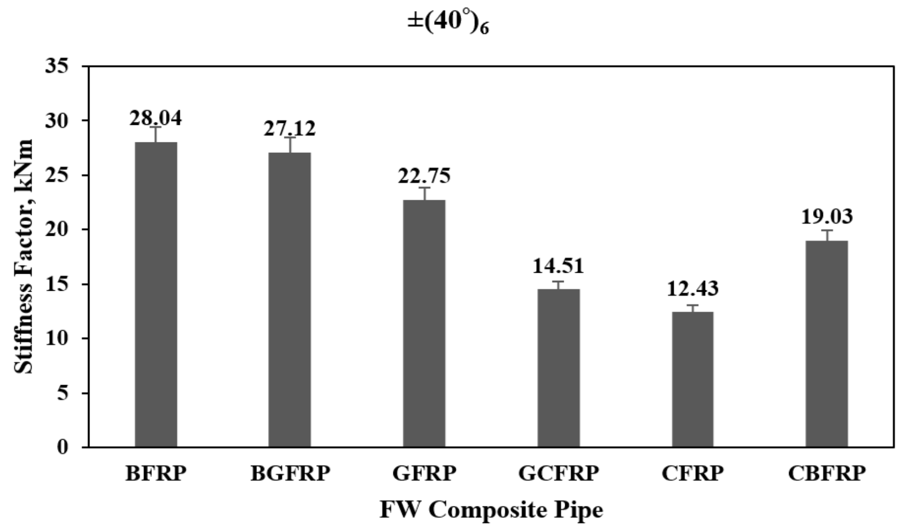

(a)

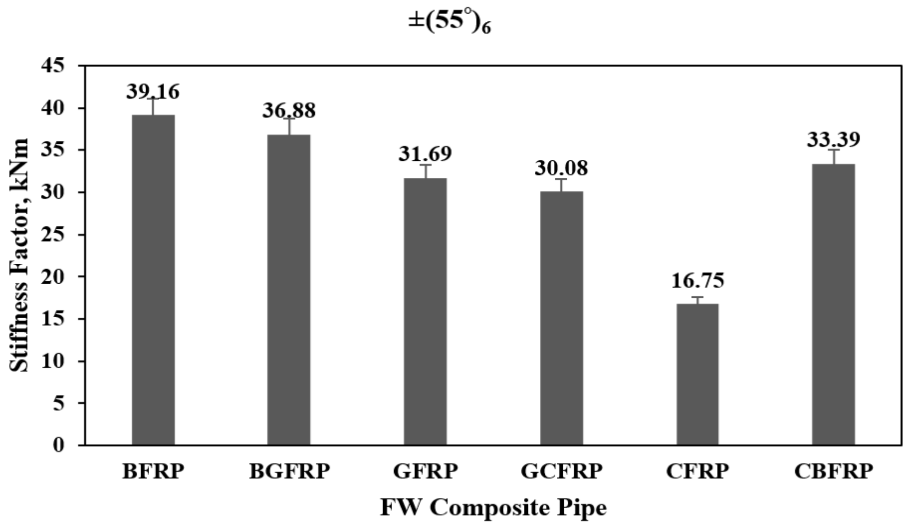

(b)

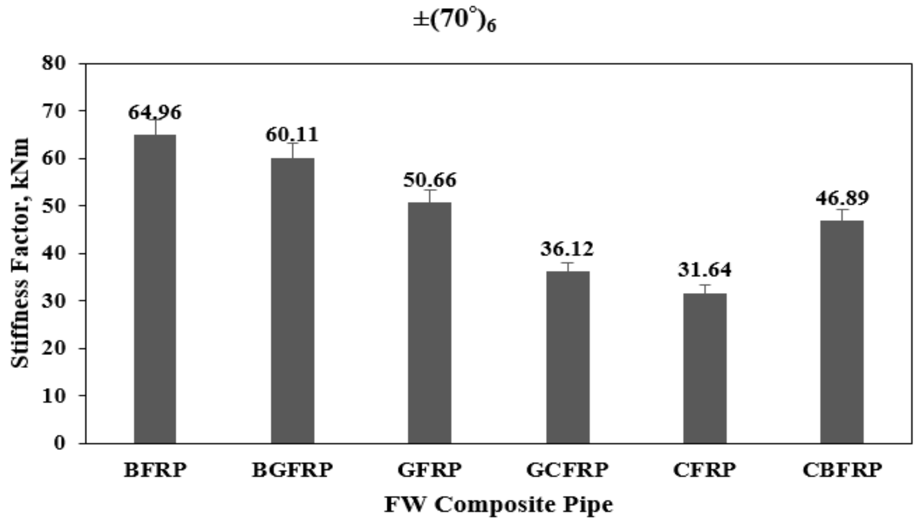

(c)

Figure 4.10 Stiffness factor for (a) ±(40°) fiber orientation, (b) ±(55°) fiber orientation, c) ±(70°) fiber orientation

Load-displacement curves of hybrid and non-hybrid samples with different fiber orientation angles were shown in Figure 4.11. There were irregular ups and downs in the graphs, caused from individual breaks in each layer. CFRP had the lowest load carrying capacity because of its thinner structure. Also, higher fiber orientation angle improved the ability to withstand more load as reported in Almeida's study [96].

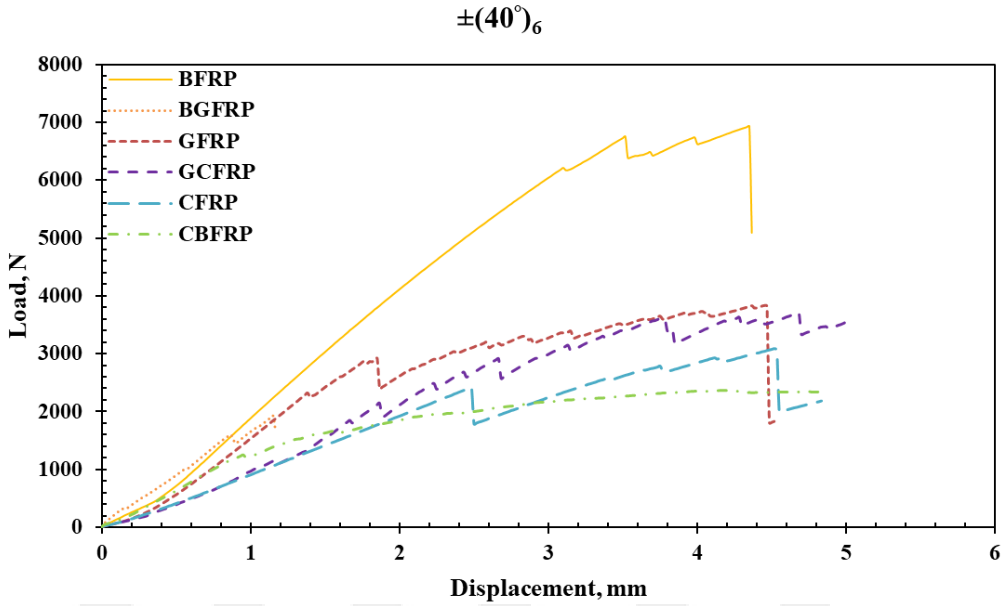

(a)

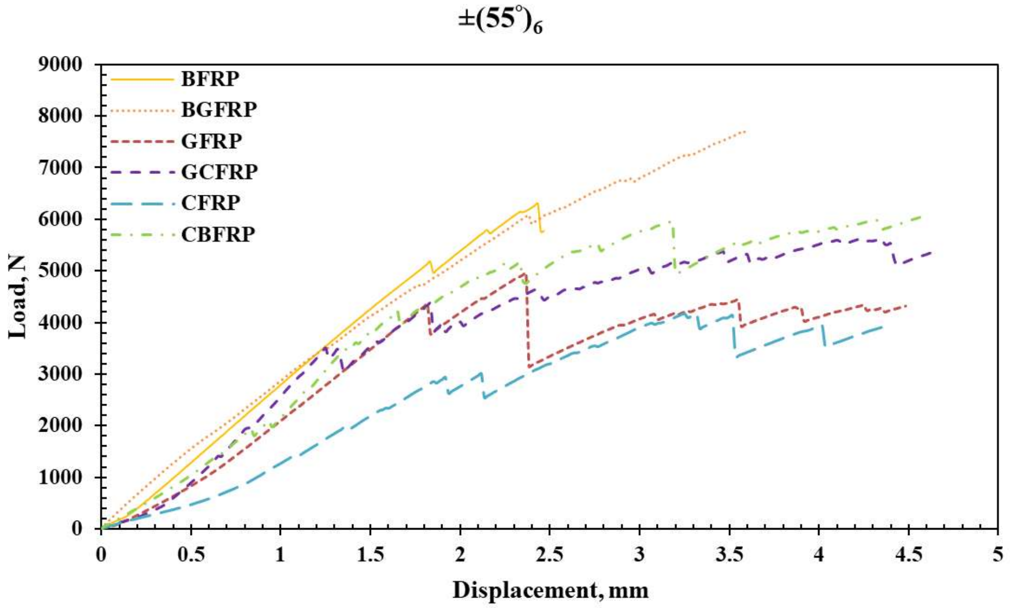

(b)

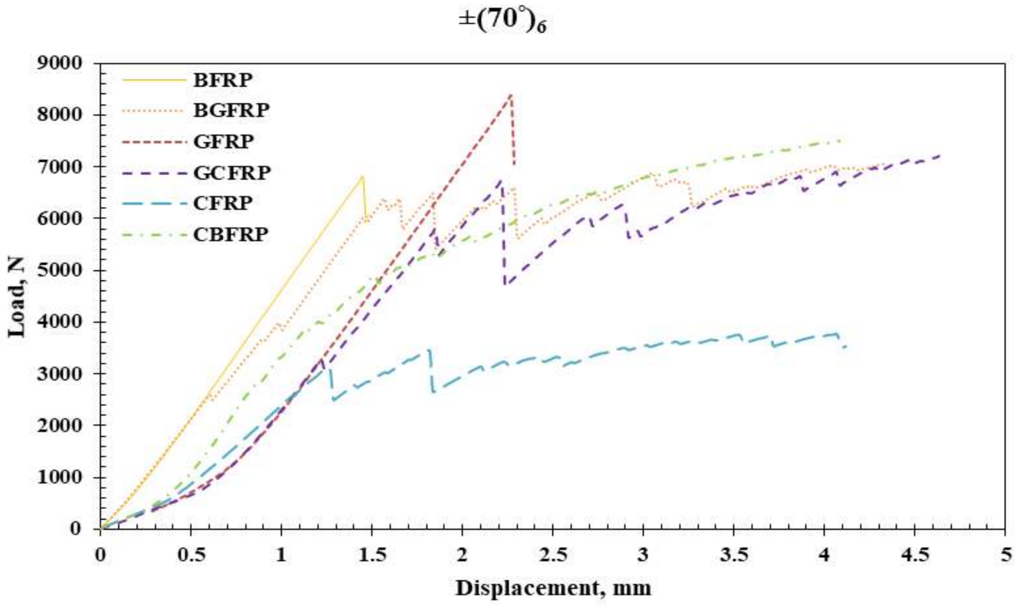

(c)

Figure 4.11 Load-displacement response for (a) ±(40°) fiber orientation, (b) ±(55°) fiber orientation, c) ±(70°) fiber orientation

The parameters of radial compression experiments such as load at first failure point, pipe stiffness, and stiffness factor and percentage pipe deflection of each sample arrangement were given in Table 4.2. The pipe deflection percentage of all intraply FRP samples had the earlier failure than non-hybrid FRPs. This can be attributed to the load carrying capacity of the constituent fibers and differences in their diameters which led variations in fiber content of different locations in a layer. Even the slightest change in surface of the samples resulted with the non-uniform contact between loading platen and samples.

Table 4.2 The parameters of radial compression test

		FW Pipe	F (N)	Δy (mm)	PS (MPa)	SF (kNm)	PPD (%)
Fiber Orientation Angle (°)	±(40°)6	BFRP	6214.99	3.10	11.83	28.04	6.69
		BGFRP	1601.41	0.87	10.82	27.12	1.82
		GFRP	2318.34	1.20	9.83	22.75	2.99
		GCFRP	1055.15	1.07	6.42	14.51	2.30
		CFRP	2417.09	2.48	5.71	12.43	5.36
		CBFRP	1253.22	0.95	7.73	19.03	2.05
	±(55°)6	BFRP	5177.59	1.83	16.52	39.16	3.96
		BGFRP	4724.55	1.77	15.56	36.88	3.81
		GFRP	4347.71	1.82	14.33	31.69	3.92
		GCFRP	1407.19	0.65	12.58	30.08	1.40
		CFRP	1407.39	1.07	7.74	16.75	2.30
		CBFRP	1939.44	0.83	13.56	33.39	1.80
	±(70°)6	BFRP	6809.19	1.45	27.65	65.96	3.13
		BGFRP	2595.38	0.60	25.36	60.11	1.29
		GFRP	8384.66	2.27	21.70	50.66	4.90
		GCFRP	3287.03	1.22	15.85	36.12	2.63
		CFRP	3100.87	1.23	14.76	31.64	2.66
		CBFRP	2764.65	0.85	18.87	46.89	1.84

The damage images of samples under radial compression were given in Figure 4.12. The cross-sectional change from circle to ellipse in all pipes was detected due to the increasein lateral dimensions caused by vertical loading [46]. All pipes showed the crazing, matrix cracking and layer delamination for the failure modes, respectively. Furthermore, intraply hybrid fiber reinforced samples showed the fiber debonding caused from weak interfacial adhesion between layers. During this test, when load was applied gradually on the sample, pipe evidenced failure mechanism like crazing, wall cracking, and wall delamination and finally ends with the rupture [97].

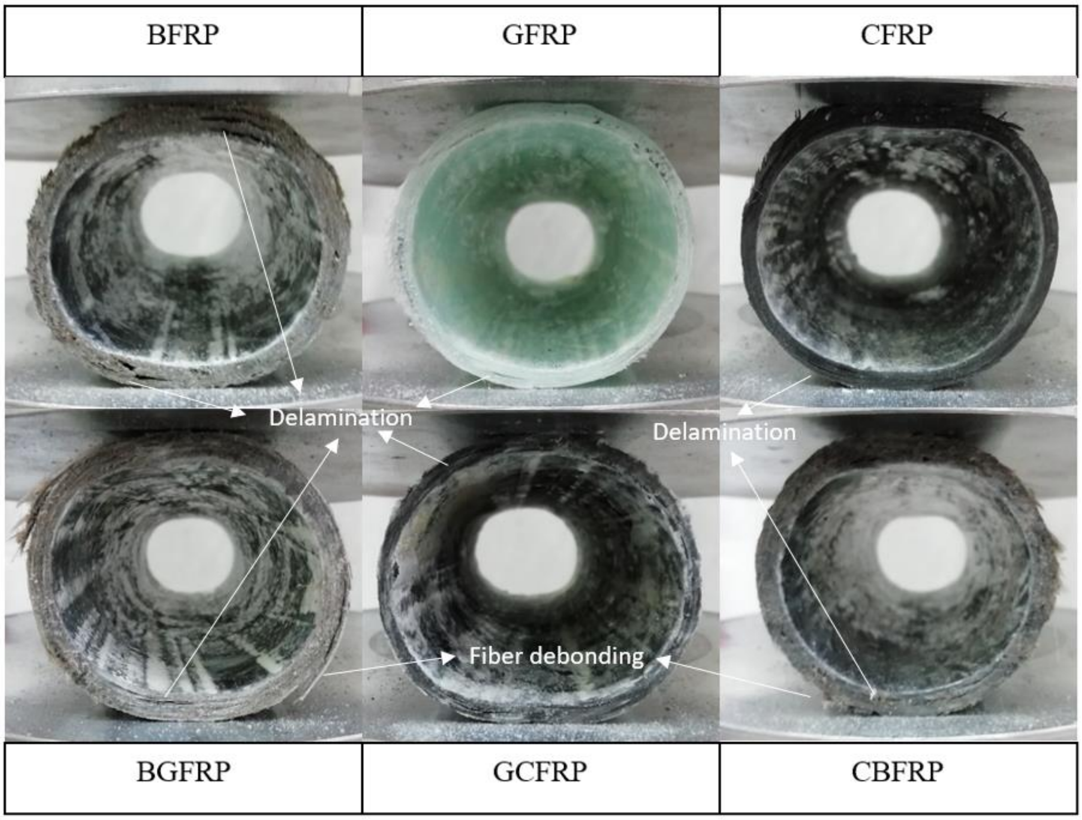

Figure 4.12 Damage images of samples under radial compression

CHAPTER V

CRASHWORTHINESS OF COMPOSITE PIPES

5.1 Introduction

Reliability of a material is an essential parameter in an engineering structure to fulfill safety requirements and to save lives by reducing casualties due to unexpected events during service operations. Crashworthiness, which takes into account for occupant protection by absorbing energy, is one of the most crucial properties of a structural material. Therefore, the energy absorption capability of a material have become a key subject that should be investigated in the event of a crash.

This chapter discusses the results of the crushing tests to meet the above requirement. Axial and lateral crushing behaviors of hybrid pipe samples have been investigated by presenting intraply fiber hybridization effects in terms of fiber orientation angles those influencing crushing modes, load carrying capacity, energy absorption capability through the crushing process. The chapter has been divided into two main parts including of four subjects related with failure modes, crushing load efficiency, energy absorption and fiber orientation influence according to direction of crushing loading application. The failure modes and corresponding to force-deflection response of the pipe samples are presented by comparing surface damages during crushing history. Key important parameters such as failure modes, load-displacement response, peak load, mean crushing load, total energy absorption, specific absorbed energy are discussed to see effects of intraply fiber hybridization of pipe samples.

5.2 Axial Crushing

5.2.1 Load-Displacement Response and Failure Modes

Load-displacement curve is the one of the main tools that gives the information about crash. The axial load-displacement curves with different fiber orientation and photographs during crushing history were presented in Figures 5.1-5.3. As seen from figures, all samples had progressive crushing with high energy absorption and good reproducibility except GFRP. BFRP and CBFRP had the earliest drastic load increase when load goes into densification phase while the hybridized BGFRP and CFRP were the latest ones. This can be explained by basalt fiber structure that causing the compaction of debris and the folded tube wall [70] before others. However, hybridization process with better repeatability enabled the more stable crushing process compared with non-hybrid FRPs for all fiber orientation.

As seen from Figure 5.1a, which presented the load-displacement response of pipes having ±(40°) fiber orientation, GFRP exhibited the highest initial peak as 45.51 kN and the lowest mean load as 23.33 kN, because of its catastrophic crushing mode. Due to interlaminar cracks growth on the tension side of the buckled fibers [51, 98] unstable local buckling was seen from Figure 5.1b, which demonstrates the crush history of the pipes. However, BFRP had the progressive folding with lamina bending mode results from short inter-/intralaminar cracks formation. CFRP showed the stable progressive crushing with parallel-to-fiber crack propagation caused from local buckling failure. Furthermore, stable cyclic crushing history was achieved for hybridized FRP samples (especially BGFRP and GCFRP) since interlaminar crack growth and parallel-to-fiber crack propagation, resulted with combination of transverse shearing and lamina bending crushing modes (brittle fracturing) [51, 93, 98], respectively.

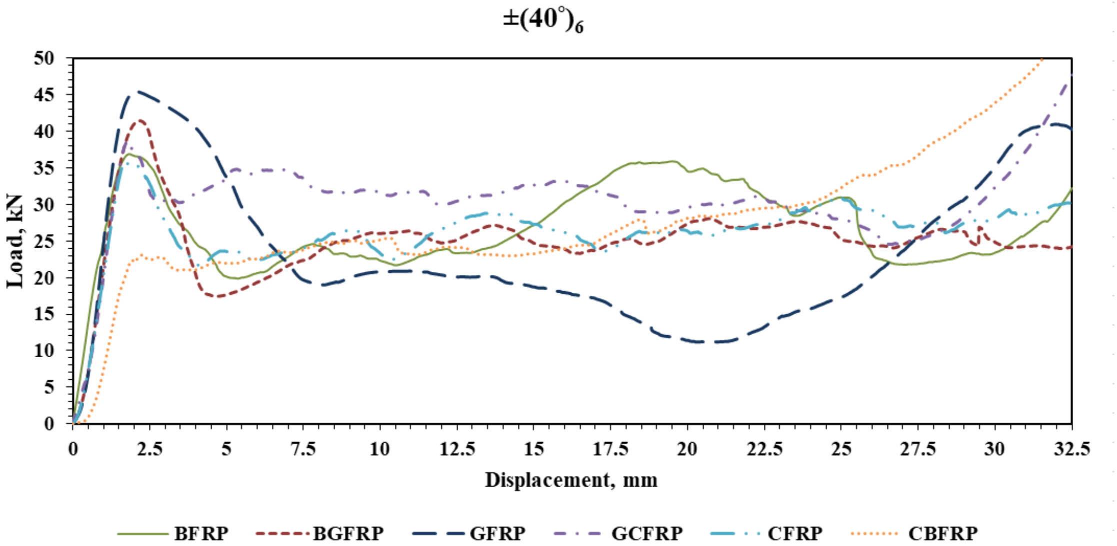

(a)

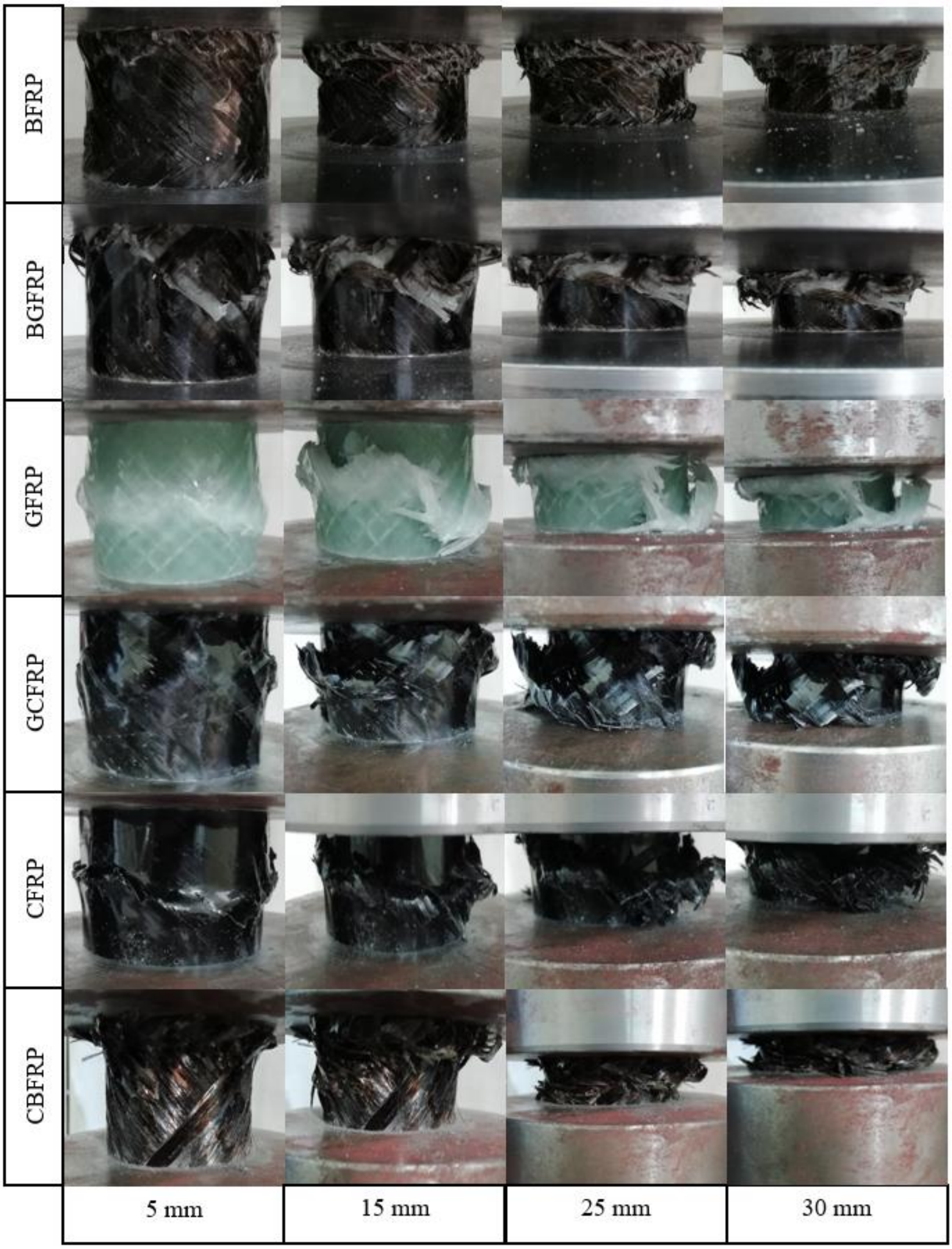

(b)

Figure 5.1 Axial crushing with ±(40°) fiber orientation; (a) load-displacement response, (b) crushing history at 5 mm, 15 mm, 25 mm and 30 mm stroke displacement

Figure 5.2a and 5.2b presented the load-displacement curve and photographs of crushing history for ±(55°) fiber orientation, respectively. BFRP and GFRP showed the unstable response of loading behavior because of local buckling crushing mode like GFRP with ±(40°) fiber orientation. The highest mean loads as 22.39 kN, 32.69 kN and 29.79 kN achieved from the samples of BGFRP, GCFRP and CBFRP, respectively, since their consistent with load response during crushing. BGFRP, CFRP and CBFRP showed the progressive end crushing with splaying fibers to outward while BFRP resulted with the inward splaying. Additionally, glass fiber-based pipes (GFRP, BGFRP and GCFRP) had the failure modes beginning with matrix fragmentation and continuing with transverse shearing and lamina bending caused by parallel-to-fiber cracks [51, 93] as depicted in Figure 5.2b.

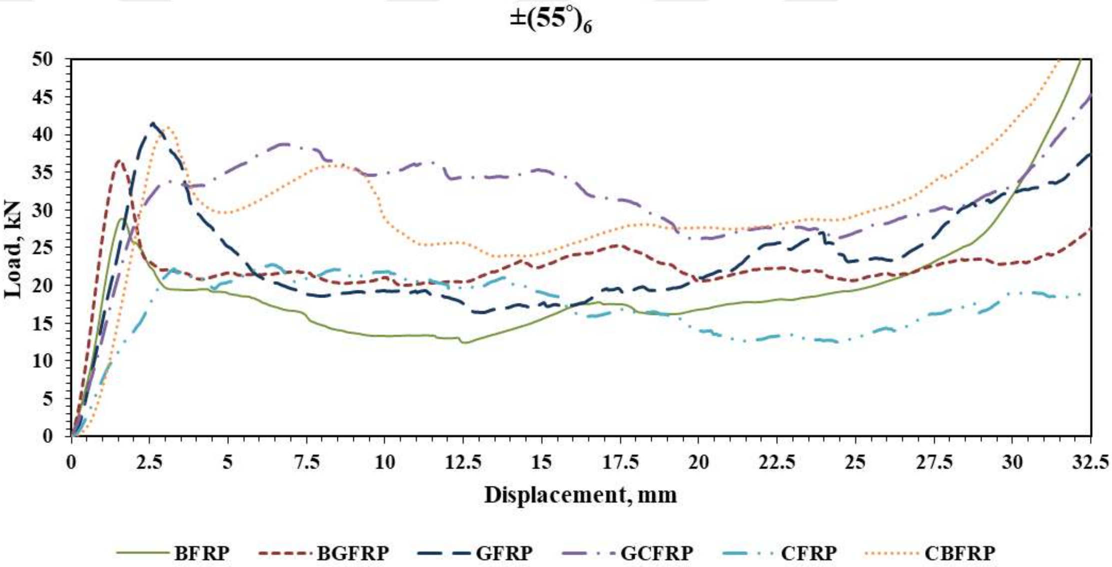

(a)

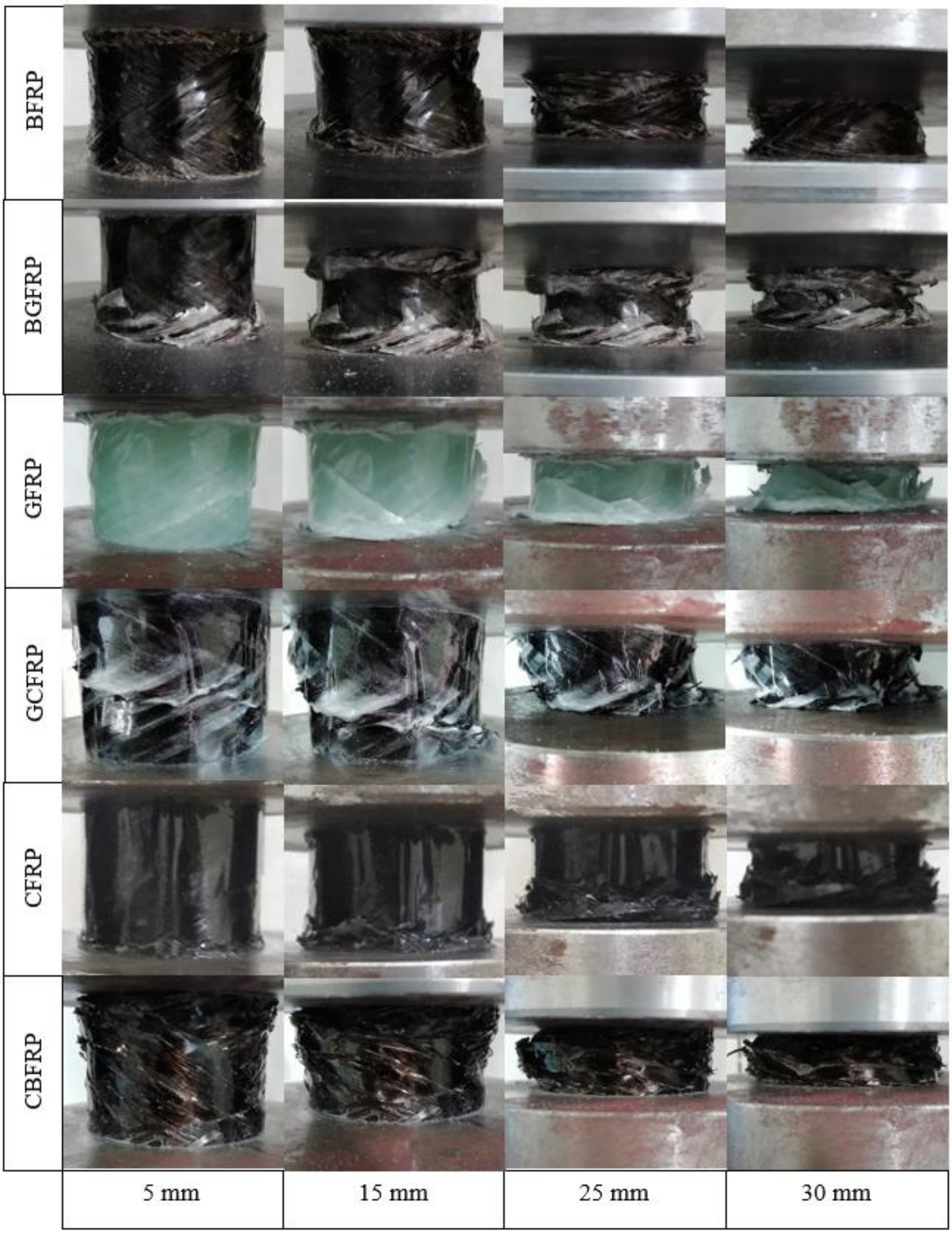

(b)

Figure 5.2 Axial crushing with ±(55°) fiber orientation; (a) load-displacement response, (b) crushing history at 5 mm, 15 mm, 25 mm and 30 mm stroke displacement

Load-displacement response and crushing history of pipes having ±(70°) fiber orientation angle were given in Figure 5.3a and 5.3b, respectively. The basalt based samples (BFRP, BGFRP and CBFRP) and CFRP developed transverse shearing crushing mode by progressive folding at various regions and early dramatically increase in load for BGFRP and BFRP caused the densification beginning. Differently, GFRP and GCFRP showed the catastrophic crushing mode by shear in fiber orientation direction. However, BGFRP sample fixing unstable load response of glass and basalt fibers had the cyclic end crushing mode progressively by interlaminar crack growth. This is consistent with a frond fracture, where the pipe wall splits into inner and outer fronds along the axial direction [99].

The photographs of samples after the crushing experiments according to fiber orientation and fiber material, provided in Figure 5.4, showed that the increase in orientation angle resulted with inner and outer irregular splaying behaviors of the fibers and intensifying of fronds. Pipe wall thickness, which had significant effect [48, 100] for failure mechanisms on crushing, led to more debris production for basalt fiber based configurations (BFRP, BGFRP and CBFRP) and more outward frond formation for others. Lastly, the combination of fiber debonding, matrix fragmentation, delamination and fiber breakage of failures were observed in most samples as seen on crushed shapes.

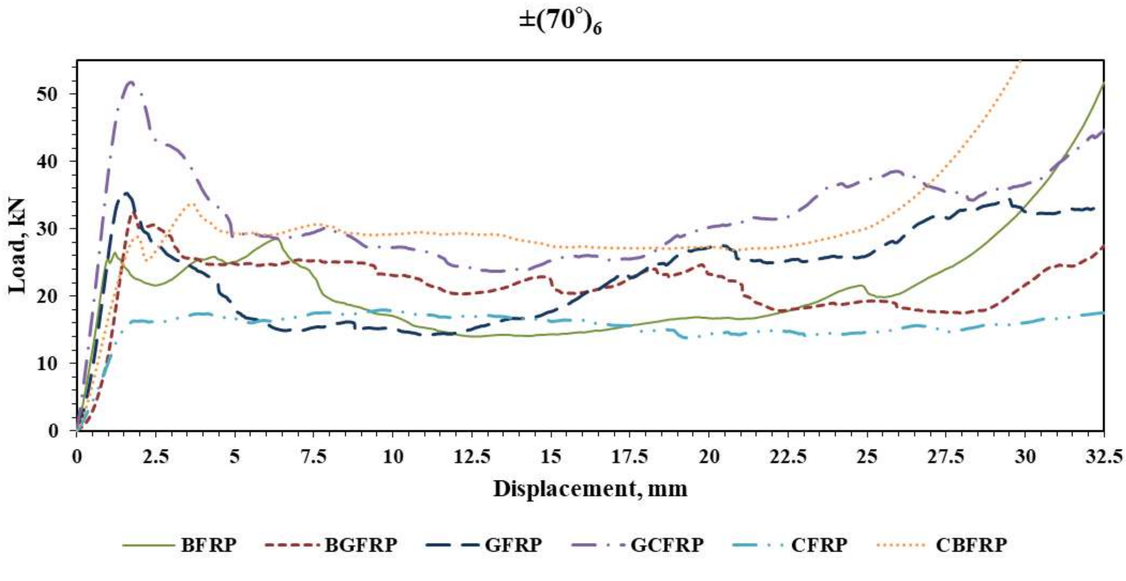

(a)

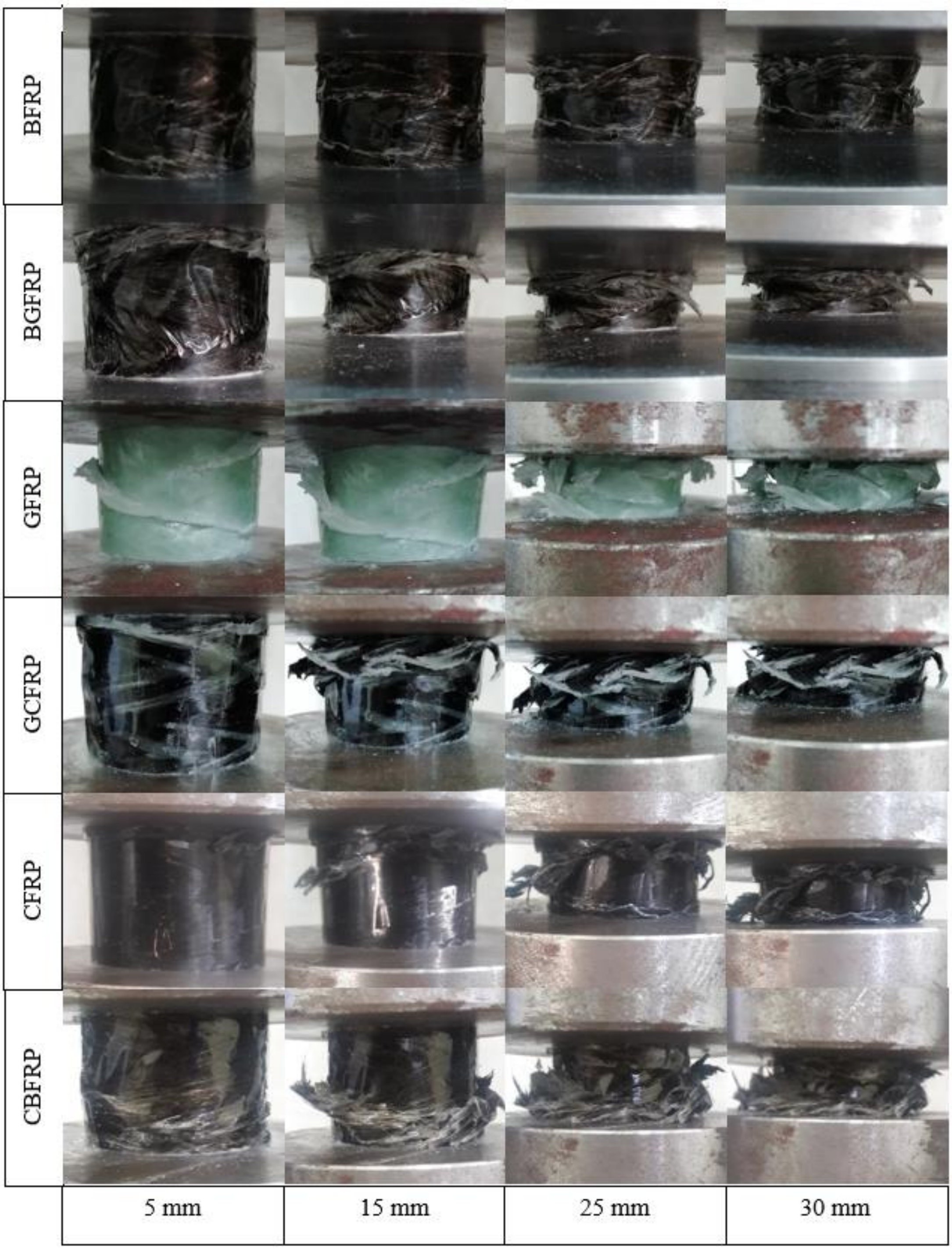

(b)

Figure 5.3 Axial crushing with ±(70°) fiber orientation; (a) load-displacement response, (b) crushing history at 5 mm, 15 mm, 25 mm and 30 mm stroke displacement

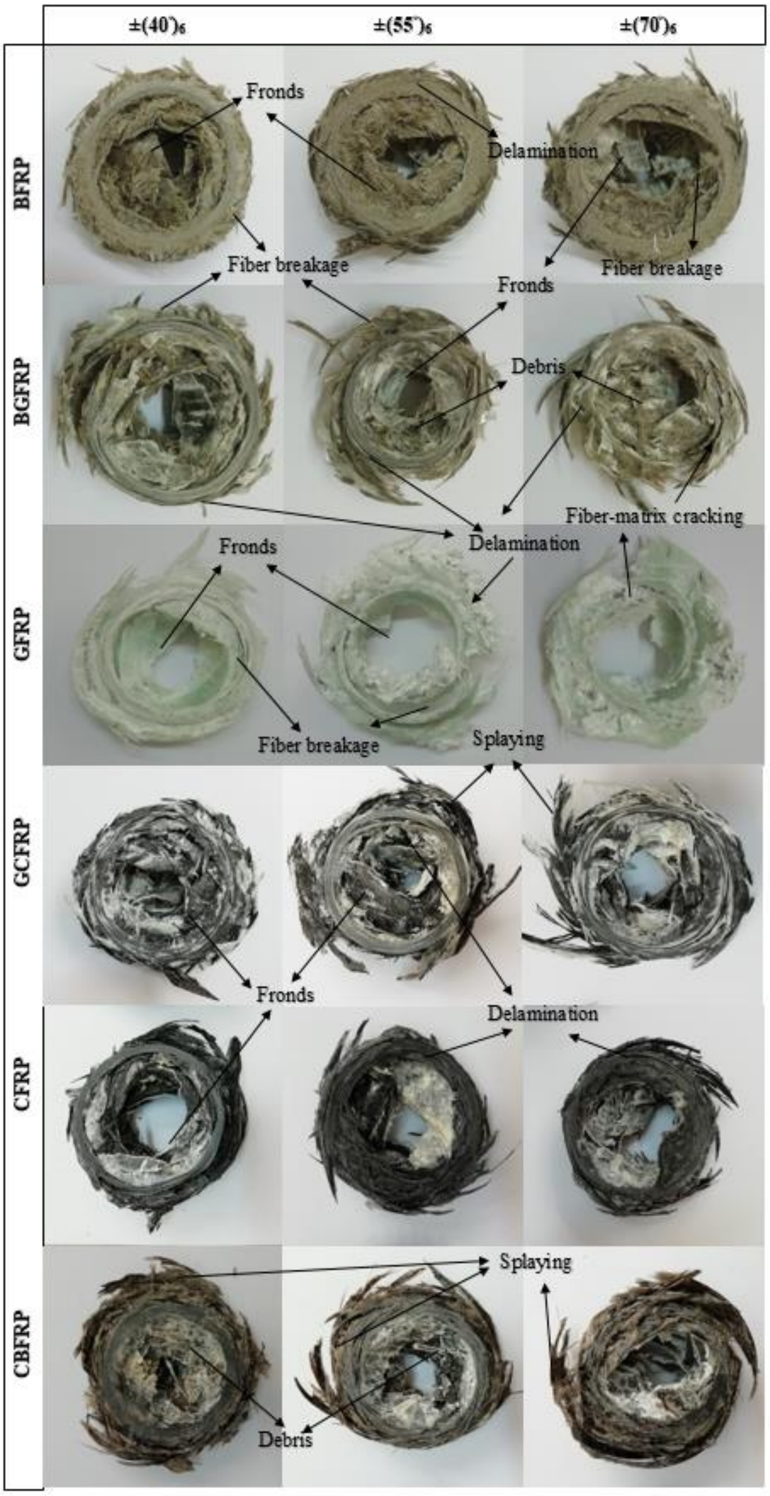

Figure 5.4 The samples after axial crushing

5.2.2 Crushing Load Efficiency

Initial peak load, P_i is a crucial parameter to understand crushing failure process beginning and also is related directly to the structure and human safety [48, 101, 102].

GFRP samples with ±(40°) fiber orientation of 45.51 kN value was achieved as maximum initial peak load, while minimum one was 16.69 kN for CFRP with ±(70°) fiber orientation as indicated in Figure 5.5. Initial peak load value of basalt fibers with inclusion of glass fibers (BGFRP) compared to BFRP were remarkably improved as %12.5, %27.8 and %23.0 for ±(40°), ±(55°), and ±(70°) fiber orientation angles, respectively. CBFRP had not regular tendency for initial peak load carrying capacity due to non-uniform load distribution on the surface of the sample that caused by the differences of basalt and carbon fiber diameters.

Mean load, P_m, represents the average value of each load application in post-crushing stage and is a good indicator of overall energy absorption capability of pipes [101]. CBFRP with ±(70°) fiber orientation had the maximum mean crushing load as 33.87 kN due to brittle fracturing crushing mode. By the way, BGFRP samples giving the results within the range of non-hybrid FRPs in mostly, in terms of both initial peak and mean load, proved that two fibers can be united functionally in applications.

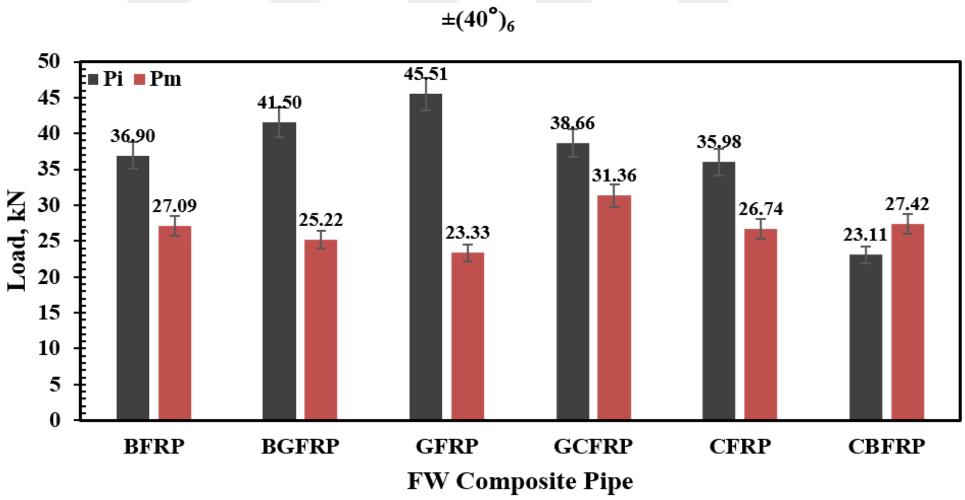

(a)

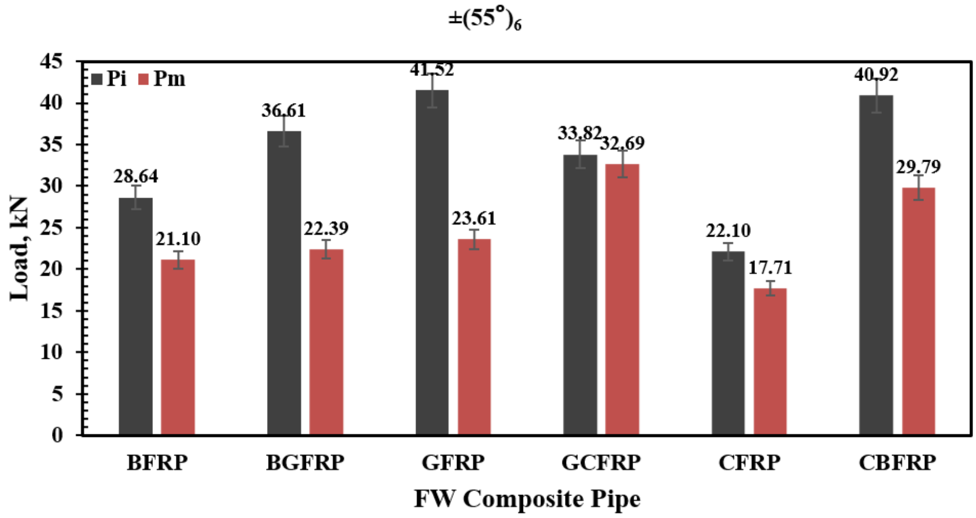

(b)

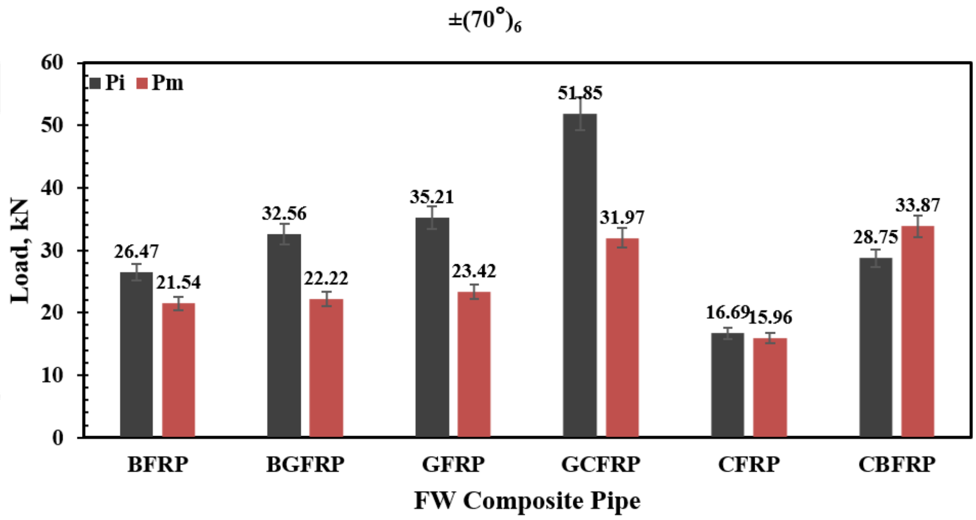

(c)

Figure 5.5 Axial loading characteristics for (a) ±(40°) fiber orientation, (b) ±(55°) fiber orientation, c) ±(70°) fiber orientation

Crushing load efficiency, η_f, which is the ratio of mean load and initial peak load, is the useful index to evaluate stability of the crushing process [21, 64, 103] and performance of the absorber [70]. Figure 5.6 revealed the crushing load efficiency of pipes at different fiber orientations. BFRP samples showed the maximum load efficiency values as 73.42%, 73.66% and 81.38% for ±(40°), ±(55°) and ±(70°) fiber orientation angles, respectively. However, the efficiency of BGFRP samples were found as 60.76%, 61.16% and 68.26% within the range of BFRP and GFRP thanks to basalt fiber addition to glass fibers. However, other hybrid samples (GCFRP and CBFRP) showed the irregular trend of load efficiency since their fiber combinations caused the unexpected load carrying capacity.

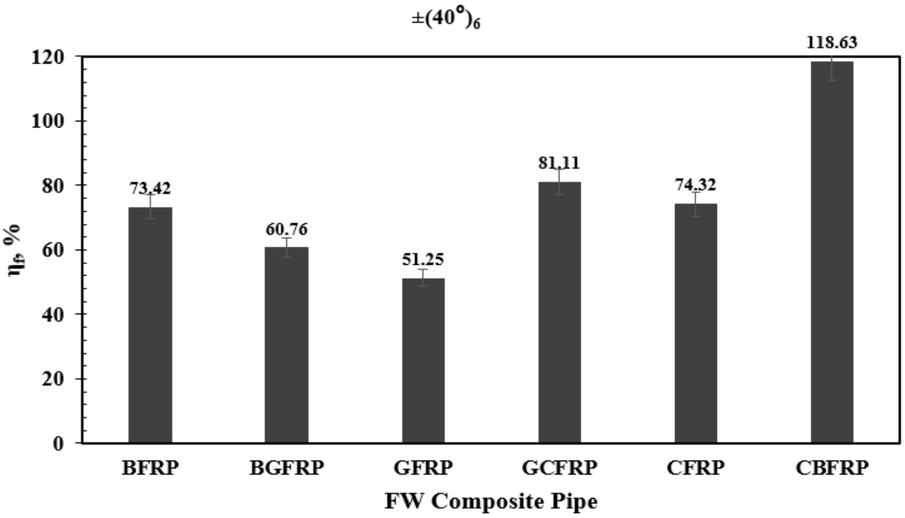

(a)

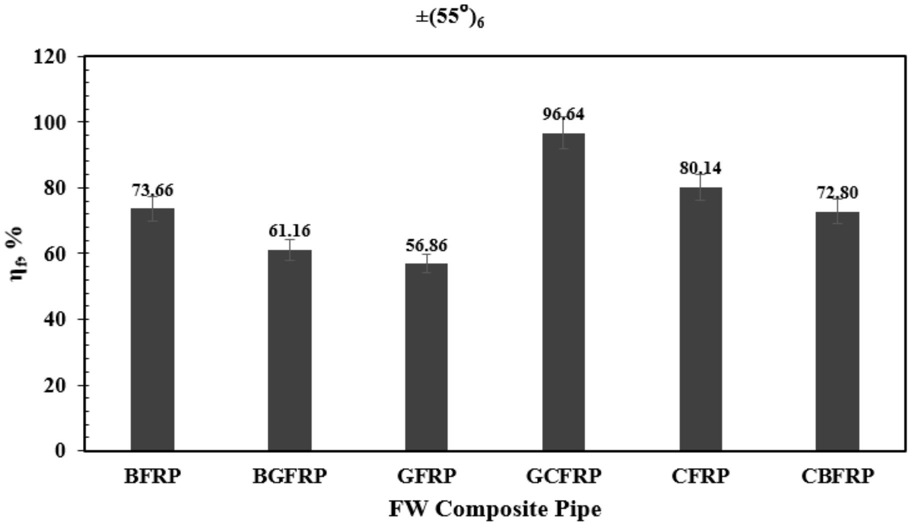

(b)

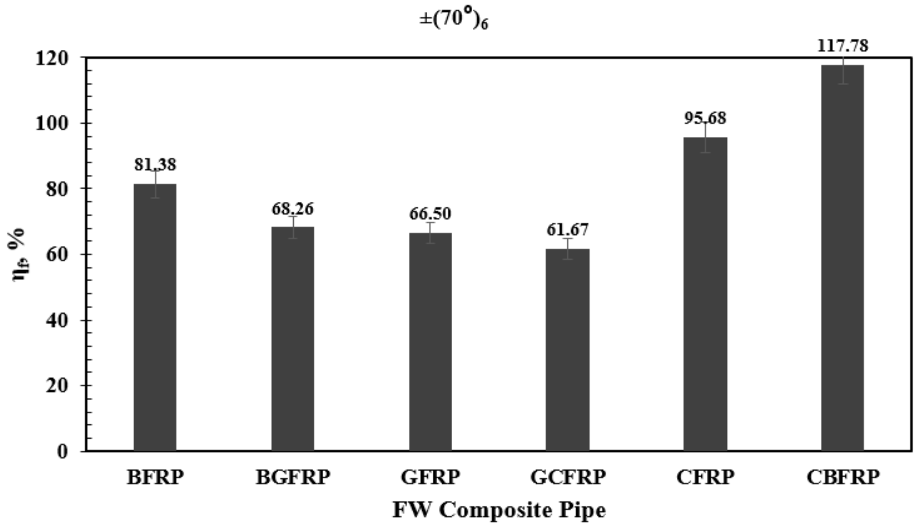

(c)

Figure 5.6 Axial crushing load efficiency for (a) ±(40°) fiber orientation, (b) ±(55°) fiber orientation, c) ±(70°) fiber orientation

5.2.3 Energy Absorption

Total energy absorption, which is the area under load-displacement curve, was presented in Figure 5.7. Hybrid GCFRP and CBFRP samples had the extreme values because of their mass caused the high crushing load efficiency, while BGFRP samples showed the values within the range of GFRP and BFRP. Also, increase in fiber orientation angle resulted with the decrease in total energy absorption.

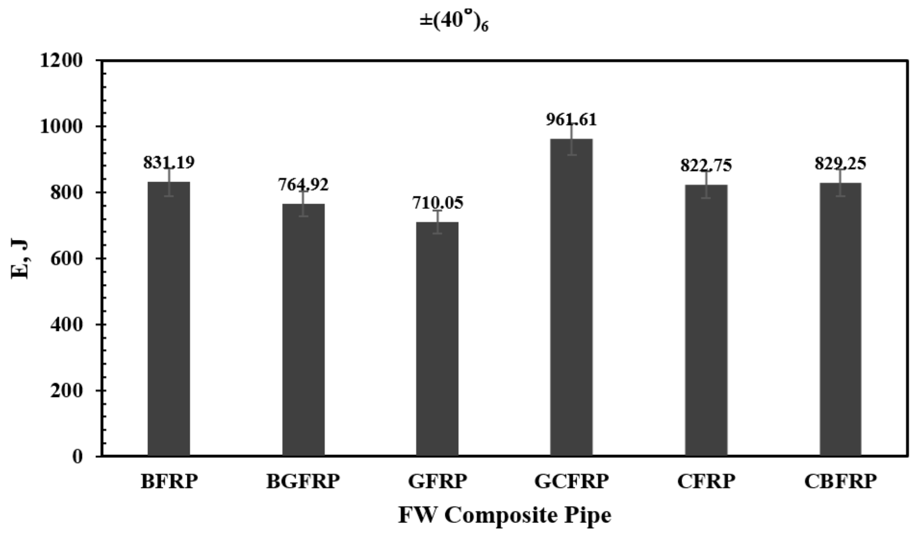

(a)

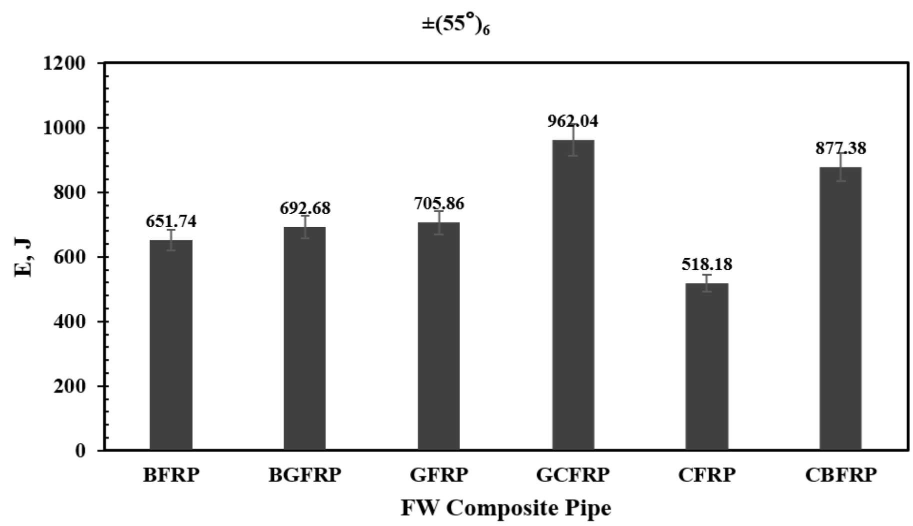

(b)

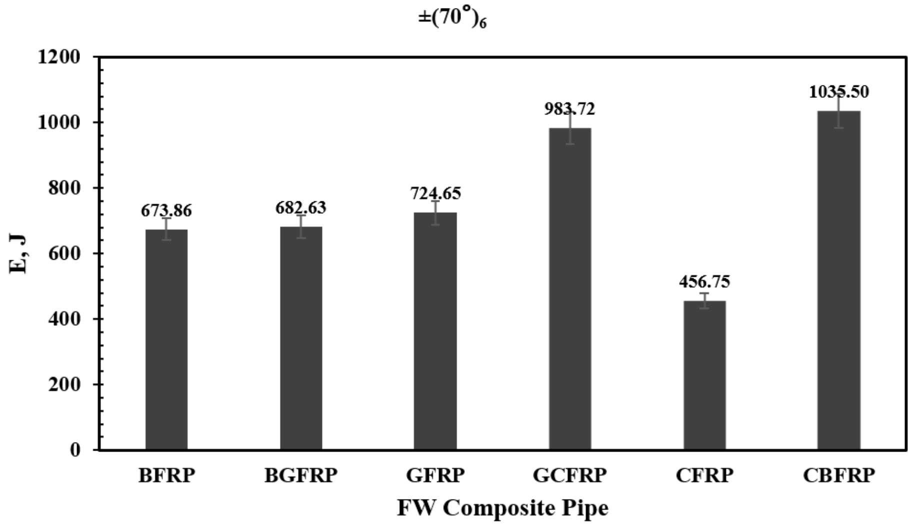

(c)

Figure 5.7 Total energy absorption in axial crushing for (a) ±(40°) fiber orientation, (b) ±(55°) fiber orientation, c) ±(70°) fiber orientation

However, specific energy absorption instead of total energy should be noted because of taking into account the mass. Figure 5.8 representing specific energy absorption results provides the reliable information to be understandable about energy absorption. GFRP showing the 29.32 J/g, 28.70 J/g, 26.32 J/g for the considered fiber orientations of ±(40°), ±(55°), and ±(70°), were 1.2, 1.34 and 1.27 times of specific energy absorption values of BFRP, respectively. BGFRP sample results remained between the GFRP and BFRP values not only in total energy absorption but also in specific energy absorption. The maximum specific absorbed energy as 47.02 J/g was found from CFRP sample with ±(40°) of fiber orientation. The carbon fiber addition to GFRP led to the 16.06%, 15.09% and 23.1% improvements for ±(40°), ±(55°), and ±(70°) fiber orientations, respectively. Also, CBFRP gave the increase in 1.1, 1.2 and 1.3 times of BFRP results.

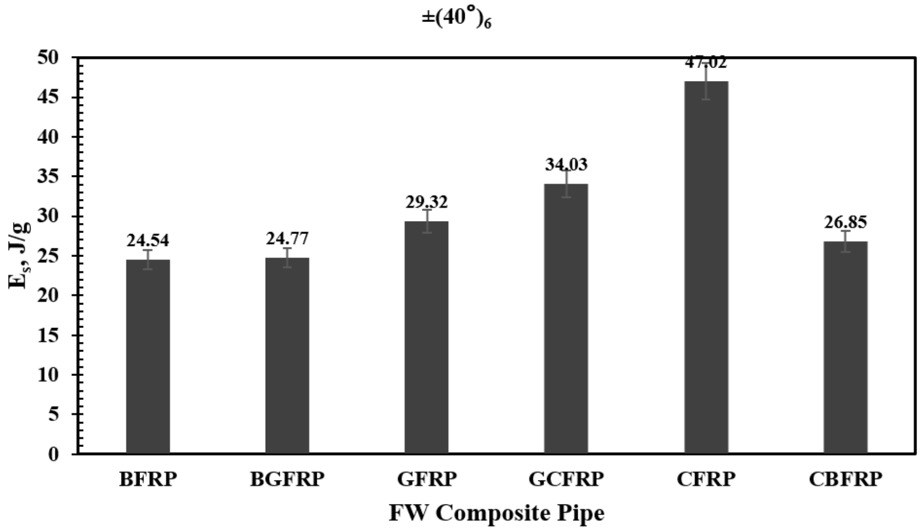

(a)

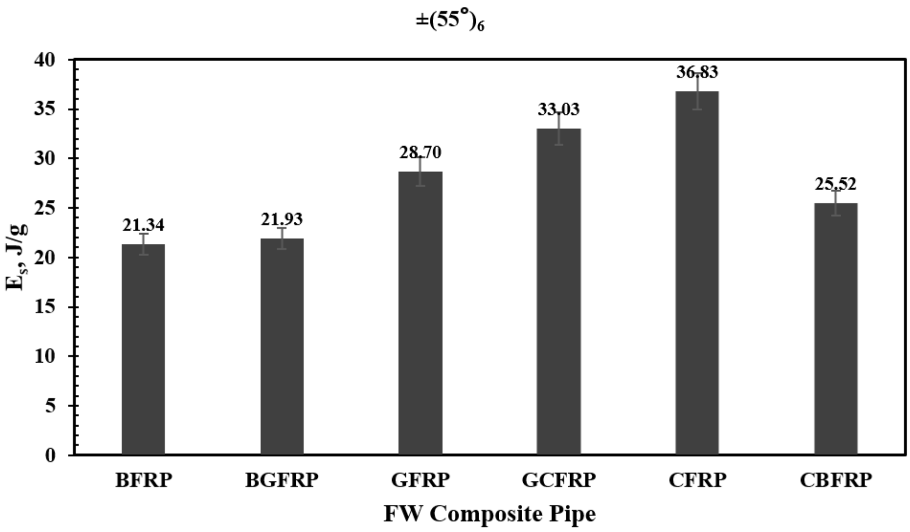

(b)

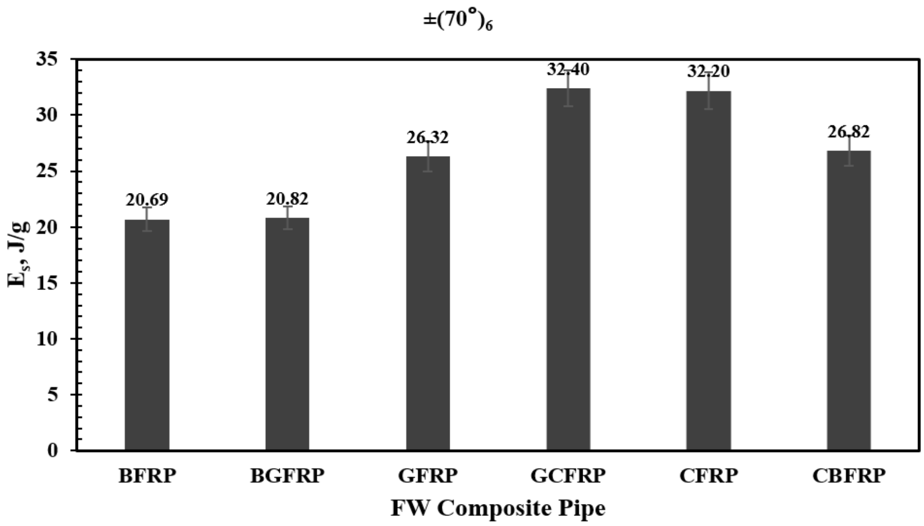

(c)

Figure 5.8 Specific absorbed energy in axial crushing for (a) ±(40°) fiber orientation, (b) ±(55°) fiber orientation, c) ±(70°) fiber orientation

5.2.4 Effect of Fiber Orientation

The characteristic parameters and mass information belong to axially crushed samples, which include initial peak load, mean load, crushing load efficiency, absorbed energy, specific energy absorption, crushing modes in accordance with Farley's classification [51], were given in Table 5.1. Fiber orientation angle had certainly significant influence on crushing behaviors of composite pipes [48, 50, 104]. The following results can be given for this study:

As seen from Figure 5.4, less debris were gradually produced with an increase in fiber orientation angle. This can be related to increasing circumferential stiffness which could give a positive contribution to enhance the resistance to interlaminar crack growth [48, 93]. For smaller angles, interlaminar cracks propagated easily along longitudinal direction and form long crack length. Nevertheless, the samples showed the short interlaminar crack length longitudinally due to the parallel-to-fiber cracking when pipe had bigger fiber orientation. Thus, transverse shearing or brittle fracturing (combination of transverse shearing and lamina bending) crushing modes were observed at ±(70°) fiber orientations. And this resulted with the higher crushing load efficiency in general while initial peak load and mean load has decreasing trend. BFRP, GFRP and CFRP samples at ±(70°) were improved by 1.11, 1.30 and 1.29 times of efficiency value compared with fiber oriented at ±(40°). The best energy absorption in specific manner as 47.02 J/g was obtained from CFRP with fiber oriented at ±(40°) while the total energy absorption was belong to CBFRP as 1035.50 J. Specific energy absorption tends to decrease with an increase in fiber orientation angle as consistent with several study in the literature [48, 50, 98]. This situation can be explained by approaching the fiber orientation to loading direction which shows maximum strength.

Table 5.1 Crashworthiness parameters under quasi-static axial compression loading

FRP	α (°)	m (g)	P_i (kN)	P_m (kN)	η_f (%)	E (J)	E_s (J/g)	Crushing Mode
BFRP	40°	33.88	36.90	27.09	73.42	831.19	24.54	Lamina bending
	55°	30.53	28.64	21.10	73.66	651.74	21.34	Local buckling
	70°	32.57	26.47	21.54	81.38	673.86	20.69	Transverse shearing
BGFRP	40°	30.89	41.50	25.22	60.76	764.92	24.77	Brittle fracturing
	55°	31.59	36.61	22.39	61.16	692.68	21.93	Brittle fracturing
	70°	32.79	32.56	22.22	68.26	682.63	20.82	Brittle fracturing
GFRP	40°	24.22	45.51	23.33	51.25	710.05	29.32	Local buckling
	55°	24.60	41.52	23.61	56.86	705.86	28.70	Transverse shearing
	70°	27.53	35.21	23.42	66.50	724.65	26.32	Transverse shearing
GCFRP	40°	28.26	38.66	31.36	81.11	961.61	34.03	Brittle fracturing
	55°	29.13	33.82	32.69	96.64	962.04	33.03	Brittle fracturing
	70°	30.37	51.85	31.97	61.67	983.72	32.40	Brittle fracturing
CFRP	40°	17.50	35.98	26.74	74.32	822.75	47.02	Local buckling
	55°	14.07	22.10	17.71	80.14	518.18	36.83	Lamina bending
	70°	14.19	16.69	15.96	95.68	456.75	32.20	Lamina bending

5.3 Lateral Crushing

5.3.1 Load-Displacement Response and Failure Modes

The load-displacement curves and the crushing history of the lateral loading application at different fiber orientations of the considered pipes were given in Figure 5.9-5.11, respectively. For all examined samples, mid-surface of samples were observed as damage region beginning with a buckling behavior of the vertical walls. This buckling allowed and encouraged the cells to readjust its position which causes a vertical crack at the samples mid plane [105]. Furthermore, first failure mode can be given as matrix cracking that triggers delamination of the layers. Most of the samples showed the fiber debonding failure mode as lateral loading continued.

The load-displacement curves of the samples with the considered fiber orientaitons were given in Figure 5.9, respectively. There were irregular ups and downs in the graphs, caused from individual breaks in each layer. As the surface contact with the load was worse than the cross-sectional flatness, cyclic load-displacement graphs could not be obtained as in axial crush. CFRP had the lowest load carrying capacity because of its thinner structure. Also, higher fiber orientation angle resulted with the increase in load carrying capacity as reported in İsmail's study [106]. GFRP with ±(70°) fiber orientation had the maximum initial loading peak value and the most regular curve.

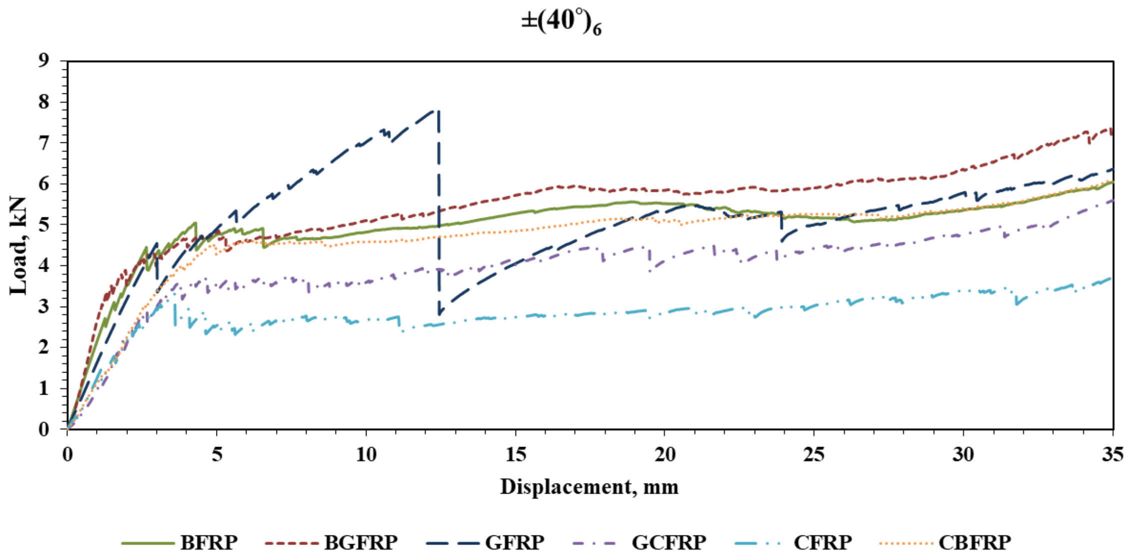

(a)

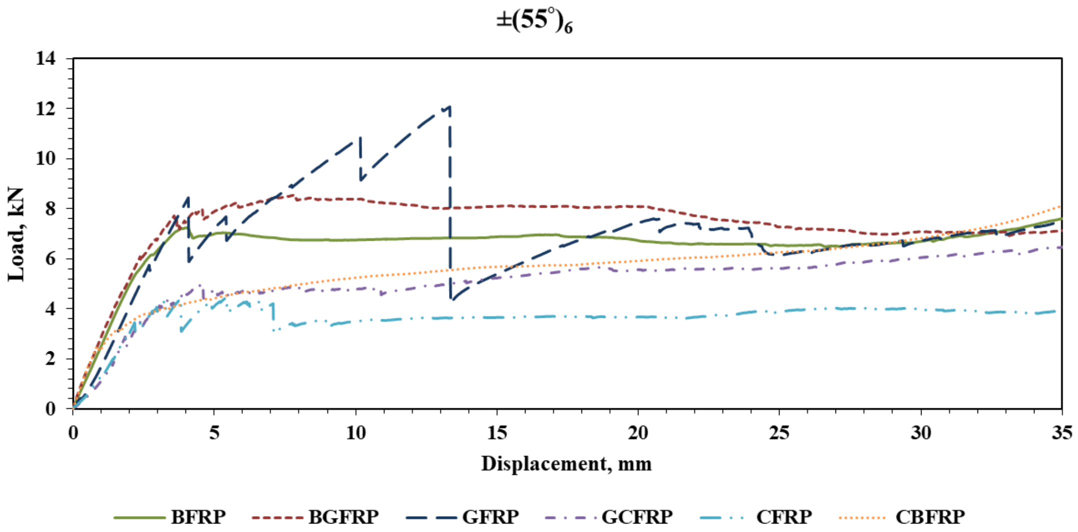

(b)

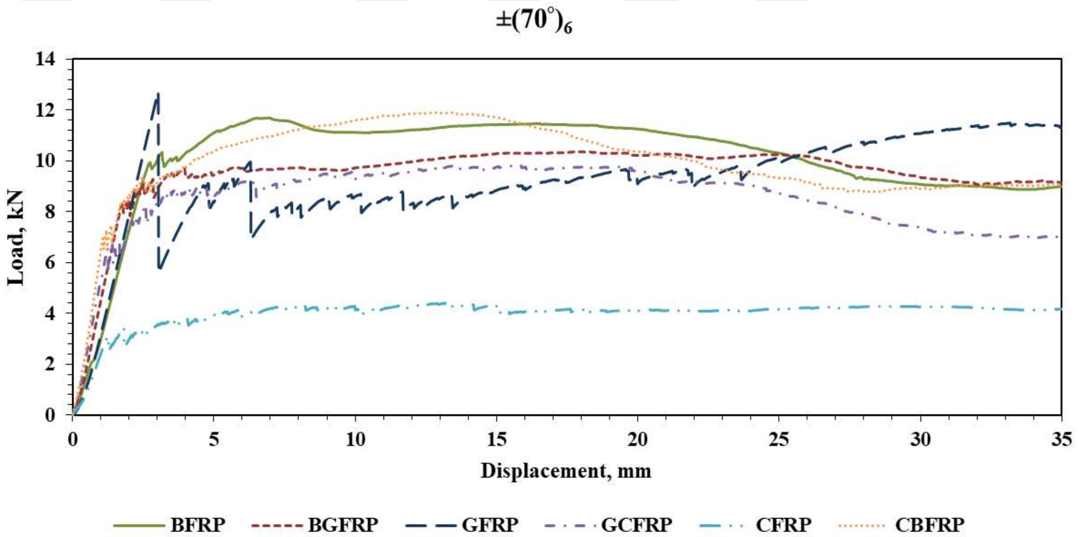

(c)

Figure 5.9 Load-displacement response for lateral crushing for (a) ±(40°) fiber orientation, (b) ±(55°) fiber orientation, c) ±(70°) fiber orientation

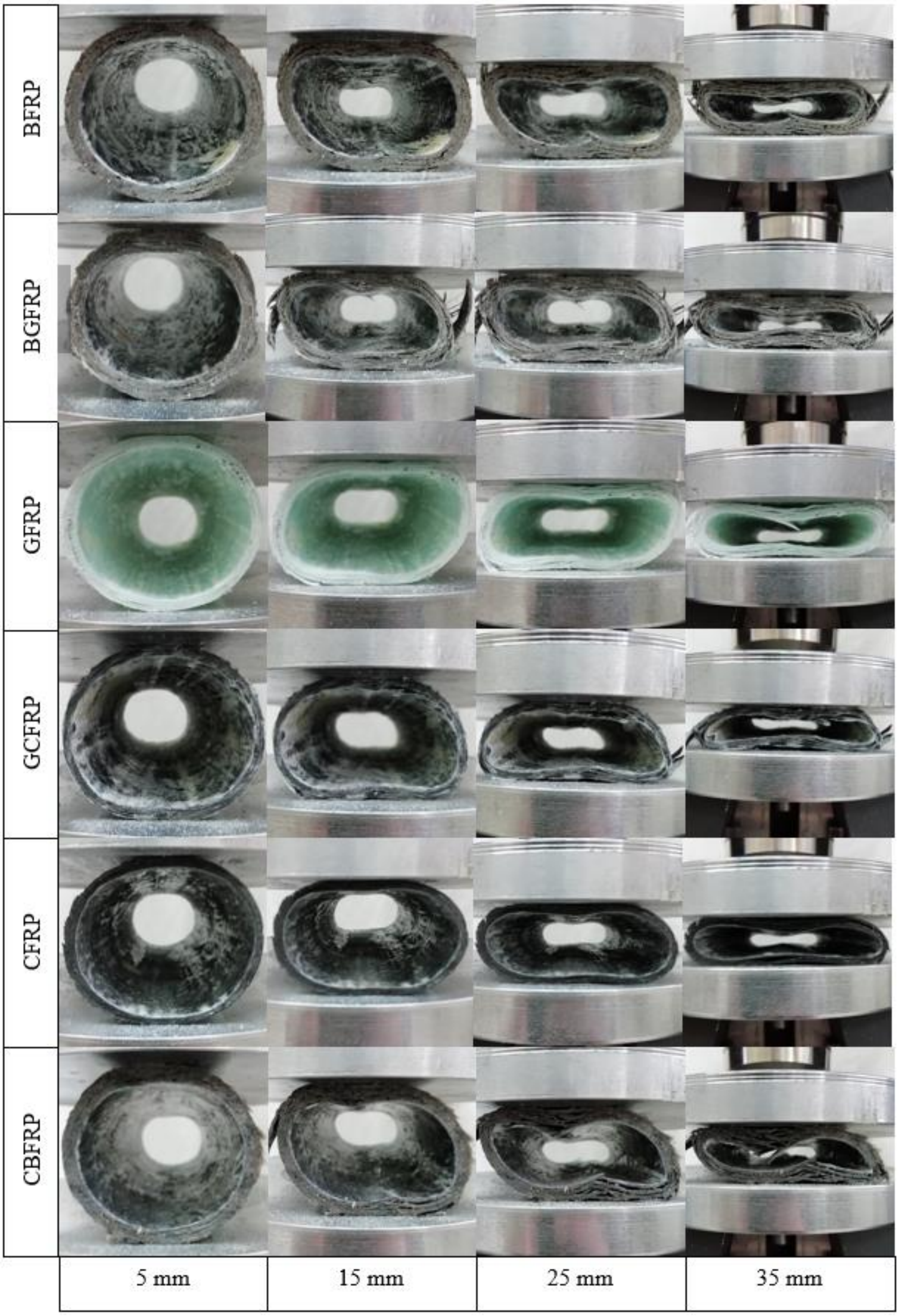

(a)

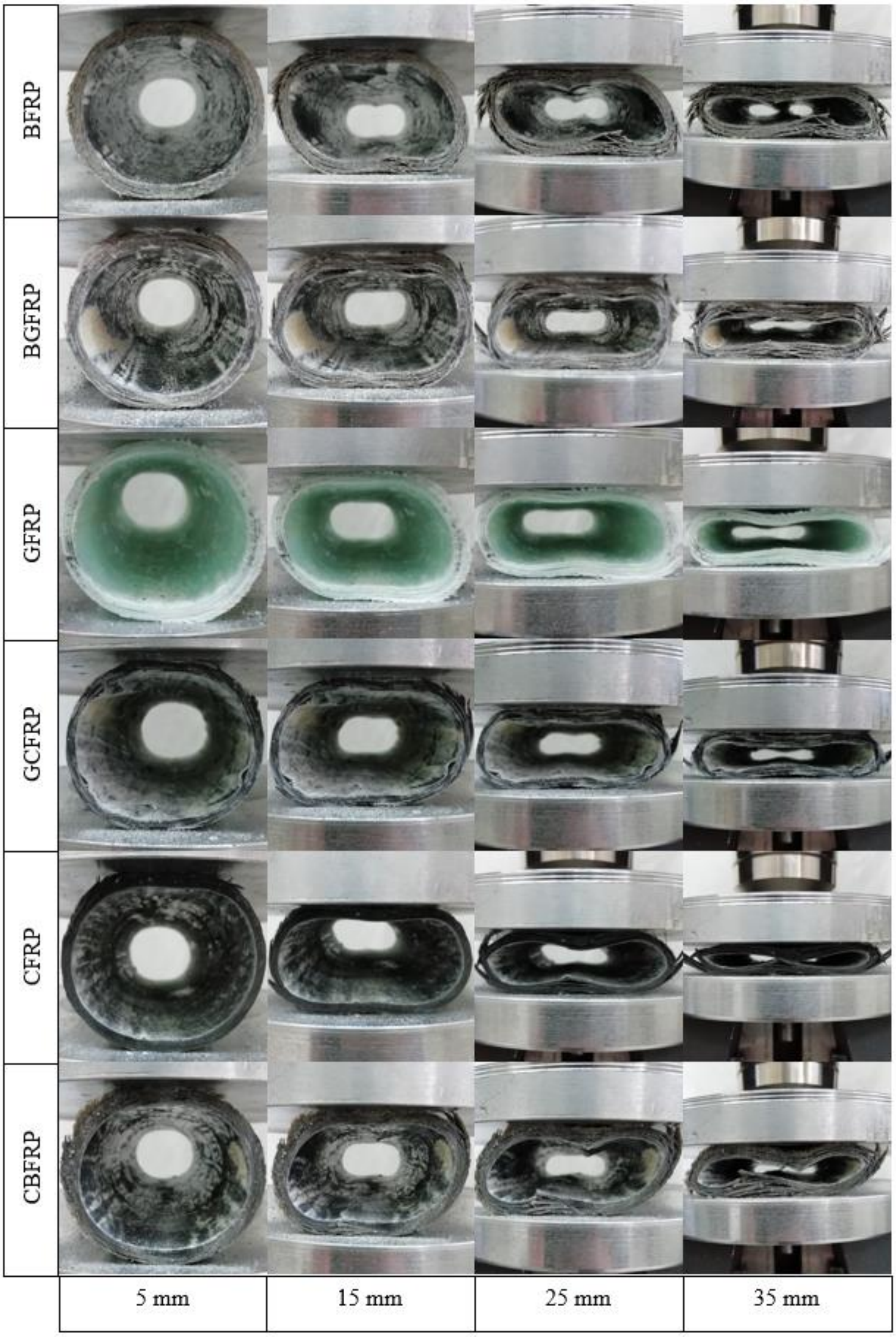

(b)

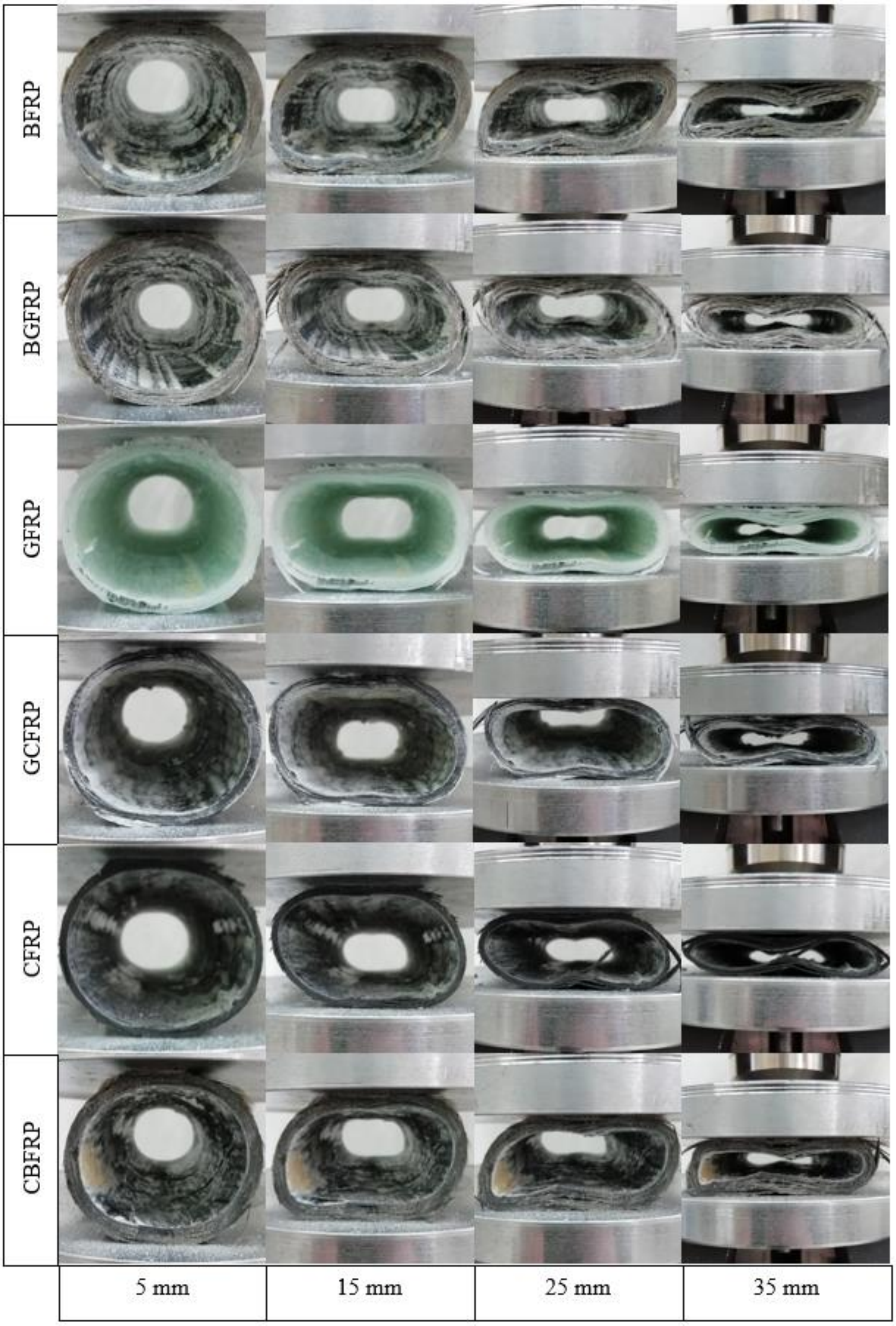

(c)

Figure 5.10 Crushing histories of the samples under lateral crushing; (a) ±(40°) fiber orientation, (b) ±(55°) fiber orientation, c) ±(70°) fiber orientation

The crushing histories of the samples with the fiber orientation of ±(40°), ±(55°) and ±(70°) were presented in Figure 5.10a-10c, respectively. For all samples, the separation between layers after matrix fragmentation was seen as main damage mechanisms. The fiber breakage was followed with delamination layer by layer. Additionally, stable lateral crushing process with buckling were obtained. The standard stable failure process as change in cross section from circular to elliptical were happened on all samples [45]. Fiber debonding as failure mode were seen on samples in mostly since weak interfacial adhesion between layers, especially in intraply ones. GCFRP samples behaved the similar characteristics with CFRP and GFRP. Basalt based intraply hybrid samples (BGFRP and CBFRP) showed the fiber debonding earlier than others. This can be attributed to the basalt fiber's thick structure caused the non-reliable bonding with related fibers.

After crushing application, the samples returned back an amount because of spring back effect. But, they did not take the original circular characteristics shapes due to plastic deformation and failure inside the samples. The last appearances of the samples with respect to different material combinations were given in Figure 5.11 as top and side view. The failure process was initiated with the matrix cracking and proceeding of delamination. Buckling of the samples, which caused the vertical cracks in mid plane, had the crucial role for fiber breakage. Fiber breakage failures were generally achieved as longitudinal cracks that happened a left and right sides of the samples. Differently, visual observations indicated that the outer skin of the BFRP having no fracture. Delamination took place as initial failure in this type of the samples. Lastly, the combination of fiber debonding, matrix cracking, delamination and fiber breakage of failures were observed in all samples as seen on crushed samples.

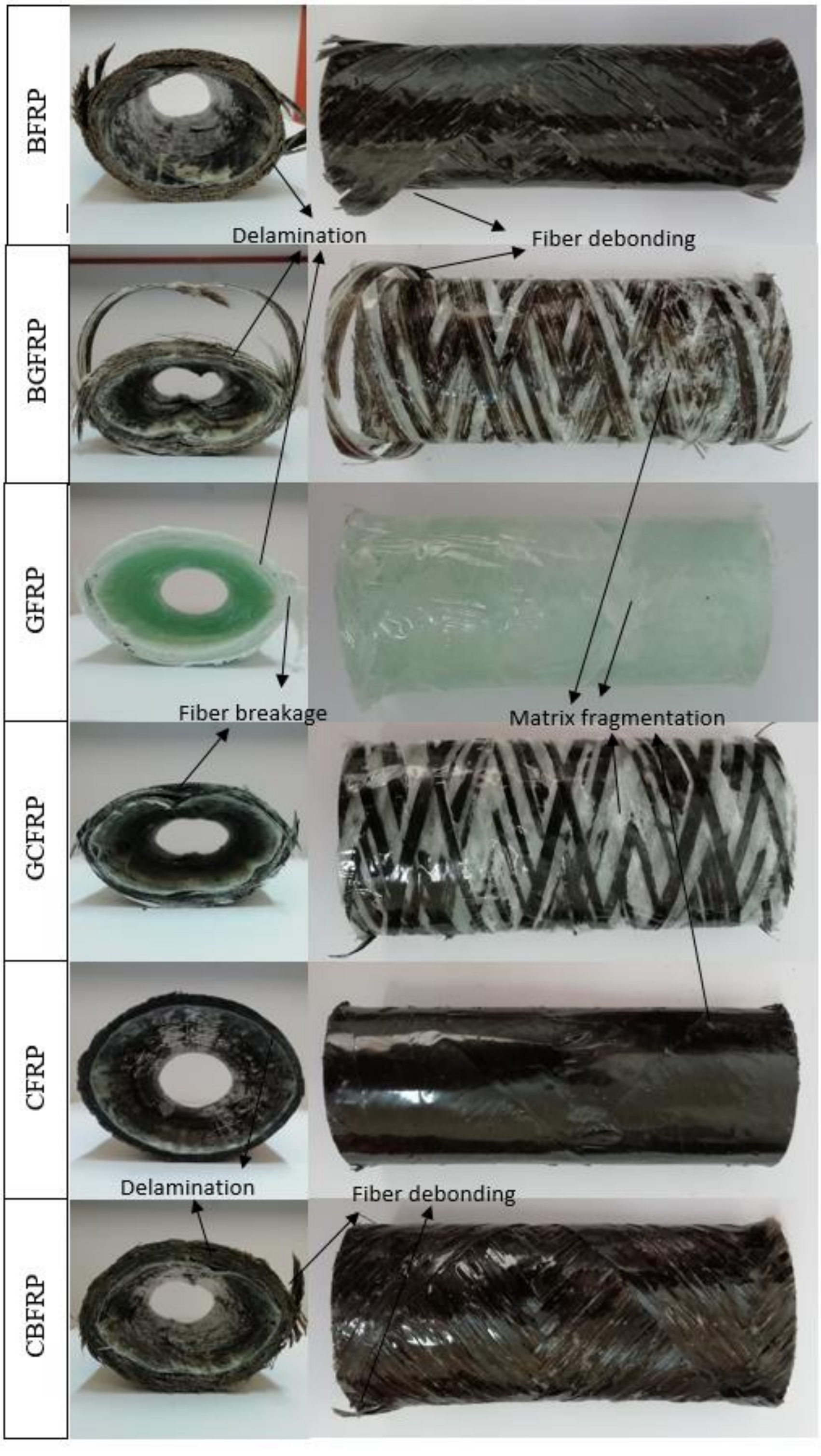

Figure 5.11 The samples after lateral crushing with front and top views

5.3.2 Crushing Load Efficiency

The initial peak load and the mean crushing load, which are references for the spring back values and the crush load stability, were shown in Figure 5.12. In general, load carrying capacity of hybrid samples had the average values of non-hybrid samples. 12.72 kN as maximum initial load was obtained from GFRP samples with ±(70°) fiber orientation. There was no regular tendency for intraply samples, but their values were in the range of non-hybrid FRPs. The mean crushing load values of CFRP were increased by addition of glass and basalt fibers (GCFRP and CBFRP). The improvements for ±(40°), ±(55°) and ±(70°) fiber orientations, were 44.86%, 43.62%, 107.63%, respectively, for glass fiber addition to CFRP. Also, CBFRP had 1.74, 1.57, 2.42 times of CFRP samples for mentioned orientations. BFRP exhibited the maximum mean crushing load values as 10.55 kN due to its heavier structure.

The lateral crushing load efficiency values for FRP samples of ±(40°), ±(55°) and ±(70°) fiber orientations were presented in Figure 5.13, respectively. In general cases of the lateral crushing application, mean load was greater than the initial peak load values. Consequently, more than 100% load efficiency, especially in intraply samples, took place on the results. It can be said that higher fiber orientation angle resulted in decrease for crushing load efficiency.

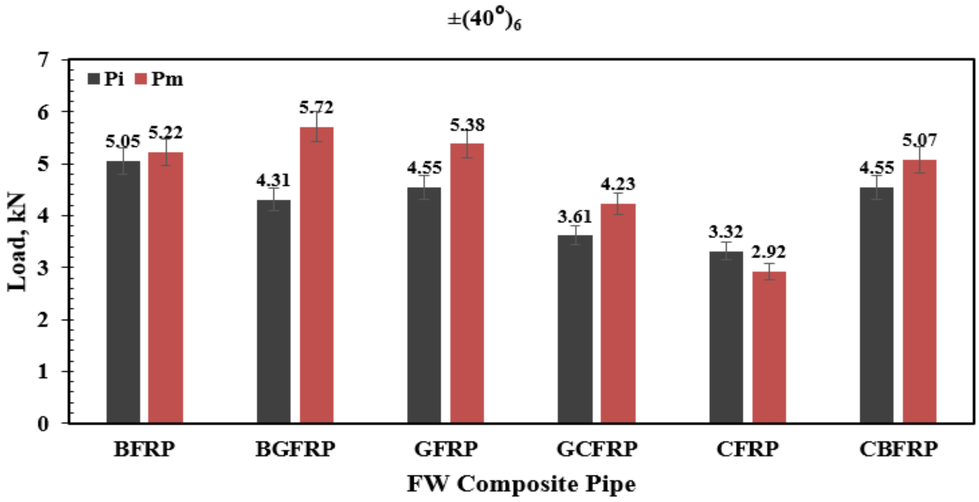

(a)

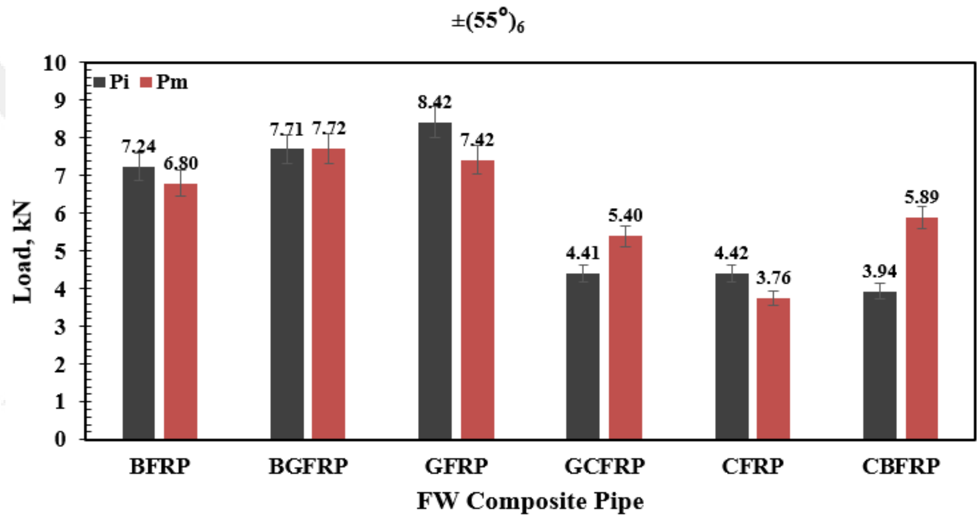

(b)

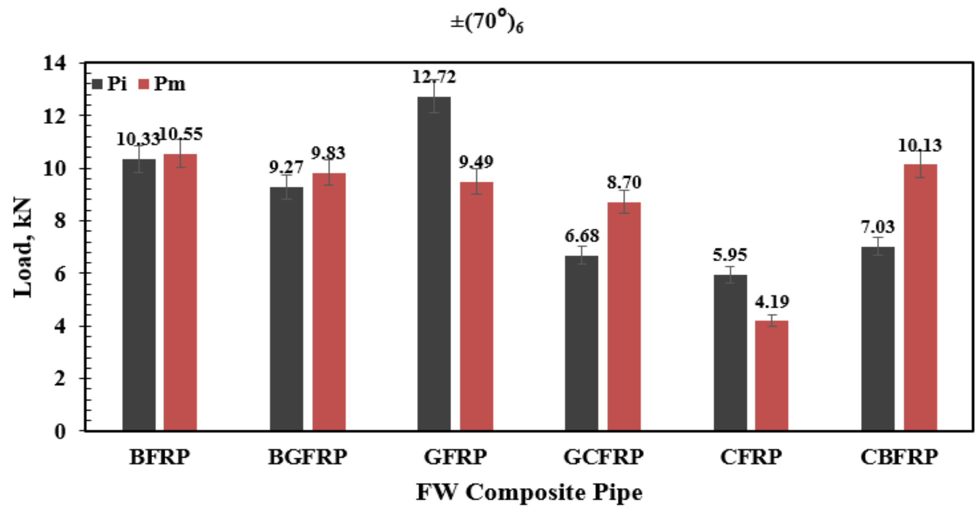

(c)

Figure 5.12 Lateral loading characteristics for (a) ±(40°) fiber orientation, (b) ±(55°) fiber orientation, c) ±(70°) fiber orientation

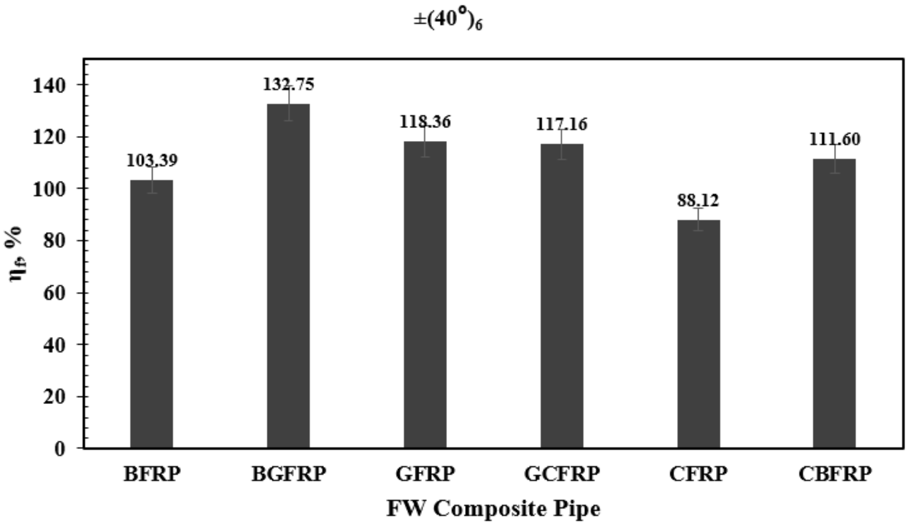

(a)

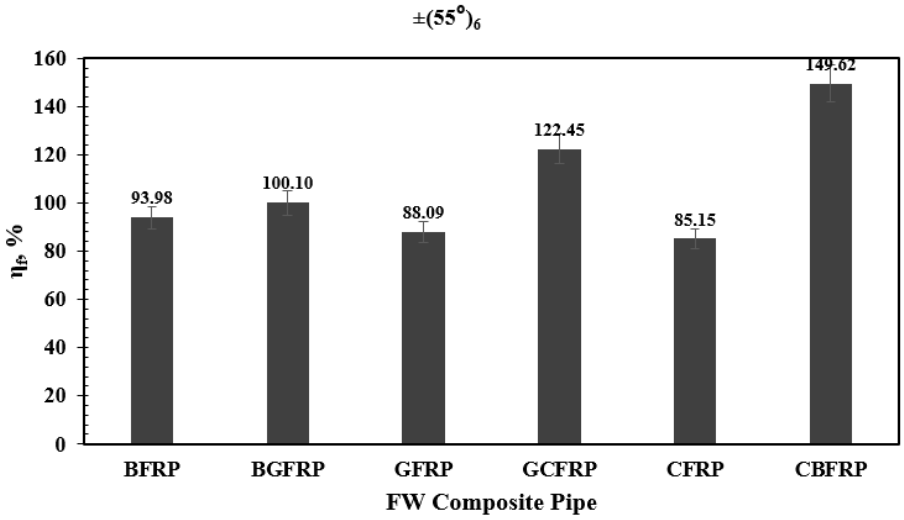

(b)

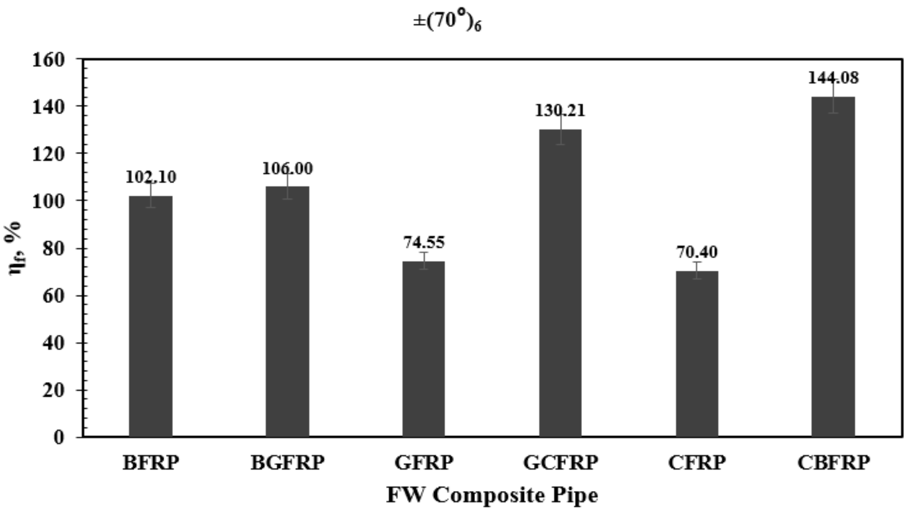

(c)

Figure 5.13 Lateral crushing load efficiency for (a) ±(40°) fiber orientation, (b) ±(55°) fiber orientation, c) ±(70°) fiber orientation

5.3.3 Energy Absorption

Total absorption energy of the samples with different fiber orientation angles were presented in Figure 5.14. GCFRP samples had the behavior between the carbon and glass fiber reinforced pipes as expected. However, basalt based intraply hybridizations (BGFRP and CBFRP) did not show the results in the range of combined fiber reinforcements. This can be explained by the heavier basalt monofilament diameter caused the more load carrying capacity. So, specific absorbed energy results can be more reliable within the aspect of energy absorption. By the way, maximum value of total energy absorption as 343.51 J was obtained from CBFRP intraply sample at ±(70°) fiber orientation.

The specific absorbed energy is a crucial parameter to understand crushing response of the samples due to mass consideration. According to different fiber orientation angles, specific absorbed energy values of the all samples were given in Figure 5.15. All intraply hybridized samples had the values in the range of non-hybrid FRPs. GCFRP had 1.15, 1.10 and 1.13 times higher values than CFRP for considered fiber orientations, so glass and carbon fiber combination gave the better material in this manner. Also, improvements as %3.54, 3.35% and 25.00% for ±(40°), ±(55°), ±(70°) configurations were achieved from the CBFRP samples compared to non-hybrid CFRP samples. Except ±(70°) fiber orientation, glass fiber inclusion to BFRP created a better material as seen from the results of BGFRP samples. In the view of above numerical results, intraply fiber hybridization was improved to absorb energy of the weaker non-hybrid fiber reinforced composite pipes.

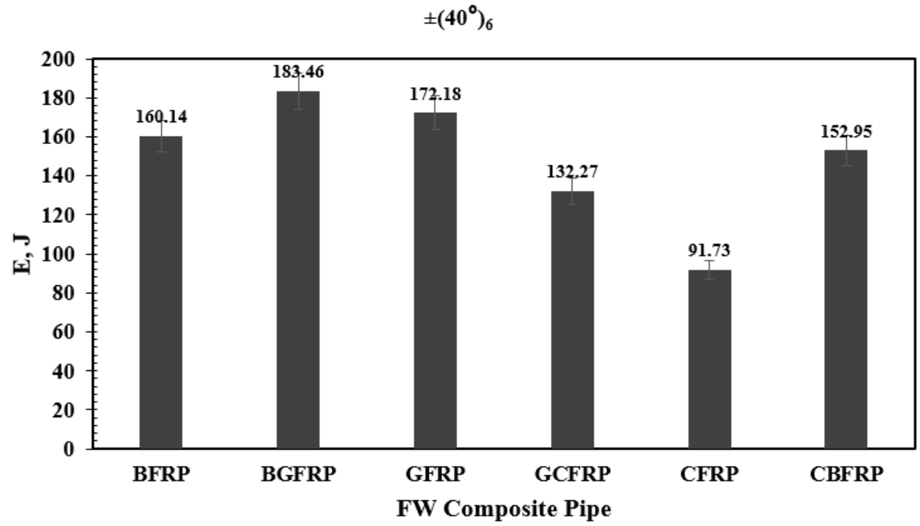

(a)

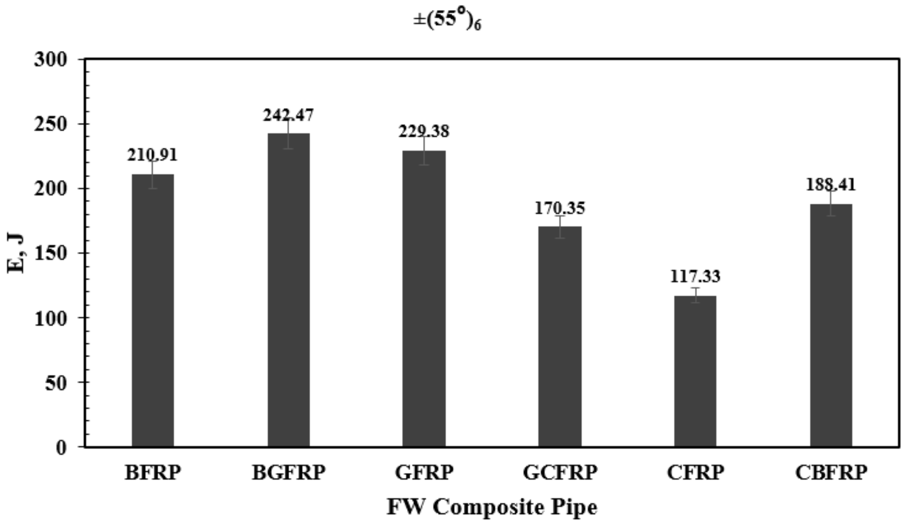

(b)

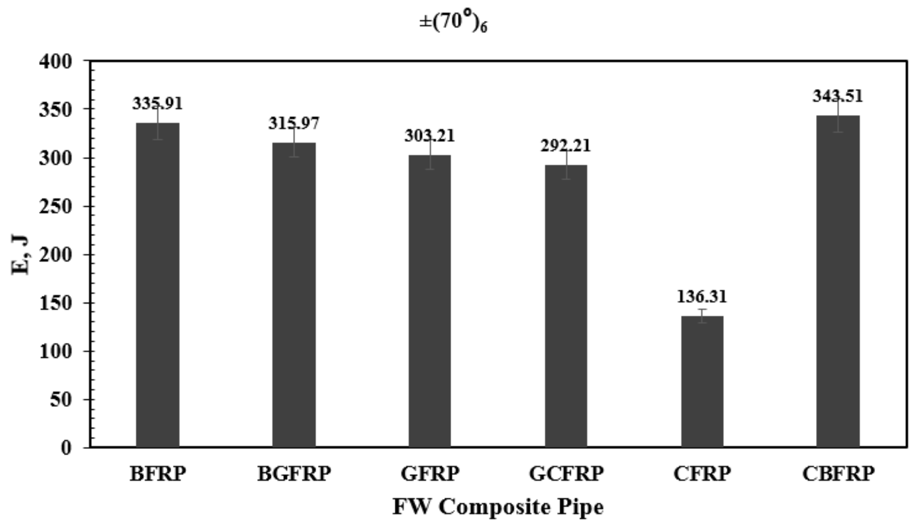

(c)

Figure 5.14 Total energy absorption in lateral crushing for (a) ±(40°) fiber orientation, (b) ±(55°) fiber orientation, c) ±(70°) fiber orientation

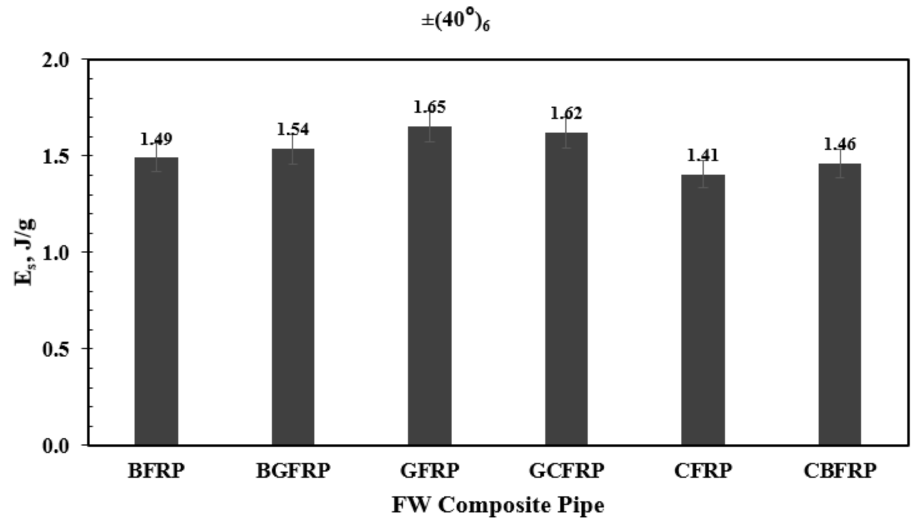

(a)

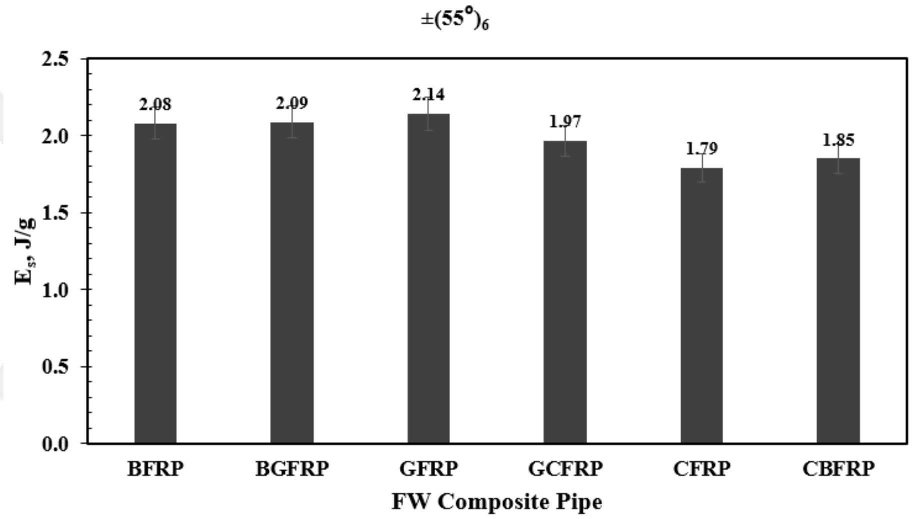

(b)

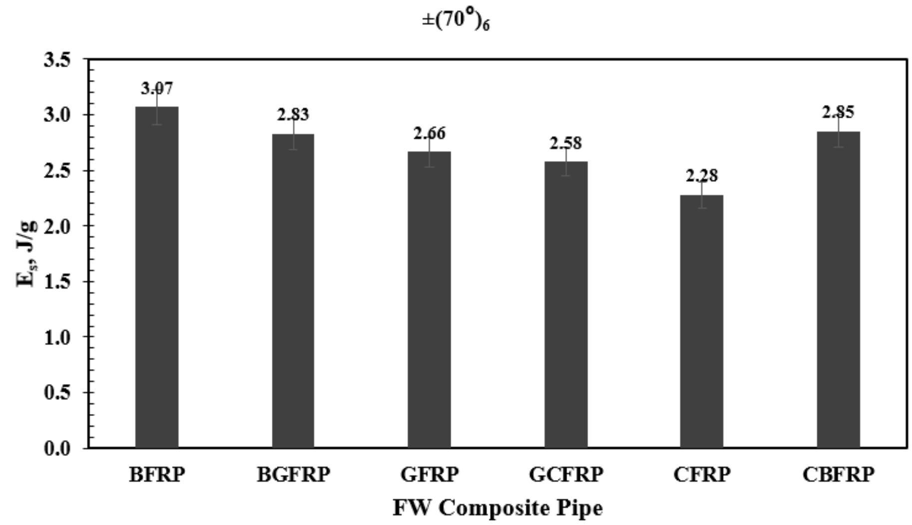

(c)

Figure 5.15 Specific absorbed energy in lateral crushing for (a) ±(40°) fiber orientation, (b) ±(55°) fiber orientation, c) ±(70°) fiber orientation

5.3.4 Effect of Fiber Orientation

The mass of the samples and the lateral crushing parameters such as initial peak load, mean load, crushing load efficiency, absorbed energy, and specific energy absorption, of the laterally crushed samples were given in Table 5.2. It could be found that the fiber orientation angle had a significant influences on all parameters. With an increase in angle, initial peak load, mean crushing load, total energy absorption and specific absorbed energy of the samples displayed the increase trend while the crush load efficiency showed the slightly decrease tendency as expected [106]. The increase in the spring back load values were 104.55%, 115.08%, 179.56%, 85.04%, 79.21%, 54.05% for BFRP, BGFRP, GFRP, GCFRP, CFRP, CBFRP, respectively. There were little tendency faults in the load efficiency of the intraply samples because of their poor surface quality compared with the non-hybrid ones. The maximum specific absorbed energy was recorded as 3.07 J/g from BFRP sample at ±(70°) fiber orientation angle. The minimum and maximum improvements of the specific absorbed energy were achieved as 59.26% and 106.04% for the GCFRP and BFRP samples, respectively. Total energy absorption and the specific absorbed energy tends to increase trend because of the approaching fiber orientation to loading direction which shows maximum strength.

Table 5.2 Crashworthiness parameters under quasi-static lateral compression loading

FRP	α (°)	m (g)	P_i (kN)	P_m (kN)	η_f (%)	E (J)	E_s (J/g)
BFRP	40°	107.37	5.05	5.22	103.39	160.14	1.49
	55°	101.33	7.24	6.80	93.98	210.91	2.08
	70°	109.51	10.33	10.55	102.10	335.91	3.07
BGFRP	40°	119.37	4.31	5.72	132.75	183.46	1.54
	55°	116.02	7.71	7.72	100.10	242.47	2.09
	70°	111.66	9.27	9.83	106.00	315.97	2.83
GFRP	40°	104.15	4.55	5.38	118.36	172.18	1.65
	55°	107.14	8.42	7.42	88.09	229.38	2.14
	70°	113.80	12.72	9.49	74.55	303.21	2.66
GCFRP	40°	81.57	3.61	4.23	117.16	132.27	1.62
	55°	86.59	4.41	5.40	122.45	170.35	1.97
	70°	113.43	6.68	8.70	130.21	292.21	2.58
CFRP	40°	65.22	3.32	2.92	88.12	91.73	1.41
	55°	65.52	4.42	3.76	85.15	117.33	1.79
	70°	59.91	5.95	4.19	70.40	136.31	2.28
CBFRP	40°	104.60	4.55	5.07	111.60	152.95	1.46
	55°	101.83	3.94	5.89	149.62	188.41	1.85
	70°	120.44	7.03	10.13	144.08	343.51	2.85

CHAPTER VI

CONCLUSIONS

The effects of intraply fiber hybridization on the tensile, compression and crushing characteristics of the filament wound composite pipes were experimentally examined to close literature gap in this subject. For this purpose, split-disk method for tensile response, external parallel-plate loading for compression and crushing characteristics of pipes were examined. Furthermore, fiber content values of the prepared samples were determined by ignition loss technique. The efficiency of hybridization with respect to fiber orientation was also analyzed by preparing composite pipes with different winding angles. The main conclusions drawn from these studies can be summarized as follows:

Ignition Loss Experiments:

- Maximum fiber content as 71.46% in average was obtained from GFRP samples.
- Intraply hybrid samples had the lowest fiber content since resin mixture having more volume caused from the difference between filament diameters of the fiber reinforcements.

Hoop Tensile Experiments by Split-Disk Method:

- Maximum apparent hoop tensile strength were found as 580.95 MPa in CFRP at $\pm(70°)_6$, while the minimum one was 72.63 MPa in GCFRP at ±(40°).
- The negative effect as deteriorations was found in the range of 9.7% (GCFRP compared to GFRP at ±(70°) fiber orientation) and 66.5% (CBFRP compared to CFRP at $\pm(40°)_6$ fiber orientation) for all intraply hybridized of FRPs because of the poor ability to merger characteristics between the fibers reinforcements.
- For the fiber orientation impression; all samples showed the remarkable apparent hoop tensile strength improvement when increasing of fiber orientation angle or, in other words, when the fiber direction was approached to loading direction.

- According to hoop tensile modulus results; all samples except ±(40°) fiber orientation gave the parallel trend with tensile characteristics.
- With the increase in fiber orientation angle, intraply hybrid fiber reinforced pipes showed the higher displacement values at break points, while non-hybrid samples exhibited decreasing trend.
- Failure modes in this test were followed as matrix fragmentation, fiber crazing, delamination, fiber breakage in winding direction for non-hybrid FRPs and finally fiber pull out for intraply hybrid FRPs, respectively.

Quasi-Static Axial Compression Experiments:

- The maximum apparent tensile strength were recorded in non-hybrid CFRP (106.59 MPa) at ±(70°), while the minimum one was obtained in non-hybrid BFRP (46.08 MPa) at ±(40°).
- Carbon fiber inclusion to GFRP and BFRP or glass fiber addition to BFRP improved the compression behaviors.
- The modulus of elasticity of intraply FRPs looked like parallel tendency with stress characteristics.
- The compression damage of non-hybrid FRPs showed the progressive failure that begins at the top or bottom cross-section of samples. Intraply FRP samples behaved three different failure types. BGFRP depending the fiber orientations had the parallel-to-fiber cracking and progressive failures. GCFRP and CBFRP samples regardless of fiber orientations resulted with the catastrophic and fiber pull out failure modes, respectively.
- Fiber orientation angles indicated no significant differences on failure modes of FRPs.
- Matrix fragmentations as first failure followed by progressive folding or parallel-to-fiber cracking were observed for all samples.

Quasi-Static Radial Compression Experiments:

- BFRP (± (70°)) with 27.65 MPa was found as the most rigid material in terms of pipe stiffness.
- The pipe stiffness characteristics of CFRP samples were increased by inclusion of glass or basalt fiber for all fiber orientation angles.

- The material gained the better rigidity in terms of pipe stiffness with increase in fiber orientation angle.
- The stiffness factor of the intraply hybrid FRP samples showed the parallel trend with the stiffness characteristics. As the fiber orientation angle increased, higher stiffness factor values were obtained for all samples.
- All pipes showed the crazing, matrix cracking and layer delamination for the failure modes, respectively. Furthermore, intraply hybrid fiber reinforced samples showed the fiber debonding caused from weak interfacial adhesion between layers.

Axial Crushing Experiments:

- All samples had progressive crushing with high energy absorption and good reproducibility for all fiber orientations except GFRP.
- Hybridization process with better repeatability enabled more stable crushing process compared with non-hybrid FRPs for all fiber orientation.
- Increase in fiber orientation angle resulted with inner and outer irregular splaying behaviors of the fibers and intensifying of fronds. The combination of failure modes of fiber debonding, matrix fragmentation, delamination and fiber breakage were observed in most samples as seen on crushed shapes.
- Increase in fiber orientation angle resulted with decrease in total energy absorption.
- BGFRP sample results remained within the range of GFRP and BFRP values not only in total energy absorption but also in specific energy absorption.
- The maximum specific absorbed energy as 47.02 J/g was found from CFRP sample at ±(40°) of fiber orientation.
- The carbon fiber inclusion to GFRP provided 16.06%, 15.09% and 23.1% improvements for ±(40°), ±(55°), and ±(70°) fiber orientations, respectively. Also, CBFRP showed increments as 1.1, 1.2 and 1.3 times of BFRP results.

Lateral Crushing Experiments:

- For all samples, the separation between layers after matrix fragmentation was seen as main damage mechanisms. The delamination followed fiber breakage layer by layer. Additionally, stable lateral crushing process with buckling were obtained.
- An increase in fiber orientation angle resulted with increase in load carrying capacity.

- GFRP at ±(70°) fiber orientation had the maximum initial loading peak value and the most regular curve.
- The standard stable failure process as change in cross section from circular to elliptical were happened on all samples.
- Fiber debonding as failure mode were seen on samples in mostly due to weak interfacial adhesion between layers, especially in intraply ones.
- In general, load carrying capacity of hybrid FRPs had the values between the results of non-hybrid constituent.
- 12.72 kN as the maximum initial load was obtained from GFRP samples having ±(70°) fiber orientation.
- The mean crushing load values of CFRP were increased with the inclusion of glass and basalt fibers (GCFRP and CBFRP). BFRP exhibited the maximum mean crushing load values as 10.55 kN due to its heavier structure.
- Higher fiber orientation angle resulted in decrease for crushing load efficiency.
- GCFRP samples showed the results between the values obtained from CFRP and GFRP. However, basalt based intraply hybridizations (BGFRP and CBFRP) did not show the results in the range of combined fiber reinforcements due to higher load carrying capacity.
- All intraply hybridized pipe samples showed the specific absorbed energy values within the range of non-hybrid composite pipe samples that composed of each fiber reinforcement.

In the view of above experimental results, intraply fiber hybridization improved to absorb energy of the non-hybrid weaker components of a composite system. Furthermore, hybrid samples giving the results within the range of non-hybrid versions of each components in mostly, in terms of examined parameters except tensile characteristics, proved that two fibers can be united functionally in applications.

CHAPTER VII

FUTURE WORKS

Following aspects are noted for the possible continuation of this study:

- Effect of intraply hybridization on impact, fatigue or pressure loading response of FRP samples,
- Influence of natural and synthetic fiber hybridization on mechanical properties of FRP structures,
- Thermal and aqueous aging effects on mechanical behaviors of FRPs,
- The effects of nanofillers on mechanical and dynamic behavior of filament wound structures,
- The performance comparison of interply and intraply fiber hybridization of FRP at different parameters (fiber orientation, mandrel diameter, number of layers etc.).

REFERENCES

[1] Koussios, S., & Bergsma, O. K. (2006). Friction experiments for filament winding applications, *Journal of Thermoplastic Composite Materials*, **19(1)**, 5-34.

[2] Abdalla, F. H., Mutasher, S. A., Khalid, Y. A., Sapuan, S. M., Hamouda, A. M. S., Sahari, B. B., & Hamdan, M. M. (2007). Design and fabrication of low cost filament winding machine, *Materials & design*, **28(1)**, 234-239.

[3] Koppert, J. J. M., De Boer, H., Weustink, A. P. D., Beukers, A., & Bersee, H. E. N. (2007). Virtual testing of dry filament wound thick walled pressure vessels, *In 16th International Conference on Composite Materials*.

[4] DuVall, F. W. (2001). Cost comparisons of wet filament winding versus prepreg filament winding for Type II and Type IV CNG cylinders, *SAMPE JOURNAL*, **37(1)**, 38-42.

[5] Peters, S. T. (Ed.). (2011). Composite filament winding. United States of America: ASM International.

[6] Peters, S. T., & Tarnopol'skii, Y. M. (1997). Filament winding. In Composites Engineering Handbook (pp. 527-560). United States: CRC Press.

[7] Hwang, J. H., Kwon, O., Lee, C. S., & Hwang, W. (2000). Interlaminar fracture and low-velocity impact of carbon/epoxy composite materials, *Mechanics of composite materials*, **36(2)**, 117-130.

[8] Bozkurt, Ö. Y., Erkliğ, A., & Bulut, M. (2018). Hybridization effects on Charpy impact behavior of basalt/aramid fiber reinforced hybrid composite laminates, *Polymer Composites*, **39(2)**, 467-475.

[9] Hanson, M. P. (1969). Tensile and cyclic fatigue properties of graphite filament-wound pressure vessels at ambient and cryogenic temperatures.

[10] Avci, A., Şahin, Ö. S., & Tarakçioğlu, N. (2007). Fatigue behavior of surface cracked filament wound pipes with high tangential strength in corrosive environment, *Composites Part A: Applied Science and Manufacturing*, **38(4)**, 1192-1199.

[11] Hernandez-Moreno, H., Douchin, B., Collombet, F., Choqueuse, D., & Davies, P. (2008). Influence of winding pattern on the mechanical behavior of filament wound composite cylinders under external pressure, *Composites Science and Technology*, **68(3-4)**, 1015-1024.

[12] Xia, M., Takayanagi, H., & Kemmochi, K. (2001). Analysis of multi-layered filament-wound composite pipes under internal pressure, *Composite Structures*, **53(4)**, 483-491.

[13] Jia, X., Chen, G., Yu, Y., Li, G., Zhu, J., Luo, X., ... & Hui, D. (2013). Effect of geometric factor, winding angle and pre-crack angle on quasi-static crushing behavior of filament wound CFRP cylinder, *Composites Part B: Engineering*, **45(1)**, 1336-1343.

[14] Soden, P. D., Kitching, R., Tse, P. C., Tsavalas, Y., & Hinton, M. J. (1993). Influence of winding angle on the strength and deformation of filament-wound composite tubes subjected to uniaxial and biaxial loads, *Composites Science and Technology*, **46(4)**, 363-378.

[15] Fitriah, S. N., Majid, M. A., Ridzuan, M. J. M., Daud, R., Gibson, A. G., & Assaleh, T. A. (2017). Influence of hydrothermal ageing on the compressive behaviour of glass fibre/epoxy composite pipes, *Composite structures*, **159**, 350-360.

[16] Misri, S., Ishak, M. R., Sapuan, S. M., & Leman, Z. (2015). The effect of winding angles on crushing behavior of filament wound hollow kenaf yarn fibre reinforced unsaturated polyester composites, *Fibers and Polymers*, **16(10)**, 2266-2275.

[17] Deniz, M. E., & Karakuzu, R. (2012). Seawater effect on impact behavior of glass–epoxy composite pipes, *Composites Part B: Engineering*, **43(3)**, 1130-1138.

[18] Sari, M., Karakuzu, R., Deniz, M. E., & Icten, B. M. (2012). Residual failure pressures and fatigue life of filament-wound composite pipes subjected to lateral impact, *Journal of Composite Materials*, **46(15)**, 1787-1794.

[19] Hawa, A., Majid, M. A., Afendi, M., Marzuki, H. F. A., Amin, N. A. M., Mat, F., & Gibson, A. G. (2016). Burst strength and impact behaviour of hydrothermally aged glass fibre/epoxy composite pipes, *Materials & Design*, **89**, 455-464.

[20] Mertiny, P., Ellyin, F., & Hothan, A. (2004). An experimental investigation on the effect of multi-angle filament winding on the strength of tubular composite structures, *Composites science and technology*, **64(1)**, 1-9.

[21] Sayman, O. (2005). Analysis of multi-layered composite cylinders under hygrothermal loading, *Composites Part A: Applied Science and Manufacturing*, **36(7)**, 923-933.

[22] Kim, C. U., Kang, J. H., Hong, C. S., & Kim, C. G. (2005). Optimal design of filament wound structures under internal pressure based on the semi-geodesic path algorithm, *Composite structures*, **67(4)**, 443-452.

[23] Kaynak, C., Erdiller, E. S., Parnas, L., & Senel, F. (2005). Use of split-disk tests for the process parameters of filament wound epoxy composite tubes, *Polymer testing*, **24(5)**, 648-655.

[24] Meijer, G., & Ellyin, F. (2008). A failure envelope for±60 filament wound glass fibre reinforced epoxy tubulars, *Composites Part A: Applied Science and Manufacturing*, **39(3)**, 555-564.

[25] Akkus, N., Genc, G., & Girgin, C. (2008). Control of the pretension in filament winding process, *acta mechanica et automatica*, **2(3)**, 5-10.

[26] Tarakçioğlu, N., Gemi, L., & Yapici, A. (2005). Fatigue failure behavior of glass/epoxy±55 filament wound pipes under internal pressure, *Composites science and technology*, **65(3-4)**, 703-708.

[27] Moon, C. J., Kim, I. H., Choi, B. H., Kweon, J. H., & Choi, J. H. (2010). Buckling of filament-wound composite cylinders subjected to hydrostatic pressure for underwater vehicle applications, *Composite Structures*, **92(9)**, 2241-2251.

[28] Arikan, H. (2010). Failure analysis of $(\pm 55)_3$ filament wound composite pipes with an inclined surface crack under static internal pressure, *Composite Structures*, **92(1)**, 182-187.

[29] Khalifa, A. B., Zidi, M., & Abdelwahed, L. (2012). Mechanical characterization of glass/vinylester±55° filament wound pipes by acoustic emission under axial monotonic loading, *Comptes Rendus Mécanique*, **340(6)**, 453-460.

[30] Sari, M., Karakuzu, R., Deniz, M. E., & Icten, B. M. (2012). Residual failure pressures and fatigue life of filament-wound composite pipes subjected to lateral impact, *Journal of Composite Materials*, **46(15)**, 1787-1794.

[31] Deniz, M. E., Ozen, M., Ozdemir, O., Karakuzu, R., & Icten, B. M. (2013). Environmental effect on fatigue life of glass–epoxy composite pipes subjected to impact loading, *Composites Part B: Engineering*, **44(1)**, 304-312.

[32] Rodriguez, E. S., Alvarez, V. A., & Montemartini, P. E. (2013). Failure analysis of a GFRP pipe for oil transport, *Engineering Failure Analysis*, **28**, 16-24.

[33] Rafiee, R. (2013). Experimental and theoretical investigations on the failure of filament wound GRP pipes, *Composites Part B: Engineering*, **45(1)**, 257-267.

[34] Martins, L. A. L., Bastian, F. L., & Netto, T. A. (2013). The effect of stress ratio on the fracture morphology of filament wound composite tubes, *Materials & Design*, **49**, 471-484.

[35] Uyaner, M., Kara, M., & Şahin, A. (2014). Fatigue behavior of filament wound E-glass/epoxy composite tubes damaged by low velocity impact, *Composites Part B: Engineering*, **61**, 358-364.

[36] Demirci, M. T., Tarakçıoğlu, N., Avcı, A., & Erkendirci, Ö. F. (2014). Fracture toughness of filament wound BFR and GFR arc shaped specimens with Charpy impact test method, *Composites Part B: Engineering*, **66**, 7-14.

[37] Perillo, G., Vedivik, N. P., & Echtermeyer, A. T. (2015). Numerical and experimental investigation of impact on filament wound glass reinforced epoxy pipe, *Journal of Composite Materials*, **49(6)**, 723-738.

[38] Pranesh, K., Majid, M. S., Afendi, M., Marzuki, H., Kazim, M., & Fakhzan, M. N. (2014). Short-Term Test of ±55° Filament Wound GRE Composite Pipes under Multiaxial Stress Ratios, *In Applied Mechanics and Materials* (**Vol. 554**, pp. 371-375). Trans Tech Publications.

[39] Perillo, G., Vacher, R., Grytten, F., Sørbø, S., & Delhaye, V. (2014). Material characterisation and failure envelope evaluation of filament wound GFRP and CFRP composite tubes, *Polymer Testing*, **40**, 54-62.

[40] Krishnan, P., Majid, M. A., Afendi, M., Gibson, A. G., & Marzuki, H. F. A. (2015). Effects of winding angle on the behaviour of glass/epoxy pipes under multiaxial cyclic loading, *Materials & Design*, **88**, 196-206.

[41] Mahdavi, H. R., Rahimi, G. H., & Farrokhabadi, A. (2016). Failure analysis of (±55) 9 filament-wound GRE pipes using acoustic emission technique, *Engineering Failure Analysis*, **62**, 178-187.

[42] TAŞYÜREK, M., & TARAKCIOĞLU, N. (2015). Karbon Nanotüp ile Modifiye Edilmiş Filaman Sarım Boruların İç Basınç Altındaki Hasar Davranış, *Politeknik Dergisi*, **18(4)**, 211-217.

[43] Hafeez, F., & Almaskari, F. (2015). Experimental investigation of the scaling laws in laterally indented filament wound tubes supported with V shaped cradles, *Composite Structures*, **126**, 265-284.

[44] Hawa, A., Majid, M. A., Afendi, M., Marzuki, H. F. A., Amin, N. A. M., Mat, F., & Gibson, A. G. (2016). Burst strength and impact behaviour of hydrothermally aged glass fibre/epoxy composite pipes, *Materials & Design*, **89**, 455-464.

[45] Almeida Jr, J. H. S., Ribeiro, M. L., Tita, V., & Amico, S. C. (2016). Damage and failure in carbon/epoxy filament wound composite tubes under external pressure: Experimental and numerical approaches, *Materials & Design*, **96**, 431-438.

[46] Üstün, T., Eskizeybek, V., & Avci, A. (2016). Enhanced fatigue performances of hybrid nanoreinforced filament wound carbon/epoxy composite pipes, *Composite Structures*, **150**, 124-131.

[47] Sebaey, T. A., & Mahdi, E. (2016). Crashworthiness of pre-impacted glass/epoxy composite tubes, *International Journal of Impact Engineering*, **92**, 18-25.

[48] Wang, Y., Feng, J., Wu, J., & Hu, D. (2016). Effects of fiber orientation and wall thickness on energy absorption characteristics of carbon-reinforced composite tubes under different loading conditions, *Composite Structures*, **153**, 356-368.

[49] Roslan, M. N., Yahya, M. Y., Ahmad, Z., Rashid, A., Hani, A., & Wang, W. X. (2018). Energy Absorption Capacity of Basalt Sandwich Composite Cylinder Subjected to Axial Compression Loadings, *In Materials Science Forum* (**Vol. 917**, pp. 7-11). Trans Tech Publications.

[50] Mahdi, E., Hamouda, A. A., & Sebaey, T. A. (2014). The effect of fiber orientation on the energy absorption capability of axially crushed composite tubes, *Materials & Design (1980-2015)*, **56**, 923-928.

[51] Farley, G. L., & Jones, R. M. (1992). Crushing characteristics of continuous fiber-reinforced composite tubes, *Journal of composite Materials*, **26(1)**, 37-50.

[52] Lapena, M. H., & Marinucci, G. (2018). Mechanical Characterization of Basalt and Glass Fiber Epoxy Composite Tube, *Materials Research*, **21(1)**.

[53] Barış Elektirik Endüstrisi A. Ş. (1996). Filaman sargı tekniği ile kompozit malzeme kullanılarak yüksek basınca dayanıklı optimum boru tasarımı, *Tübitak*, MİSAG-39.

[54] Pivacek, A. (2001). A computer controlled filament winding technique for manufacturing cement based composite laminates (Master's thesis, Arizona State University).

[55] Genç, G. (2008). Elyaf sarma yöntemiyle üretilen karbon elyaf kompozitlerde ön gerilme parametrelerinin elyaf ve kompozit mukavemetine etkisi (PhD thesis, Marmara University).

[56] Sarı, M. (2010). Sea water effect on composite pipes subjected to impact loading (Master's thesis, Dokuz Eylül University).

[57] Skjærholt, I. (2012). Integration Tools for Design and Process Control of Filament Winding (Master's thesis, Norwegian University of Science and Technology).

[58] Görücü, Ü. (2011). Elyaf takviyeli boğumla kuvvetlendirilmiş kompozit boruların sonlu elemanlar yöntemi ile geometric optimizasyonu (PhD thesis, Marmara University).

[59] Deniz, M. E. (2011). Sea water effect on behaviors of impact and axial compression-after impact of composite pipes (Master's thesis, Dokuz Eylül University).

[60] Balya, B. (2004). Design and analysis of filament wound composite tubes (Master's thesis, Middle East Technical University).

[61] Erdiller, E. S. (2004). Experimental investigation for mechanical properties of filament wound composite tubes (Master's thesis, Middle East Technical University).

[62] Dons, K. (2013). Filament winding of composite tubes (Master's thesis, Norwegian University of Science and Technology).

[63] Ha, S. K., Kim, S. J., Nasir, S. U., & Han, S. C. (2012). Design optimization and fabrication of a hybrid composite flywheel rotor, *Composite Structures*, **94(11)**, 3290-3299.

[64] Xu, J., Ma, Y., Zhang, Q., Sugahara, T., Yang, Y., & Hamada, H. (2016). Crashworthiness of carbon fiber hybrid composite tubes molded by filament winding, *Composite Structures*, **139**, 130-140.

[65] Esnaola, A., Ulacia, I., Aretxabaleta, L., Aurrekoetxea, J., & Gallego, I. (2015). Quasi-static crush energy absorption capability of E-glass/polyester and hybrid E-glass–basalt/polyester composite structures, *Materials & Design*, **76**, 18-25.

[66] Ma, Y., Sugahara, T., Yang, Y., & Hamada, H. (2015). A study on the energy absorption properties of carbon/aramid fiber filament winding composite tube, *Composite Structures*, **123**, 301-311.

[67] Zuraida, A., Khalid, A. A., & Ismail, A. F. (2007). Performance of hybrid filament wound composite tubes subjected to quasi static indentation, *Materials & design*, **28(1)**, 71-77.

[68] Cicala, G., Cristaldi, G., Recca, G., Ziegmann, G., El-Sabbagh, A., & Dickert, M. (2009). Properties and performances of various hybrid glass/natural fibre composites for curved pipes, *Materials & Design*, **30(7)**, 2538-2542.

[69] Talib, A. A., Ali, A., Badie, M. A., Lah, N. A. C., & Golestaneh, A. F. (2010). Developing a hybrid, carbon/glass fiber-reinforced, epoxy composite automotive drive shaft, *Materials & Design*, **31(1)**, 514-521.

[70] Kim, J. S., Yoon, H. J., & Shin, K. B. (2011). A study on crushing behaviors of composite circular tubes with different reinforcing fibers, *International Journal of Impact Engineering*, **38(4)**, 198-207.

[71] Ha, S. K., Kim, S. J., Nasir, S. U., & Han, S. C. (2012). Design optimization and fabrication of a hybrid composite flywheel rotor, *Composite Structures*, **94(11)**, 3290-3299.

[72] Kim, S. J., Hayat, K., Nasir, S. U., & Ha, S. K. (2014). Design and fabrication of hybrid composite hubs for a multi-rim flywheel energy storage system, *Composite structures*, **107**, 19-29.

[73] Kumar, K. V., Sait, A. N., & Panneerselvam, K. (2014). Machinability study of hybrid-polymer composite pipe using response surface methodology and genetic algorithm, *Journal of Sandwich Structures & Materials*, **16(4)**, 418-439.

[74] Häußler, M., Schatz, M., Baier, H., & Mertiny, P. (2015, July). Optimization of Polymer Composite Pipe Under Consideration of Hybridization. *In ASME*

2015 Pressure Vessels and Piping Conference (pp. V003T03A010-V003T03A010).

[75] Gemi, L., Kara, M., & Avci, A. (2016). Low velocity impact response of prestressed functionally graded hybrid pipes, *Composites Part B: Engineering*, **106**, 154-163.

[76] Wakayama, S., Kobayashi, S., Imai, T., & Matsumoto, T. (2006). Evaluation of burst strength of FW-FRP composite pipes after impact using pitch-based low-modulus carbon fiber, *Composites Part A: Applied Science and Manufacturing*, **37(11)**, 2002-2010.

[77] Rosato, D. V., & Grove, C. S. (1964). Filament winding: its development, manufacture, applications, and design. New York: Interscience Publishers.

[78] Peters, S. T. (Ed.). (2013). Handbook of composites. California: Springer Science & Business Media.

[79] Allen, A. K. (2004). A Method for Winding Advanced Composites of Unconventional Shapes using Continuous and Aligned Fibers, (Master's thesis, Brigham Young University - Provo)

[80] Lifshitz, J. M., & Dayan, H. (1995). Filament-wound pressure vessel with thick metal liner, *Composite Structures*, **32(1-4)**, 313-323.

[81] Shen, F. C. (1995). A filament-wound structure technology overview, *Materials Chemistry and Physics*, **42(2)**, 96-100.

[82] Hazra, T. (2011). A low cost 2-axis plc controlled filament winding machine with simplified fiber winding angle and tension control system.

[83] Swolfs, Y., Gorbatikh, L., & Verpoest, I. (2014). Fibre hybridisation in polymer composites: a review, *Composites Part A: Applied Science and Manufacturing*, **67**, 181-200.

[84] ASTM D2584. (2002). Standard test method for ignition loss of cured reinforced resins. In American Society for Testing and Materials (Vol. 100).

[85] Wang, H., Bouchard, R., Eagleson, R., Martin, P., & Tyson, W. R. (2002). Ring hoop tension test (RHTT): A test for transverse tensile properties of tubular materials, *Journal of Testing and Evaluation*, **30(5)**, 382-391.

[86] ASTM, D. (2004). 2290. Apparent tensile strength of parallel reinforced plastics by split disk method.

[87] Kinna, M. A. (1964). NOL Ring Test Methods (No. NOLTR-64-156). NAVAL ORDNANCE LAB WHITE OAK MD.

[88] https://en.wikipedia.org/wiki/Compressive_strength. Accessed 03.07.2019

[89] ASTM, D. (2002). 695. Standard test method for compressive properties of rigid plastics.

[90] ASTM, D. 2412 (2010). Standard Test Method for Determination of External Loading Characteristics of Plastic Pipe by Parallel-Plate Loading, American Society for Testing and Materials.

[91] Rabiee, A., & Ghasemnejad, H. (2017). Progressive crushing of polymer matrix composite tubular structures, *Open Journal of Composite Materials*, **7**, 14-48.

[92] Thornton, P. H. (1990). The crush of fiber-reinforced plastics, *Handbook of ceramics and composites*, **1**, 307-337.

[93] Farley, G. L. (1992). Relationship between mechanical-property and energy-absorption trends for composite tubes, Virginia: NASA Technical Paper 3284.

[94] Pegoretti, A., Fabbri, E., Migliaresi, C., & Pilati, F. (2004). Intraply and interply hybrid composites based on E-glass and poly (vinyl alcohol) woven fabrics: tensile and impact properties, *Polymer International*, **53(9)**, 1290-1297.

[95] Nosraty, H., Tehrani-Dehkordi, M., Shokrieh, M. M., & Minak, G. (2015). Intraply hybrid composites based on basalt and nylon woven fabrics: tensile and compressive properties, *Iran J Mater Sci Eng*, **12**, 1-11.

[96] Almeida Jr, J. H. S., Tonatto, M. L., Ribeiro, M. L., Tita, V., & Amico, S. C. (2018). Buckling and post-buckling of filament wound composite tubes under axial compression: linear, nonlinear, damage and experimental analyses, *Composites Part B: Engineering*, **149**, 227-239.

[97] Suresh, G., & Jayakumari, L. S. (2016). Analyzing the mechanical behavior of E-glass fibre-reinforced interpenetrating polymer network composite pipe, *Journal of composite materials*, **50(22)**, 3053-3061.

[98] Farley, G. L. (1989). Energy-absorption capability of composite tubes and beams (Doctoral dissertation, Virginia Polytechnic Institute and State University).

[99] Xin, Z., Duan, Y., Zhou, J., & Xiao, H. (2019). Effect of tailored plies on the energy absorption capability of square CFRP tubes with discontinuous fibers, *Composite Structures*, **209**, 150-159.

[100] Kalhor, R., & Case, S. W. (2015). The effect of FRP thickness on energy absorption of metal-FRP square tubes subjected to axial compressive loading, *Composite Structures*, **130**, 44-50.

[101] Chiu, L. N., Falzon, B. G., Ruan, D., Xu, S., Thomson, R. S., Chen, B., & Yan, W. (2015). Crush responses of composite cylinder under quasi-static and dynamic loading, *Composite Structures*, **131**, 90-98.

[102] Liu, Q., Xing, H., Ju, Y., Ou, Z., & Li, Q. (2014). Quasi-static axial crushing and transverse bending of double hat shaped CFRP tubes, *Composite Structures*, **117**, 1-11.

[103] Palanivelu, S., Van Paepegem, W., Degrieck, J., Van Ackeren, J., Kakogiannis, D., Van Hemelrijck, D., ... & Vantomme, J. (2010). Experimental study on the axial crushing behaviour of pultruded composite tubes, *Polymer testing*, **29(2)**, 224-234.

[104] Pickett, L., & Dayal, V. (2012). Effect of tube geometry and ply-angle on energy absorption of a circular glass/epoxy crush tube–A numerical study, *Composites Part B: Engineering*, **43(8)**, 2960-2967.

[105] Mahdi, E., & Sebaey, T. A. (2014). Crushing behavior of hybrid hexagonal/octagonal cellular composite system: Aramid/carbon hybrid composite, *Materials & Design*, **63**, 6-13.

[106] Ismail, A. E., & Sahrom, M. F. (2015). Lateral crushing energy absorption of cylindrical kenaf fiber reinforced composites, *International Journal of Applied Engineering Research*, **10(8)**, 19277-19288.

CURRICULUM VITAE

PERSONAL INFORMATION

Name and Surname: Özkan ÖZBEK

Nationality: T.C.

E-mail: ozkanozbek@gantep.edu.tr/ozkanozbek@windowslive.com

EDUCATION

	Graduate School	Year
Master	Gaziantep University, Mechanical Engineering Department	2015
Bachelor	Gaziantep University, Mechanical Engineering Department	2013
High School	Mersin Dumlupınar High School	2005

WORK EXPERIENCES

	Place	Enrollment
2014-Present	Gaziantep University, Mechanical Engineering Department	Research Asst.
2013-2014	Kilis 7 Aralık University, Mechanical Engineering Department	Research Asst.

INTERNATIONAL VISITING

Period	Visiting Institution	Programme
15.06.2015 18.06.2015	University of West Bohemia, Mechanical Engineering Department Plzen/CZECH REPUBLIC	Erasmus+ Staff Mobility for Training
01.07.2019 03.07.2019	Opole University of Technology, Faculty of Mechanical Engineering Opole/POLAND	Erasmus+ Staff Mobility for Training

INTERNATIONAL RESEARCH EXPERIENCE

1) Numerical Modeling and Testing of Filament Wound Pressure Pipes and Vessels, (Elyaf sarım yöntemi ile üretilen kompozit malzemelerin farklı tasarım parametrelerinde ANSYS programı üzerinde sayısal analizleri), Malta University, Researcher Visiting, 11.06.2018 -12.08.2018 (Uluslararası).

PUBLICATIONS

Papers Published in International indexed Journals

1) ÖZBEK ÖZKAN,BOZKURT ÖMER YAVUZ,ERKLİĞ AHMET (2019). An experimental study on intraply fiber hybridization of filament wound composite pipes subjected to quasi-static compression loading. Polymer Testing, 79, 106082, Doi: 10.1016/j.polymertesting.2019.106082 (Yayın No: 5203218)
2) ÖZBEK ÖZKAN,BOZKURT ÖMER YAVUZ (2019). Hoop tensile and compression behavior of glass-carbon intraply hybrid fiber reinforced filament wound composite pipes. Materials Testing, 61(8), 763-769, Doi:10.3139/120.111395 (Yayın No: 5162311)
3) BOZKURT ÖMER YAVUZ,ÖZBEK ÖZKAN,ABDO ATBAN RAFEA (2017). The Effects of Nanosilica on Charpy Impact Behavior of Glass/EpoxyFiber Reinforced Composite Laminates. Periodicals of Engineering and Natural Sciences, 5(3), 322-327., Doi: 10.21533/pen.v5i3.119 (Yayın No: 3623881)
4) BOZKURT ÖMER YAVUZ,DAİ İHSAN CİHAN,ÖZBEK ÖZKAN (2017). The Finite Element Analysis and Geometry Improvements of Some Structural Parts of a Diesel Forklift Truck. Periodicals of Engineering and Natural Sciences (PEN), 5(2), 202-209., Doi: 10.21533/pen.v5i2.118 (Yayın No: 3561344)
5) BOZKURT ÖMER YAVUZ,ÖZBEK ÖZKAN,BULUT MEHMET (2016). The Influence of Fiber Orientation Angle on Damping and Vibration Properties of Basalt Fiber Reinforced Composite Laminates. Journal of Civil, Structural and Transportation Engineering(2), 12-16., Doi: TBA (Yayın No: 2898454)
6) BOZKURT ÖMER YAVUZ,ÖZBEK ÖZKAN (2016). Analysis Of Laminated Composite Plates Using Element Free Galerkin Method. European Journal of Engineering and Natural Sciences , 1(1), 1-8. (Yayın No: 2577384)

7) BOZKURT ÖMER YAVUZ,mustafa barbar,ÖZBEK ÖZKAN (2015). Investigation of Effects of Parameters in Element Free Galerkin Method for Bending Analysis of Mindlin Reissner Plates. Acta Physica Polonica A, 128(2B), 208-210., Doi: 10.12693/APhysPolA.128.B-208 (Yayın No: 1929204)

Papers Published in National indexed Journals

1) BOZKURT ÖMER YAVUZ,ÖZBEK ÖZKAN,BULUT MEHMET (2016). Damping and Vibration Behavior of Adhesively Bonded Glass Fiber Reinforced Composite Laminates. Çukurova Üniversitesi Mühendislik-Mimarlik Fakültesi Dergisi, 31, 61-67., Doi: 10.21605/cukurovaummfd.311885 (Kontrol No: 2909284)

International Conference Papers Published in Proceedings

1) ÖZBEK ÖZKAN,BOZKURT ÖMER YAVUZ,GÖKDEMİR MUHAMMET ENVER (2019). Tensile and Flexural Characteristics of Glass/Epoxy Reinforced Structures Fabricated by Filament Winding Technique. 6th International Multidisciplinary Studies Congreess, 1, 95-105. (Tam Metin Bildiri/Sözlü Sunum)(Yayın No:5062801)
2) ÖZBEK ÖZKAN,BOZKURT ÖMER YAVUZ,KANAT MEHMET SAMİ,GÖKDEMİR MUHAMMET ENVER (2019). The Influence of Loading Rate on Axial Compression Characteristics of Carbon/Epoxy Fiber Reinforced Composite Pipes Fabricated by Filament Winding Technique. 6th International Multidisciplinary Studies Congreess, 1, 107-114. (Tam Metin Bildiri/Sözlü Sunum)(Yayın No:5062802)
3) GÖKDEMİR MUHAMMET ENVER,BOZKURT ÖMER YAVUZ,ÖZBEK ÖZKAN (2019). Effect of water aging on vibration damping behavior of basalt fiber reinforced composites. III. Uluslararası AVRASYA Multidisipliner Çalışmalar Kongresi, 173-178. (Tam Metin Bildiri/Sözlü Sunum)(Yayın No:5035546)
4) GÖKDEMİR MUHAMMET ENVER,BOZKURT ÖMER YAVUZ,ÖZBEK ÖZKAN (2019). Effect of hydrothermal aging on vibration-damping behavior of basalt fiber reinforced composite laminates. III. Uluslararası AVRASYA

Multidisipliner Çalışmalar Kongresi, 179-185. (Tam Metin Bildiri/Sözlü Sunum)(Yayın No:5035545)

5) BOZKURT ÖMER YAVUZ,ERKLİĞ AHMET,ÖZBEK ÖZKAN,FAYADH WALEED AHMED (2018). THE INFLUENCE OF FIBER ORIENTATION ANGLE ON TENSILE AND FLEXURAL CHARACTERISTICS OF GLASS FIBER REINFORCED COMPOSITE LAMİNATES WİTH 1 NANOCLAY PARTICLE. III. Uluslararası Mesleki ve Teknik Bilimler Kongresi, 3499-3504. (Tam Metin Bildiri/Sözlü Sunum)(Yayın No:4350627)
6) BOZKURT ÖMER YAVUZ,ERKLİĞ AHMET,ÖZBEK ÖZKAN,FAYADH WALEED AHMED (2018). THE RADIAL COMPRESSION BEHAVIOUR OF GLASS FIBER REİNFORCED COMPOSİTE PİPES. III. ULUSLARARASI MESLEKİ VE TEKNİK BİLİMLER KONGRESİ, 3505-3512. (Tam Metin Bildiri/Sözlü Sunum)(Yayın No:4350629)
7) ÖZBEK ÖZKAN,BOZKURT ÖMER YAVUZ,KANAT MEHMET SAMİ (2018). The Effect of Winding Angle on Hoop Tensile Characteristics of the Glass Fiber Reinforced Composite Pipes. International Congress on Engineering and Life Science, 825-829. (Tam Metin Bildiri/Sözlü Sunum)(Yayın No:4267919)
8) ÖZBEK ÖZKAN,BOZKURT ÖMER YAVUZ,MAHMOOD MUHAMMED HUSSEIN (2018). On the Tensile and Flexural Behavior of Basalt-Epoxy Fiber Reinforced Composite Laminates with Nanoclay. International Congress on Engineering and Life Science, 830-834. (Tam Metin Bildiri/Sözlü Sunum)(Yayın No:4267925)
9) BOZKURT ÖMER YAVUZ,ÖZBEK ÖZKAN,Waleed A FAYADH (2017). THE EFFECT OF NANOCLAY ON DAMPING AND VIBRATIONCHARACTERISTICS OF GLASS/EPOXY FIBER REINFORCEMENT COMPOSITE LAMINATES. 2nd International Energy and Engineering Conference, 1177-1183. (Tam Metin Bildiri/Sözlü Sunum)(Yayın No:3975475)
10) KILIÇ ALİ,BOZKURT ÖMER YAVUZ,ÖZBEK ÖZKAN (2017). Design and Construction of 2-Axis Filament Winding Machine. 4th International Conference on Computational and Experimental Science and Engineering (ICCESEN 2017), 373 (Özet Bildiri/Sözlü Sunum)(Yayın No:3632238)
11) BOZKURT ÖMER YAVUZ,ALAZZAWI WALEED KADHIM,ÖZBEK ÖZKAN (2017). The Effect of Nanosilica on Tensile and Flexural Behavior of

Glass Fiber reinforced Composite Laminates. Academics World (Tam Metin Bildiri/Sözlü Sunum)(Yayın No:3573108)

12) BOZKURT ÖMER YAVUZ,ÖZBEK ÖZKAN,ABDO ATBAN RAFEA (2017). The Effects of Nanosilica on Charpy Impact Behavior of Glass/Epoxy Fiber Reinforced Composite Laminates. 3rd International Conference on Engineering and Natural Sciences, 464 (Özet Bildiri/Sözlü Sunum)(Yayın No:3575229)
13) BOZKURT ÖMER YAVUZ,DAİ İHSAN CİHAN,ÖZBEK ÖZKAN (2017). The Finite Element Analysis and Geometry Improvements of Some Structural Parts of a Diesel Forklift Truck. 3rd International Conference on Engineering and Natural Sciences, 470 (Özet Bildiri/Sözlü Sunum)(Yayın No:3575239)
14) BOZKURT ÖMER YAVUZ,MAHMOOD MOHAMMED HUSSEIN,ÖZBEK ÖZKAN (2016). The Effect of Nanoclay on Tensile and Flexural Behavior of Glass Fiber Reinforced Composite Laminates. International Conference on Advanced Technology & Sciences, 1183-1185. (Tam Metin Bildiri/Sözlü Sunum)(Yayın No:2888178)
15) BOZKURT ÖMER YAVUZ,ÖZBEK ÖZKAN,ABDO ATBAN RAFEA (2016). Investigation of the Effect of Nanoclay Inclusion on Charpy Impact Behavior of the Glass Fiber Reinforced Composite Laminate. International Conference on Advanced Technology & Sciences, 1179-1182. (Tam Metin Bildiri/Sözlü Sunum)(Yayın No:2888182)
16) BOZKURT ÖMER YAVUZ,ÖZBEK ÖZKAN,BULUT MEHMET (2016). Damping and Vibration Behavior of Adhesively Bonded Composite Laminates. International Conference on Welding Technologies and Exhibition, 412-418. (Tam Metin Bildiri/Sözlü Sunum)(Yayın No:2874917)
17) BOZKURT ÖMER YAVUZ,BULUT MEHMET,ÖZBEK ÖZKAN (2016). Effect of Fibre Orientations on Damping and Vibration Characteristics of Basalt Epoxy Composite Laminates. International Conference on Structural, Engineering, New Technology and Methods, Doi: 10.11159/icsenm16.115 (Tam Metin Bildiri/Sözlü Sunum)(Yayın No:2636675)
18) ÖZBEK ÖZKAN,BOZKURT ÖMER YAVUZ (2015). Analysis of Laminated Composite Plates Using Element Free Galerkin Method. International Conference on Engineering and Natural Sciences (Tam Metin Bildiri/Sözlü Sunum)(Yayın No:1981763)

19) BOZKURT ÖMER YAVUZ,MUSTAFA BARBAR,ÖZBEK ÖZKAN (2014). Investigation of Effects of Parameters in Element-Free Galerkin Method for Bending Analysis of Mindlin-Reissner Plates. International Conference on Computational and Experimental Science and Engineering (Özet Bildiri/Sözlü Sunum)(Yayın No:3575243)
20) BOZKURT ÖMER YAVUZ,ÖZBEK ÖZKAN (2014). Study of Selectable Parameters in Element Free Galerkin Method for Bending Analysis of Mindlin Reissner Plates. 3rd International Eurasian Conference on Mathematical Sciences and Applications, 498-498. (Özet Bildiri/Sözlü Sunum)(Yayın No:2888188)

National Conference Papers Published in Proceedings

1) BOZKURT ÖMER YAVUZ,ÖZBEK ÖZKAN (2015). Tabakalı Kompozit Plakaların Eleman Bağımsız Galerkin Yöntemi İle Analizinde Kayma Düzeltme Katsayısının Etkisi. XIX. Ulusal Mekanik Kongresi, 237-246. (Tam Metin Bildiri/Sözlü Sunum)(Yayın No:3459049)
2) ÖZBEK ÖZKAN,BOZKURT ÖMER YAVUZ (2015). Eleman Bağımsız Galerkin Yöntemindeki Çözümü Etkileyen Seçilebilir Parametrelerin Tabakalı Plakaların Eğilme Problemlerinde İncelenmesi. XIX. Ulusal Mekanik Kongresi, 733-742. (Tam Metin Bildiri/Sözlü Sunum)(Yayın No:3459051)

TASKS IN PROJECTS

1) Yükleme Hızının Cam ve Karbon Fiber Takviyeli Kompozit Boruların Çekme ve Eğme Özellikleri Üzerine Etkilerinin Deneysel İncelenmesi, Yükseköğretim Kurumları tarafından destekli bilimsel araştırma projesi, Araştırmacı:Kanat Mehmet Sami,Yürütücü:BOZKURT ÖMER YAVUZ,Araştırmacı:ÖZBEK ÖZKAN, , 20/03/2018 - 21/01/2019 (ULUSAL)
2) Nano kil Katılmış Epoksi Matriks Tabanlı Kompozit Laminatların Çekme ve Eğilme Davranışları, Yükseköğretim Kurumları tarafından destekli bilimsel araştırma projesi, Yürütücü:BOZKURT ÖMER YAVUZ,Araştırmacı:ÖZBEK ÖZKAN,Araştırmacı:MAHMOOD MUHAMMED HUSSEIN, , 01/08/2016 - 24/08/2017 (ULUSAL)
3) Elyaf Sarma İşleminde Üretim Hızını Ve Esnekliğini Artırmaya Yönelik Yeni Bir Yöntem Uygulaması, -Tübitak 1005, Yürütücü:ERKLİĞ AHMET,Bursiyer:BULUT MEHMET,Bursiyer:DOĞAN NURETTİN

FURKAN,Araştırmacı:BOZKURT ÖMER YAVUZ,Bursiyer:ÖZBEK ÖZKAN, , 01/09/2015 - 22/02/2018 (ULUSAL)

4) Elyaf Melezlemenin Elyaf Sarma Yöntemi ile Üretilen Kompozit Boruların Mekanik Özelliklerine Etkisi, Yükseköğretim Kurumları tarafından destekli bilimsel araştırma projesi, Araştırmacı:TOKUR BOZKURT YÜKSEL,Araştırmacı:ÖZBEK ÖZKAN,Yürütücü:BOZKURT ÖMER YAVUZ, , 01/08/2016 - 01/05/2018 (ULUSAL)
5) Nano silis Katılmış Epoksi Matris Tabanlı Laminatların Darbe Davranışları, Yükseköğretim Kurumları tarafından destekli bilimsel araştırma projesi, Araştırmacı:ABDO ATBAN RAFEA,Yürütücü:BOZKURT ÖMER YAVUZ,Araştırmacı:ÖZBEK ÖZKAN, , 01/08/2016 - 26/07/2017 (ULUSAL)
6) Su Yaşlanmasının Elyaf Takviyeli Kompozit Laminatların Titreşim Sönümleme Davranışına Etkisi, Yükseköğretim Kurumları tarafından destekli bilimsel araştırma projesi, Yürütücü:BOZKURT ÖMER YAVUZ,Araştırmacı:ÖZBEK ÖZKAN,Araştırmacı:GÖKDEMİR MUHAMMET ENVER, , 07/05/2018 (Devam Ediyor) (ULUSAL)